

INFORMATION TO USERS

This manuscript has been reproduced from the microfilm master. UMI films the text directly from the original or copy submitted. Thus, some thesis and dissertation copies are in typewriter face, while others may be from any type of computer printer.

The quality of this reproduction is dependent upon the quality of the copy submitted. Broken or indistinct print, colored or poor quality illustrations and photographs, print bleedthrough, substandard margins, and improper alignment can adversely affect reproduction.

In the unlikely event that the author did not send UMI a complete manuscript and there are missing pages, these will be noted. Also, if unauthorized copyright material had to be removed, a note will indicate the deletion.

Oversize materials (e.g., maps, drawings, charts) are reproduced by sectioning the original, beginning at the upper left-hand corner and continuing from left to right in equal sections with small overlaps. Each original is also photographed in one exposure and is included in reduced form at the back of the book.

Photographs included in the original manuscript have been reproduced xerographically in this copy. Higher quality 6" x 9" black and white photographic prints are available for any photographs or illustrations appearing in this copy for an additional charge. Contact UMI directly to order.

UMI

A Bell & Howell Information Company
300 North Zeeb Road, Ann Arbor MI 48106-1346 USA
313/761-4700 800/521-0600

HARVARD UNIVERSITY
Graduate School of Arts and Sciences



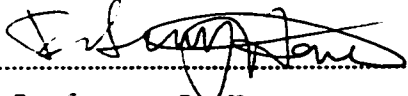
THESIS ACCEPTANCE CERTIFICATE


The undersigned, appointed by the
Division of Engineering and Applied Sciences
Department
Committee

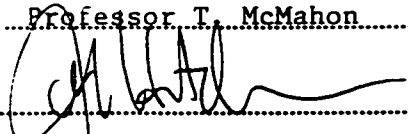
have examined a thesis entitled
"Remote Palpation Instruments for
Minimally Invasive Surgery"

presented by William Jeane Peine

candidate for the degree of Doctor of Philosophy and hereby
certify that it is worthy of acceptance.

Signature 
Typed name Professor R. Howe

Signature 
Typed name Professor T. McMahon

Signature 
Typed name Professor J. Hutchinson

Date October 16, 1998

Remote Palpation Instruments for Minimally Invasive Surgery

A thesis presented
by

William Jeane Peine

to

The division of Engineering and Applied Sciences
in partial fulfillment of the requirements
for the degree of
Doctor of Philosophy
in the subject of
Engineering Sciences

Harvard University
Cambridge, Massachusetts

October 1998

UMI Number: 9921526

**Copyright 1998 by
Peine, William Jeane**

All rights reserved.

**UMI Microform 9921526
Copyright 1999, by UMI Company. All rights reserved.**

**This microform edition is protected against unauthorized
copying under Title 17, United States Code.**

UMI
300 North Zeeb Road
Ann Arbor, MI 48103

© 1998 by William J. Peine
All Rights Reserved

Abstract

New minimally invasive surgical techniques prevent surgeons from directly touching and palpating internal tissue. Palpation tasks that are trivial to complete with the fingers are time consuming or impossible with current surgical tools. Remote palpation systems are needed to allow surgeons to use their highly developed sense of touch. These systems include tactile sensors to measure distributed contact information as the tissue is probed, signal processing algorithms to determine what the surgeon's finger would feel if it were touching the tissue, and tactile displays that recreate this information on the finger. Development of these devices is difficult due to the complexity of palpation and the human sense of touch. This thesis investigates design specifications for remote palpation instruments. A three-prong approach is taken. First, palpation is studied through observation and measurement. Second, design specifications are determined, and third, prototypes are designed, constructed, and tested based on these principles. To focus the research, a target application of locating hard nodules in the lung during thoracic surgery was chosen. To provide insight to the sensitivity requirements of the tactile sensor, an experiment measured the tactile stimulus on the finger when a lump could just be detected. Based on these results, the prototype sensor was designed to measure distributed pressure. One important design parameter for tactile displays is temporal bandwidth. Adequate speed is required for the display to produce correct tactile sensations as the finger moves over a structural feature. A human factors experiment measured maximum finger velocities during a lump localization task, and it was determined that a 30 Hz bandwidth display is needed. The surgical instrument carries the tactile feedback and allows internal tissues to be probed. Effective designs must allow the surgeon to use natural hand and finger motions. To provide insight for the design process, a taxonomy of palpation was developed to characterize hand configurations and finger motions used during surgery. The prototype remote palpation instrument incorporating all of the components was able to locate lumps in rubber models using minimally invasive techniques.

This thesis is dedicated to my parents, Thomas and Susan Peine.

Acknowledgments

The research involved in this thesis work utilized the ideas, talents, and enthusiasm of many individuals. The relationships developed with these people will be some of my most treasured memories of this effort. I owe all of them my thanks and appreciation for their help.

I would like to express my deepest thanks to my advisor, Professor Robert Howe, for his guidance, creativity, and support. As an excellent scientist, he provided vision about the scope and usefulness of the research and generated many insightful technical ideas. He instructed me in the importance of communication and integrity, and never let me settle for the easier to obtain less important result.

The other members of my thesis committee were an indispensable part of this research as well. Professor Thomas McMahon is an excellent teacher and inspiration. His undying devotion to understanding how nature works and his ability to distill a problem down and focus on critical aspect are marvelous. The support and enthusiasm from Professor John Hutchinson always buoyed my spirits. He enhanced my ability to form appropriate assumptions and correctly qualify simplified analyses.

Dr. John Wain of Massachusetts General Hospital provided critical instruction about the target application of minimally invasive thoracic surgery. Much of the technical success of the surgical instrument design is due his guidance and the time I spent in the operating room with him.

The insightful conversations with Professors Susan Lederman and Roberta Klatzky were valuable in designing, conducting, and analyzing the psychophysics experiments in this thesis research. Professor Ken Johnson provided important understanding about the relation of experimental results to biomechanics and neurophysiology research.

A tremendous amount of support and education came from the many graduate students and post-docs in the lab. I appreciate Eric Dunn's help with circuit and

software design. Dimitri Kontarinis's research provided much of the foundation for the shape display development. Dianne Pawluk's understanding of biomechanics and tactile perception were extremely valuable. Jae Son's work with the tactile sensor design was key. Aram Hajian provided insight to various problems and was always available for much-needed comic relief. I am especially appreciative of the help of Parris Wellman. He was instrumental to this research and contributed years of effort to the shape display and system design. Jack Dennerlein and Paul Millman also contributed with their insight and ideas.

Many undergraduate students also contributed to this work. Danny Sanchez helped with the array sensor development and calibration and produced much of the actuated positioner used in the lump detection experiments. Kharma Foucher collected much of the data for the finger velocity experiment. Felix Chung helped with many aspects of the apparatus and analysis for the lump detection experiment. Matthew Emans provided key insight to the surgical instrument design and machined and constructed the finger-based prototype. Andrew Goldman helped with the arm-based surgical instrument design.

Finally, I would like to thank my family for all their support and love during this process. My wife, Gina, gave me confidence and carried me when I felt like stopping. She brings stability and purpose to my life and I appreciate all her big and little acts of love. In many ways, I am most thankful for my parents' contributions. They provided me with the education and drive to accomplish this dream and never faltered in their devotion. I am deeply thankful for their generosity, guidance, and love they continually show.

This research was funded by a generous grant from the Whitaker Foundation.

Table of Contents

Abstract	iii
Acknowledgements	v
Chapter 1. Introduction	1
1.1 Minimally Invasive Surgery	1
1.2 Remote Palpation Systems	3
1.3 Complexities of Medical Palpation	7
1.4 Remote Palpation Instrument System Design Issues	9
1.5 Research Approach and Target Application	10
1.6 Thesis Overview	12
Chapter 2. Human Sensing Limits for Lump Detection	15
2.1 Motivation for Lump Detection Experiment	15
2.2 Experimental Methods	17
2.3 Results	23
2.4 Discussion	30
2.5 Resulting Design Specifications for Remote Palpation Instruments	35
Chapter 3. Tactile Sensor and Signal Processing	36
3.1 Prototype Tactile Array Sensor	38
3.2 Signal Processing for Lump Localization	43
3.3 Haptic Rendering Model to Simulate Soft Tissue Contact	50
Chapter 4. Finger Speed during Lump Localization	56
4.1 Experimental Methods	58
4.1.1 Apparatus and Experimental Setup	58
4.1.2 Experimental Procedure	61
4.2 Results	63
4.3 Discussion	70
4.4 Resulting Design Specifications for Tactile Display	72
Chapter 5. Tactile Shape Display	75
5.1 Previous Research on Tactile Shape Displays	76

5.2	Mechanical Design of Prototype Shape Display	77
5.2.1	Configuration Design	77
5.2.2	Mechanical Design	79
5.3	Thermal Design	81
5.4	Controller Design	82
5.5	Display Performance Characterization	82
5.6	Effect of Bandwidth on Performance of Lump Localization	86
5.7	Discussion	88
Chapter 6.	Taxonomy of Palpation	90
6.1	Taxonomy of Palpation: Hand Postures and Finger Motions	91
6.2	Resulting Design Specifications for Remote Palpation Instrument	96
Chapter 7.	Remote Palpation Instrument	99
7.1	Design Approaches	100
7.2	Finger-Based Motion Design	101
7.3	Arm-Based Motion Design	104
7.3.1	Sensor to Instrument Shaft Joint Design	105
7.3.2	Handle to Instrument Shaft Joint Design	109
7.4	Final Prototype Performance	111
7.5	Lump Localization Experiment with Remote Palpation Instrument	114
7.5.1	Experimental Methods	115
7.5.2	Results	119
7.5.3	Discussion	124
Chapter 8.	Conclusions and Future Work	128
8.1	Improvements for Prototype System	129
8.1.1	Tactile Sensor and Signal Processing Design	129
8.1.2	Tactile Shape Display Design	130
8.1.3	Surgical Instrument Design	132
8.2	Advanced Signal Processing Techniques	133
8.2.1	Measured Model Based Haptic Rendering	134
8.2.2	3D Tissue Model Generation from Tactile Signals	136
8.2.3	Haptic Interface of Finger Contact with 3D Tissue Model	139
8.3	The Fundamental Importance of Touch	141
Bibliography		142

Chapter 1. Introduction

1.1 Minimally Invasive Surgery

For centuries, surgery has been performed using traditional, open-incision methods. Large incisions are necessary to access internal organs and provide surgeons with room for their hands and tools to work. Unfortunately, this damages a great deal of healthy tissue. A relatively new surgical technique, minimally invasive surgery, sometimes called “keyhole” surgery, is challenging this traditional method. It reduces damage to healthy tissues by allowing surgeons to operate inside the patient’s body through a few small incisions. Endoscopic cameras are used to view the surgical site while long handled instruments or specialized robotic arms manipulate the internal organs. By minimizing incision size and decreasing trauma, patients heal more quickly with less pain. Hospital stays are shortened from weeks to days or eliminated completely – freeing up valuable hospital resources. Recovery times are reduced from months to weeks - allowing people to rapidly return to normal life and get back to work. This dramatically lowers the costs for insurance companies and society. These tremendous health and financial benefits are driving the development of advanced technology to increase the range of minimally invasive procedures. Ultimately, these techniques have the power to revolutionize the way all types of surgery are performed.

Minimally invasive surgery is currently in its infancy and applied to a limited number of procedures. This is largely due to the present state of surgical instrument designs, which fall far short of the dexterity and sensitivity of the human hand [Melzer, Buess,

and Cuschieri 1994]. Simple, long handled tools able to fit through the small incisions are used to grasp, cut, cauterize, and staple tissue. Figure 1.1 shows an example of a typical minimally invasive grasper (manufactured by Karl Storz GmbH & Co., Tuttlingen, Germany). These tools often use a single degree of freedom mechanism operated by a scissors handle to open and close the jaws. The fixed point of rotation imposed by the entry location at the incision restricts manipulation because the orientation of the gripper must be inline with the instrument shaft. As a result, only simple tasks that do not require complex motions or high dexterity can be performed.

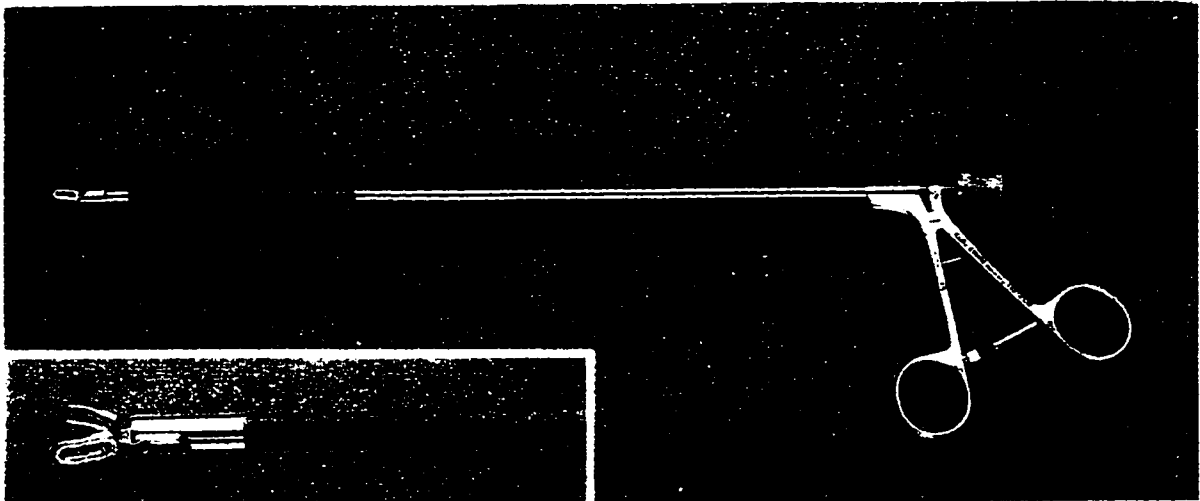


Figure 1.1. *Typical Minimally Invasive Grasper.* A rod running the length of the instrument shaft connects the motions of the scissors grip handle with the jaws of the gripper. Internal tissues are grasped by passing the instrument through a small incision in the patient's body. (Manufactured by Karl Storz GmbH & Co., Tuttlingen, Germany)

Another major problem with current minimally invasive surgical instruments is they deprive surgeons of one of their most valuable diagnostic tools: the sense of touch. The awkward instruments provide some force information, but this is vastly inferior to the distributed, time-varying tactile sensations felt by touching and palpating tissue directly.

The small incision sizes used in minimally invasive procedures often make direct contact between the fingers and tissue impossible. This is a great loss because palpation provides important information about material and structural properties of soft tissues and is a vital part of traditional, open-incision surgery. In some procedures tactile sensations are essential to quickly complete a task. For example, hard lumps in soft organs are detected by probing the tissue with the fingers; arteries are localized during dissection by feeling for a time varying pressure; or the structural integrity of a blood vessel wall is assessed by rolling it between the fingers. These tasks are time consuming, frustrating, and sometimes impossible without the sense of touch. In other procedures, the sense of touch is used to discriminate between healthy and diseased tissue. Surgeons will quickly examine all of the accessed organs in a body cavity, for example, feeling for abnormalities. Previously unknown problems can then be caught before they become critical. The sense of touch is clearly important to surgery and provides valuable information to the surgeon. Minimally invasive surgery is considerably limited by the inability to palpate internal organs [Melzer et al 1993].

1.2 Remote Palpation Systems

In order to utilize a surgeon's extensive palpation skills in minimally invasive procedures, special surgical instruments are needed that remotely measure tactile sensations from inside the patient's body and display this information to the surgeon. This would allow internal tissues to be manipulated and palpated to gather tactile information useful for diagnosis and localization. Figure 1.2 shows a conceptual representation of a remote palpation instrument. By extending the length of the surgeon's

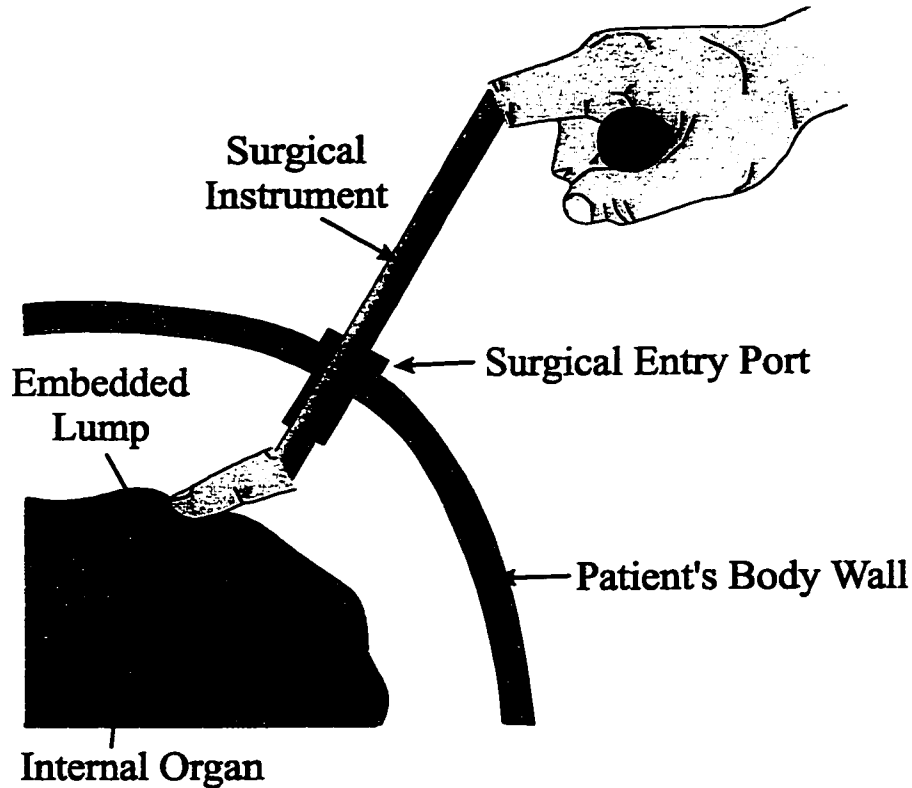


Figure 1.2. *Conceptual Idea of a Remote Palpation Instrument.* The remote palpation instrument allows internal tissues to be probed through the small entry incisions by acting as a remote finger. Ideally, the instrument would reproduce tactile sensations such that the surgeon feels as if the inaccessible tissues are being directly touched.

finger, internal tissues can be probed through the small entry incisions. Transposing the fingertip is obviously impossible, and special hardware is needed to provide a remote sense of touch to the surgeon. To be effective, these devices should naturally tie into the human sense of touch.

Tactile perception through palpation is composed of two distinct modalities: tactile or cutaneous sensing and kinesthetic sensing [Loomis and Lederman 1986]. Tactile sensing refers to distributed sensations from the skin such as local pressure or curvature. Kinesthetic sensing refers to sensations of the internal state of the limb through

parameters such as joint angle and muscle effort. The combination of these sensations, often referred to as haptics, allows tactile exploration by integrating local shape or curvature information with overall finger location and contact force. Hardware for remote palpation instruments must allow the surgeon to use both sensing modalities.

Figure 1.3 shows a surgical instrument that accomplishes this goal. It uses sensors, located at the tip of the instrument, to measure contact information (such as distributed pressure, shape, temperature, or vibration) as internal tissues are probed. A signal processing algorithm changes these measured signals into drive commands for tactile display devices in the instrument handle. Thus, sensations of the remote tissue are recreated directly on the surgeon's fingertip. The surgical instrument provides kinesthetic feedback by coupling the motions of the surgeon's finger to the motions of the sensor. Internal organs are palpated by scanning the sensor probe across the tissue surface while feeling the induced tactile sensations.

The ultimate goal of these devices is to provide "transparent" tactile feedback so the surgeon feels as if he or she is palpating internal tissues directly. Surgeons could then use their highly developed tactile perception for effective, natural palpation while retaining the benefits of minimally invasive surgery. The development of transparent tactile feedback systems is extremely challenging and current hardware is far from obtaining this goal. Even though initial efforts may produce less-than-perfect systems, they can still be quite effective in many procedures. New technology and advanced signal processing should strive to synchronize with natural palpation motions and sensations. This requires a thorough understanding of palpation to aid the design process.

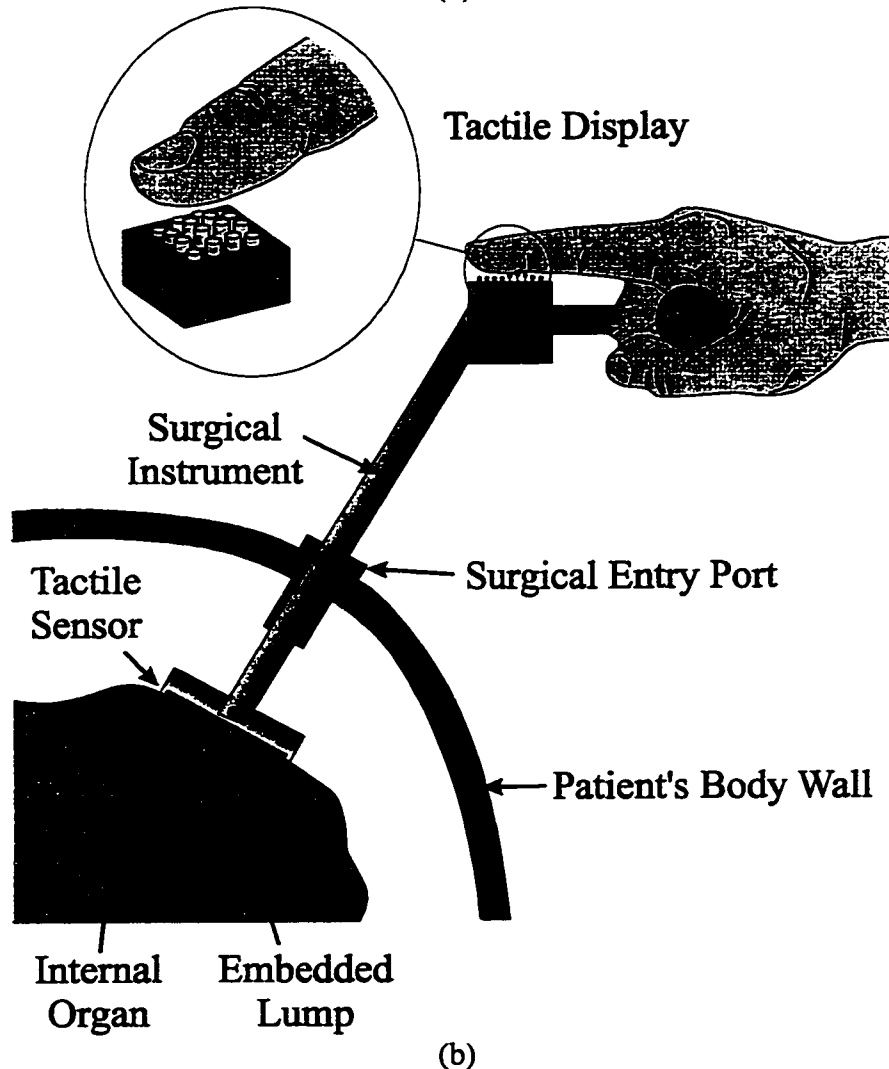
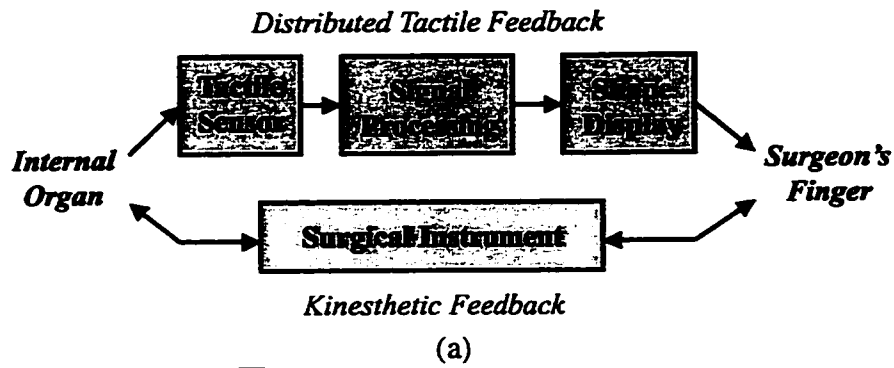


Figure 1.3. Hardware Components of a Remote Palpation Instrument. (a) Block diagram showing integration of a tactile feedback system into a surgical instrument. (b) Tactile sensors at the instrument tip measure distributed contact information. These sensations are recreated on the surgeon's finger using a tactile display (tactile feedback). The instrument couples the surgeon's finger motions and forces to the movements of the sensor (kinesthetic feedback). Properly designing and integrating these components allows natural palpation motions while producing realistic tactile sensations.

1.3 Complexities of Medical Palpation

Palpation is a difficult problem to study because it involves many complex components, such as large-deformation contact mechanics, nonlinear biological materials, human tactile perception, and sensory-motor control. These are extensive research areas by themselves and palpation intimately combines them. Successful investigations will require small pieces of the process to be analyzed separately. Then a more complete picture can be built up from these individual studies.

In chapter 6, we will look at palpation in detail, but for now a broad overview of the palpation process is beneficial to understanding how these components interact and provides important clues for surgical instrument designs. A wide variety of palpation techniques are utilized in medical procedures. Tissues are probed using many different hand configurations and motions, and tactile sensations of interest depend on specific task objectives. Despite these differences, the same basic technique is used in all palpation procedures. Figure 1.4 shows a block diagram of the palpation process. The first step is to configure the hand so the fingers can contact the tissue and probe it using specific motions. Often the position of the hands and fingers is determined by what types of motions are necessary and geometric constraints imposed by the location of the organ.

Contact between the fingers and tissue creates tactile sensations on the skin of the fingerpad. These are complex to analyze because large-deformations are induced in the soft tissue and fingerpad flesh. Also, the finger and tissue exhibit nonlinear viscoelastic behavior [Fung 1993, Pawluk 1997]. These tactile stimuli created by contact are sensed by thousands of mechanoreceptors in the skin [Johansson and Valbo 1983]. Neural signals encoding this information are then sent to the brain. Cognitive perception of the

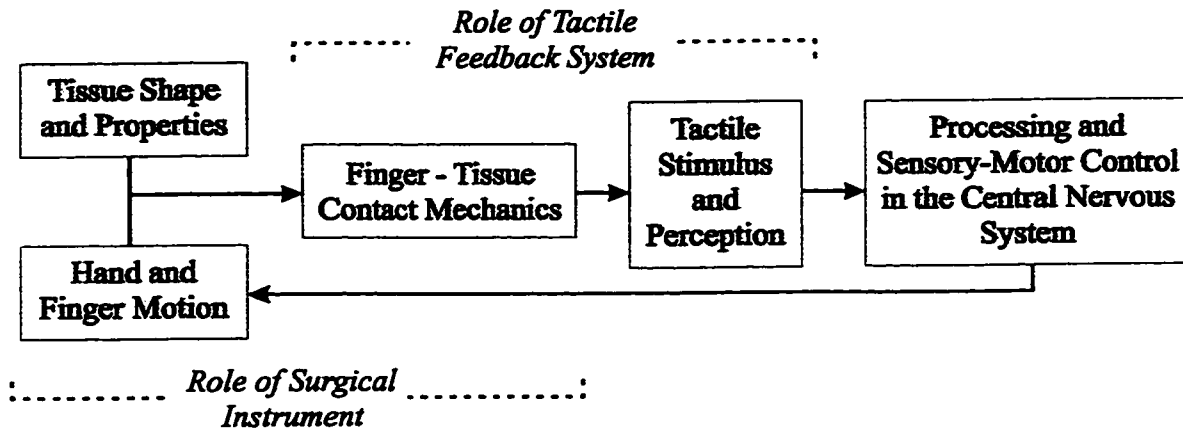


Figure 1.4. *Block Diagram Showing Important Components of Palpation.*

distributed information allows the tactile sensations of interest to be detected. Additionally, this information is used for sensory-motor control of the fingers so large areas can be explored and the orientations of the fingers can be adjusted to maintain a consistent contact with the tissue.

Despite the frequent and important use of palpation in medicine, few studies have investigated tactile perception techniques during contact with soft materials. One study that specifically looked at palpation quantified the main psychophysical parameters for lump detection in breast self-examination [Pennypacker and Iwata 1990], but did not investigate mechanical issues such as finger motions and forces or induced pressures distributions on the fingerpad. Other studies have looked at the relation between tactile stimuli, mechanoreceptor response, and cognitive perception. Many of these, however, generated tactile stimuli by pressing rigid objects against the fingerpad [Philips and Johnson, 1981; Johansson and Valbo 1983; Srinivasan and Lamotte 1987]. There are many fundamental holes in palpation and tactile sensing research. The development of remote palpation technology requires a more focused understanding.

1.4 Remote Palpation Instrument System Design Issues

The development of transparent remote palpation systems is a tremendous challenge because the design space for these devices is enormous. Palpation is a complex process, and constructing hardware to provide a seamless interface between the internal tissue and the surgeon's hands is therefore difficult.

One main reason why the development of tactile feedback systems has been slow is the immense design complexities associated with producing tactile displays. The prototypes developed to date are limited in performance and suffer from poor reliability. Typically, displays consist of a dense array of individually controlled "tactors" used to create a distributed pressure or shape against the fingerpad. The actuators driving each tactor need to produce fairly large displacements with adequate force and be quick enough to keep up with the speed of the operator's motions. Additionally, the display needs to be small and lightweight to avoid restricting finger motion. Meeting all of these design requirements is often impossible and simplifications and tradeoffs are necessary.

It is best to base important design decisions on a detailed scientific understanding of the palpation process. This approach would incorporate the most important aspects of tactile sensations and finger motions into the instrument design. Unfortunately, performance requirements for these devices has not been explored and many important and fundamental questions concerning the development of remote palpation instruments need to be answered.

1.5 Research Approach and Target Application

The goal of this thesis is to illuminate the design space for remote palpation instruments. In this context, design space refers to all possible hardware solutions that fulfill the task requirements and specifications necessary for them to adequately function. A three pronged approach was chosen to accomplish this objective. First, palpation is studied in detail through scientific observation, experimentation, and measurement. This allows important aspects of palpation to be understood, such as what tactile sensations surgeons are using and why particular finger motions are chosen. The second part of the approach involves determining important design specifications for palpation instruments from these observations. This will indicate what to build and how well it must perform. Finally, prototypes of the tactile feedback system and instrument are developed based on the determined design specifications. Building and testing simple prototypes can teach important lessons that are difficult to learn any other way and are essential for experiments carried out in the first and second parts of this research approach.

Because the design space for remote palpation instruments is large, this thesis can realistically explore only a small portion of this space. This is appropriate given the lack of study in the areas of palpation, the human sense of touch, minimally invasive surgical tools, and tactile feedback system. One way to limit the scope is to pick a target application and focus on a specific type of palpation.

A promising application of remote palpation instruments is localizing hard inclusions in the lung during minimally invasive thoracic surgery. This is an important part of a commonly performed procedure where cancerous nodules are surgically removed by sectioning off the small peripheral portion of the lung that contains the lump. The

location of the nodules is determined using preoperative imaging, such as x-ray, CT scan, or MRI. During the operation, however, the lung is partially deflated to make room in the chest cavity, and the spatial relationships present in the image data are no longer valid. This requires the lumps to be located during the operation. When palpation is possible, as is the case in open-incision surgery, the nodules are trivial to locate. As the fingers probe the lung, the sensation of the lump is obvious due to its large stiffness compared to the partially deflated lung tissue. During minimally invasive surgery, this task becomes difficult and time consuming. Localization is typically accomplished by using a long slender probe (approximately 5 mm in diameter) held in the surgeon's hand outside the rib cage to scan the surface of the lung. When the probe passes over the hard lump, a small amount of force information is felt. This process can take 15 to 30 minutes. Some nodules can be visually detected because of puckering of the lung surface, but most require localization through other methods. This has been identified as a major problem of video-assisted lung resection procedures [Mack et al. 1993].

A few preoperative localization techniques have been proposed to mark the location before the lung is deflated. These involve marking the nodule percutaneously through the chest wall with dyes and hook wires using computerized tomographic guidance. These techniques have been shown to be effective [Plunket et al. 1992], but require complex hardware and sometimes fail. Intraoperative techniques involve ultrasound probes and blunt grasping instruments or cylindrical rods to probe the tissue. Searching with an instrument is much simpler, but less precise because the tools provide little force feedback to the surgeon. Often, this technique is inconclusive and surgeons insert their index finger through one of the entry incisions to digitally palpate the lung directly. The

fact that surgeons go out of their way to use their fingers is a good indication that remote palpation instruments could be a benefit to these procedures.

For a number of reasons, locating nodules in the lung is a good initial target application for remote palpation instruments. The localization task does not require high fidelity tactile signals for completion. The tactile feedback system needs to provide enough information such that the surgeon can confidently determine the presence or absence of a lump. The instrument design is also simplified because the palpation technique uses a single finger and manipulation of the tissue is not necessary. The design space for this simplified instrument is much more tractable to explore. Studying single finger palpation is much easier than dealing with all the fingers at once, making analytic observation and experimentation straightforward.

This thesis therefore focuses on the design issues for remote palpation instruments used to localize hard lumps in soft materials. The prototypes and investigations of palpation are geared to the development of these types of instruments.

1.6 Thesis Overview

The organization of this thesis follows the approach described above. Studies provide insight into palpation technique and human tactile sensing, and help determine important specifications for remote palpation instrument designs. Prototypes are then developed and tested based on these findings. This process is followed for each of the main components in a remote palpation instrument: the tactile sensor, the tactile display, and the surgical instrument. The chapters are paired based on the hardware. The first chapter of the pair presents an experiment, measurement, or observation of surgical palpation.

The second chapter of the pair describes the prototype hardware developed for the remote palpation instrument. All of these studies and prototypes were geared toward the target application of localizing lumps in soft materials using single finger palpation.

The first pair of chapters deals with the design of the tactile sensor and signal processing. The design of the sensor hinges on an understanding of tactile sensations created when the finger or sensor scans over the top of a lump. Important design questions to answer include: What parameters should the sensor measure? and What sensitivity is necessary to match human ability? Chapter 2 describes an experiment that determined human sensing limits for lump detection using passive palpation. Total indentation forces were determined for a subject to just detect an embedded lump. Finger shape and pressure distribution on the finger were measured the threshold detection force. Chapter 3 describes the prototype tactile array sensor. It measures distributed pressure. Also described in this chapter are a real time signal processing technique to enhance the sensation of the lump and a more sophisticated processing algorithm to simulate soft tissues.

The second pair of chapters focuses on the design of the tactile display. This is used to recreate the tactile sensations on the surgeon's finger. From previous research on tactile displays, temporal bandwidth has been shown to be an important design specification. A quick display is necessary for the tactile sensations to synchronize with the motions of the surgeon's finger. Chapter 4 describes a human factors experiment where finger speed during a lump localization task was measured. This provides insight to the kinds of motions utilized while finding a lump and the necessary temporal bandwidth for the tactile display. Chapter 5 describes the high-speed tactile shape

display prototype we developed, consisting of line of individually controlled pins. Also discussed in this chapter is a virtual lump localization experiment using the prototype display, which quantified the tradeoffs between display speed and performance.

The third pair of chapters deals with surgical instrument design. The instrument carries the tactile feedback system and couples the motions of the surgeon's finger to the motions of the sensor. It is important for the instrument to synchronize with natural motions of surgeon and avoid ergonomic problems. This requires understanding how the hands are used in palpation. Chapter 6 describes a taxonomy showing different hand configurations and finger motions used during palpation. Based on these findings, chapter 7 presents the design of two prototypes: a finger-based motion design and an arm-based motion design. This chapter also presents an experiment using the prototype remote palpation instrument to localize lumps in rubber models in a minimally invasive setting.

Finally, chapter 8 discusses the conclusions of this research and the future work necessary to further the design of remote palpation instruments and other surgical tactile feedback systems. An advanced signal processing algorithm is discussed that allows the surgeon to feel a virtual model of the tissue through haptic feedback devices. The model is developed during the palpation task from tactile information collected by the contact sensors inside the patient's body.

Chapter 2. Human Sensing Limits for Lump Detection

The mechanical interaction between the surgeon's fingers and tissue is one of the most important parts of the palpation process. The tactile sensations induced by this contact provide the necessary information for completing the task. Understanding this interaction is therefore crucial to developing a complete picture of palpation. This analysis is difficult because the mechanics involve large deformations of two compliant objects, nonlinear rate-dependent material behavior, and surface interactions at the contact interface. The motion of fingers relative to the tissue further complicates this process.

This chapter describes an experiment where key aspects of the mechanical stimulus to the fingers (distributed pressure and shape) were measured during a simplified lump detection task. This information will provide important design specification for the development of remote palpation instruments. It is important to match the tactile feedback system's sensitivity to the human sense of touch. This requires an understanding of what humans are detecting when they just begin to feel the sensation of a lump.

2.1 Motivation for Lump Detection Experiment

There has been some work to understand the relationship between mechanical stimulus to the finger, neural signals, and perception. Many of these studies, however, have looked at rigid surfaces in contact with the fingerpad [Phillips and Johnson, 1981;

Johansson and Vallbo, 1983; Srinivasan and Lamotte, 1987]. In palpation, the finger is often in contact with surfaces of similar or greater compliance. This changes the stimulus to the finger as both the finger and tissue deform. One study involving soft materials investigated the ability to determine material stiffness through touch, but the stimulus to the finger was not analyzed [Srinivasan and Lamotte, 1995]. Pennypacker and Iwata [1990] have conducted experiments to quantify the ability to locate lumps in soft rubber models. This study examined perceptual abilities, but did not investigate the mechanics of detection during palpation.

The goal of this study is to determine the relationship between physical stimulus and detection of a hard ball embedded in a soft rubber material. We vary important parameters in the experiment (ball size and indentation speed) while measuring the mechanical stimulus to the finger (skin deformation and pressure distribution). The study consists of three parts. The first is a psychophysics experiment to determine the minimum indentation force needed for subjects to just detect the presence of the balls in the rubber models. The next step involves measuring the shape of the subject's finger at the threshold force by photographing the finger through the side of the rubber model. Finally, the pressure distribution on the finger due to the contact with the model is measured using a localized pressure sensing technique. These three parts provide a detailed description of the mechanical stimulus to the finger when the ball is just noticeable.

2.2 Experimental Methods

Studying palpation in a medical setting is difficult due to the complexity of the stimulus and interaction. To simplify our experiment, we designed models for subjects to palpate that simulated biological tissues and used a mechanical device to press the models against the subject's finger. The models were made of a clear, soft silicone rubber (General Electric Co., GE6166, Young's Modulus $\cong 2.5$ kPa). Hard plastic balls were embedded in the rubber to stimulate tumors (Figure 2.1). Four models were produced with ball diameters of 6.4, 12.7, 19.1 and 25.4 mm. An additional model contained no ball. The models were constructed in boxes (100 x 100 mm base and 50 mm height) with glass sides. The distance between the top of the rubber surface and the top of the ball was 12.7 mm in all cases. As the subject's finger indented into the model, the ball

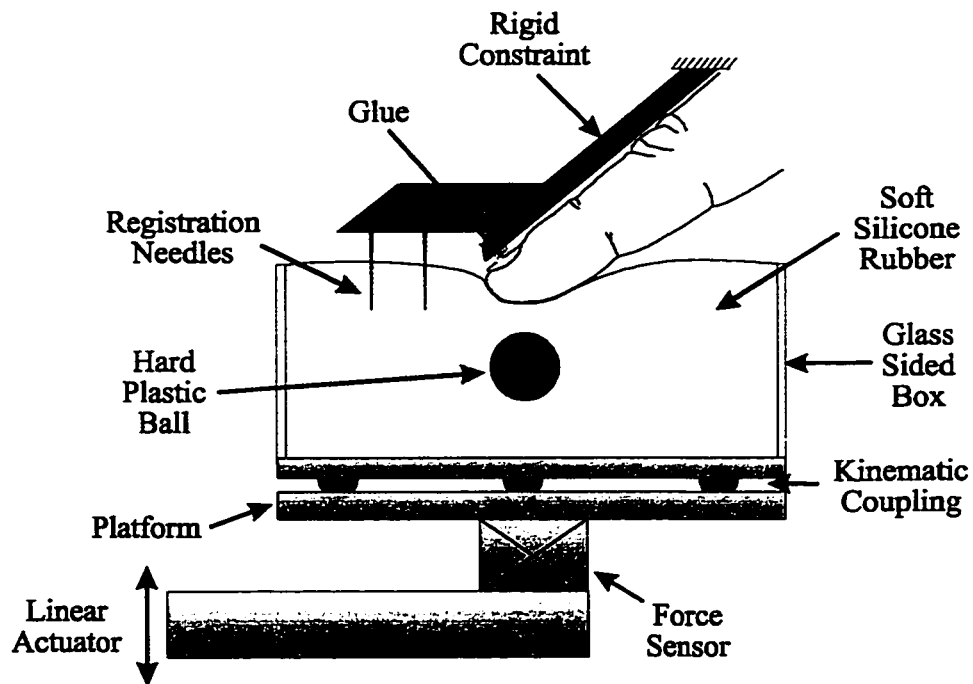


Figure 2.1. *Apparatus for Detection Experiment.* The linear actuator raises the rubber model against the subject's fixed finger to a specific contact force. The shape of the finger and location of the ball is visible through the side of the model.

and finger were visible through the sides of the model. A thin layer of oil was used to lubricate the rubber surface and minimize the friction between the subject's finger and model.

Subjects touched the models with the index finger of their right hand. Voluntary movements of the finger were precluded by gluing the fingernail and securing the forearm to a rigid support fixed to the table. The index finger was held at approximately 45 degrees by the constraint. Needles for image registration were also attached to the constraint.

A linear actuator raised the models against the finger. Although this is a deviation from typical palpation motions, a passive experiment allows accurate control over important parameters such as indentation speed and contact location. The mechanism consisted of a translation stage with 30 cm of travel that moved a cantilevered beam and platform that held the model. A force sensor under the platform measured indentation force (RMS noise 0.005 N, range 10 N) and an optical encoder (resolution 0.013 mm) measured displacement. The motion of the model was position controlled using a PD controller. The RMS position tracking error was less than 0.2 mm, and the force plateaus were accurate to within 3% with a repeatability of 0.02 N RMS. A kinematic coupling between the platform and model ensured that the location of the model (and thus the ball) was consistent from trial to trial relative to the subject's fixed finger. The balls in the models were aligned directly under the lowest point of the finger.

A psychophysics experiment used the method of limits to determine the minimum force required for subjects to just detect the presence of the ball in the rubber. This involved raising the models at a constant velocity against the finger to a specific force,

maintaining that force level for one second, retracting the model away from the finger, and then asking the subject if they could feel the ball in the rubber during this process. By varying the force “plateau” levels, the detection force could be determined. In this protocol the detection force is the average of two different types of trials. The first starts with the force plateaus at a level well below the detection point. The force plateau level is slowly increased in repeated indentations. As the force level crosses the detection point, the subject indicates they felt the ball. In the second type of trial, the force plateaus start well above the detection point and are slowly lowered. In this case the subjects indicate when they can no longer feel the ball in the rubber.

There are a large number of parameters that can be varied in this experiment. Through pilot studies, we found a significant variation in detection force due to changes in ball size and indentation speed. Additional parameters of interest we did not investigate include ball depth, stiffness, and shape; rubber stiffness; and inhomogeneous rubber models (e.g. models with a thin, stiffer skin). Our experiment consisted of seven cases: four with a fixed indentation speed of 20 mm/s with ball diameters of 6.4, 12.7, 19.1, and 25.4 mm, and three additional cases with the 19.1 mm ball at indentation speeds of 5, 10 and 40 mm/s. This provided four data points with variation in ball size and four with variation in indentation speed. Each subject completed 16 trials for each case: 8 with increasing forces and 8 with decreasing forces. The trials were broken into sets of 14 with rests between sets. All the cases in one set were of the same type (increasing or decreasing force). The order of presentation of ball size and indentation velocity in a set, as well as order of set type, was randomized. Periodically the model without a ball was presented to ensure the subjects were actually sensing the ball. Subjects never incorrectly

detected a ball when it was absent. The data was taken over two days. A total of five unpaid subjects participated (mean age 22 years, 4 male and 1 female).

Once detection levels for each combination of ball size and indentation speed were determined, the shape of the finger at the detection force for each case was measured using photographs taken through the side of the rubber models. The camera was fixed to the apparatus and had a field of view of 40 x 60 mm. A flash lamp located on the opposite side of the model back lit the finger and ball. This created an image with high contrast allowing the profile of the finger and ball to be easily extracted. The flash was electronically synchronized to fire at the beginning of the force plateau. Photographs were taken of the finger indenting into models with and without a ball at the detection forces measured for each case. By registering these images, a comparison between the shape of the finger with and without the ball at the same force was determined. Thus, the shape change of the finger induced by the presence of the ball could then be measured. This technique only works if the finger remains convex. No concavity was observed for any of the subjects at threshold.

The photographs of the finger were digitally scanned, with a resulting image pixel size of approximately 13 μm . A contour detection algorithm located the edge of the finger and ball. The edges were spatially filtered using a fourth-order low-pass filter with a cutoff frequency of 1.6 cycles/mm in each direction to remove high frequency noise. Using the outline of the needles penetrating into the rubber, the finger edges from all the images were aligned and registered. Fifth order polynomials were then fit to the finger shapes. The relative deformation induced by the ball could then be determined by subtracting the shape of the finger measured when the ball was present from the finger

shape when the ball was absent. Due to the complexity of the signal processing, only one set of finger pictures was analyzed for each case. To estimate the repeatability of the measurement, relative deformation curves were measured for one case seven times from seven independent indentations into the model with the ball, and seven indentations into the model without a ball. The RMS error between the seven relative deformation curves was less than 0.025 mm across the entire finger length.

The final step of the experiment was to measure the approximate pressure distribution on the fingerpad at the detection force levels for each of the seven cases. An apparatus was constructed to measure the local contact pressure at any point on the finger. Wax replicas of a subject's index finger were made from a plaster of paris mold. A tube running the length of the wax finger was inserted into the mold during the construction process. To measure the pressure at a specific point on the finger, a 0.75 mm hole was drilled normal to the local surface through the wax finger into the central tube, which connected to a compressed air supply. After the wax finger was indented into the rubber to the appropriate detection force level (using the same apparatus described above), the air pressure was slowly increased. When the air pressure inside the hole in the finger equaled the contact pressure at the surface of the rubber around the hole, air would escape. Using an electronic pressure sensor (RMS noise 0.01 kPa; range 20 kPa), the transient in the pressure created by the air escaping around the finger determined the contact pressure at the location of the hole. By drilling holes in different locations on the wax finger, the pressure distribution along the midline of the finger was measured. Standard deviations of repeated measurements at the same hole location and indentation force were less than 0.07 kPa.

The wax replicas used to take the pressure measurements have a much greater stiffness than the human finger. Therefore, the shape change of the subject's fingerpad induced by the ball will not be present in these replicas during indentation. It is possible that these small deformations significantly change the pressure distributions. This would cause the measurements taken with the wax finger to be incorrect. To quantify this effect, pressures on the finger directly above the ball were measured using replicas with slightly different shapes. By removing wax with sandpaper, shape changes were produced similar to actual deformations measured on the subject's finger. The amount of wax removed at the location of the hole was measured using a jig to insure consistency. Using a 1.0 N indentation force, a deformation of 0.262 mm produced a 2.44 percent change in pressure from measurements taken with the undeformed finger shape. When 0.423 mm of wax was removed, the change increased to 3.46 percent. A higher indentation force level of 1.4 N was also tested and resulted in 3.85 percent and 6.62 percent changes using the same modified wax replicas. Results show the pressure does change, but not enough to cause the results of the measurements to be invalid.

2.3 Results

Figure 2.2 shows the detection forces required for each of the five subjects for variations in ball size (2a) and indentation velocity (2b). The same trends were observed for all subjects: detection required more force as the ball size decreased or the curvature increased. We found an approximately linear relation between detection force and curvature of the ball. Least squared error fits to lines are listed in Table 2.1. We also found a linear relation between the log of the indentation speed and the required force for detection: the slower the indentation, the higher the detection force. Table 2.2 lists linear fits for this data. Using t tests, we found most of the variations in detection forces were significant ($p < 0.05$). The only cases where significant variations were not obtained occurred between the 19.1 and 25.4 mm ball size detection forces.

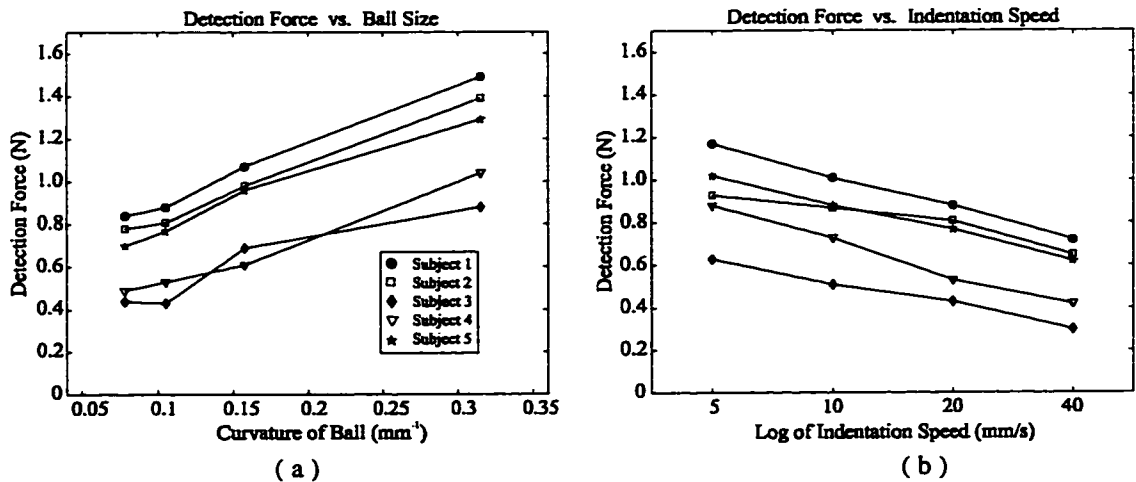


Figure 2.2. *Indentation Force Required for Detection.* Indentation force required by all subjects for variations in (a) ball size and (b) indentation speed.

Subject	Slope (N/mm ⁻¹)	Offset (N)	r ²
1	2.806	0.610	0.996
2	2.649	0.555	0.996
3	1.946	0.291	0.905
4	2.378	0.277	0.987
5	2.478	0.524	0.986
Mean	2.451	0.451	---

Table 2.1. *Linear fit relating detection force and ball curvature.*

Subject	Slope (N/log ₁₀ (mm/s))	Offset (N)	r ²
1	-0.492	1.511	0.998
2	-0.299	1.159	0.931
3	-0.355	0.876	0.993
4	-0.525	1.244	0.989
5	-0.435	1.323	0.997
Mean	-0.421	1.223	---

Table 2.2. *Linear fit relating detection force and log₁₀ of indentation speed.*

The deformations induced on the fingerpad by the ball were measured for all cases. Figure 2.3a shows a photograph of a typical subject at the detection force for the 19.1 mm ball using a 5 mm/s indentation speed. Figure 2.3b shows the same subject at the same indentation force contacting the model without a ball. The extracted and registered profile shapes of the finger, ball, and needles in these photos are shown in Figure 2.3c. The relative deformation of the finger induced by the ball was found by subtracting the finger shapes shown. Figure 2.4 shows the relative deformation curves measured for the same subject for the different ball sizes (2.4a) and indentation speeds (2.4b). The shape of the relative deformation curves was approximately the same for all cases. This shape could be described many ways (e.g. curvature).

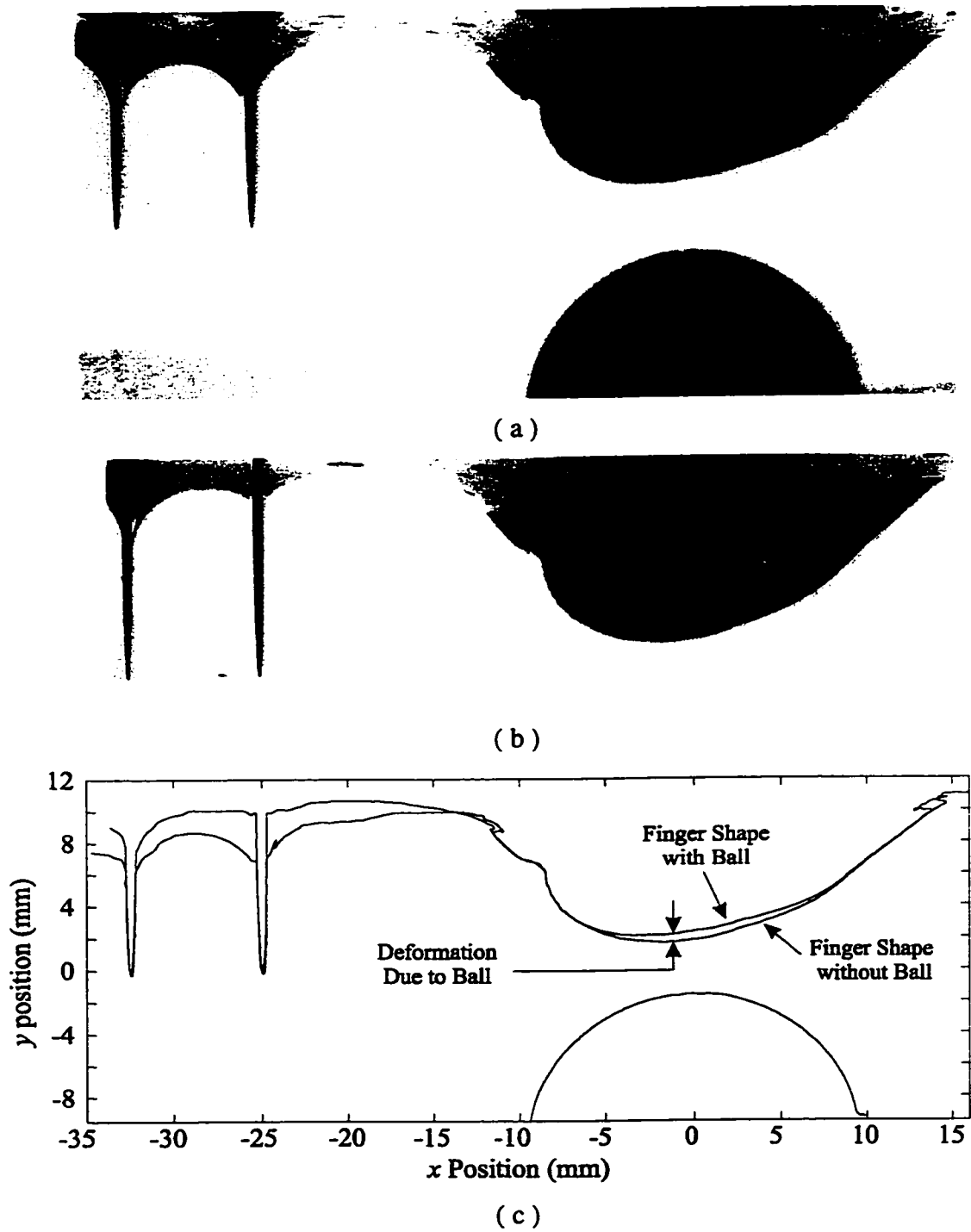


Figure 2.3. *Measurement of Finger Shape at Detection.* (a) Subject 4 at threshold force for the model with 19.1 mm ball, (b) same indentation force for model without a ball, (c) extracted and registered edges from images. Relative deformation of the finger caused by the ball is determined by subtracting the two finger shapes.

We chose to use maximum deformation because it was most straightforward to measure. Figure 2.5 shows the maximum deformation induced by the ball versus ball size (2.5a) and indentation speed (2.5b) for all subjects. As with the detection force, all subjects showed the same trends. The maximum deformations induced by the ball were relatively constant for the different ball sizes, but they significantly increased as the indentation speed decreased. Lines where least square fit to the data for the relation between maximum deformation and ball curvature (Table 2.3) and indentation velocity (Table 2.4).

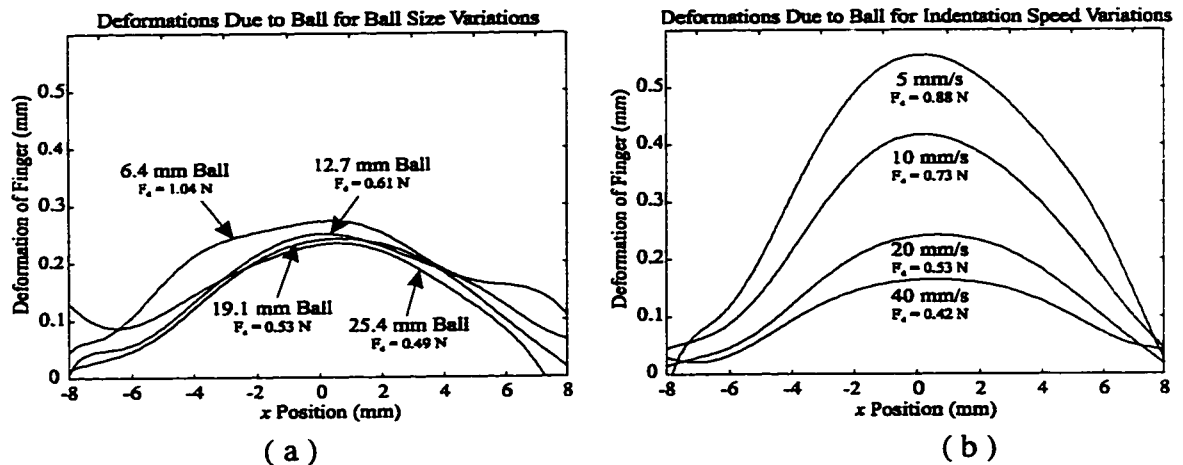


Figure 2.4. Deformation of Finger Caused by Ball. Relative deformations at threshold from Subject 4 for variation in (a) ball size and (b) indentation speed.

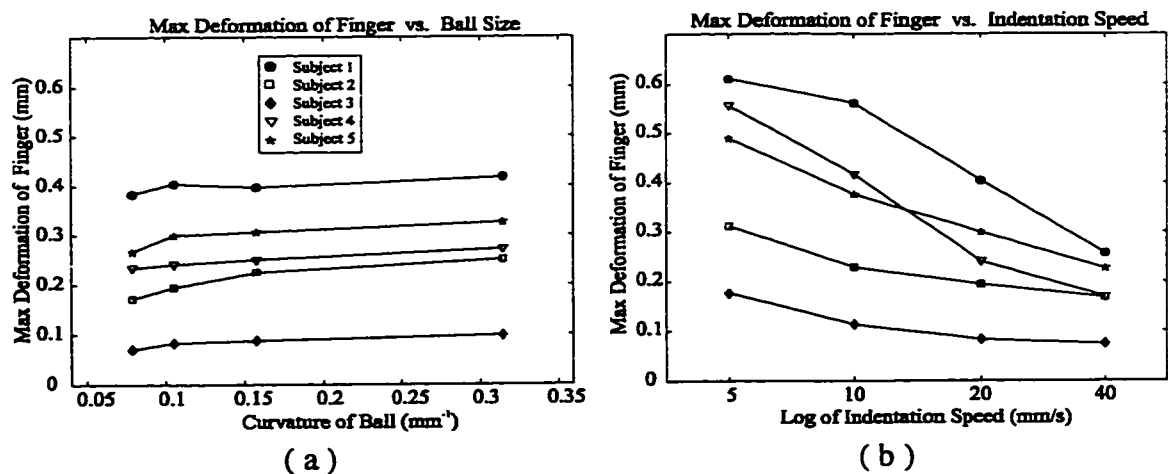


Figure 2.5. Maximum Relative Deformation of Finger Caused by Ball. Maximum deformations at threshold for all subjects for variation in (a) ball size and (b) indentation speed.

Subject	Slope (mm/mm ⁻¹)	Offset (N)	r ²
1	0.118	0.381	0.873
2	0.309	0.160	0.895
3	0.100	0.068	0.823
4	0.158	0.223	0.982
5	0.204	0.266	0.814
Mean	0.177	0.220	---

Table 2.3. *Linear fit relating maximum finger deformation and ball curvature.*

Subject	Slope (mm/log ₁₀ (mm/s))	Offset (N)	r ²
1	-0.404	0.923	0.960
2	-0.155	0.404	0.925
3	-0.112	0.240	0.877
4	-0.445	0.858	0.977
5	-0.288	0.679	0.987
Mean	-0.281	0.621	---

Table 2.4. *Linear fit relating maximum finger deformation and log₁₀ of indentation speed.*

The local pressure measurements taken with the wax finger indenter show the distributed pressure on the finger when contacting the models with a ball is different from the pressure distribution created when contacting the model without a ball. Figure 2.6a and 2.6b shows the pressure distribution along the centerline of the finger for the 6.4 and 25.4 mm ball cases, respectively. The solid squares show the measurements taken using the model with the ball and the open circles show the pressures measured using the model without a ball. Figure 2.6c shows the locations of the pressure measurements on the finger. Because the same indentation forces were used when taking measurements using the models with and without a ball, the integral of the pressures is the same. The

difference in the pressure distributions caused by the ball was calculated by subtracting the two curves. Figure 2.6d shows the measured pressure difference for each of the two ball sizes. The 6.4 mm ball causes a high, narrow pressure concentration above the ball, while the 25.4 mm ball causes a lower, wider pressure concentration.

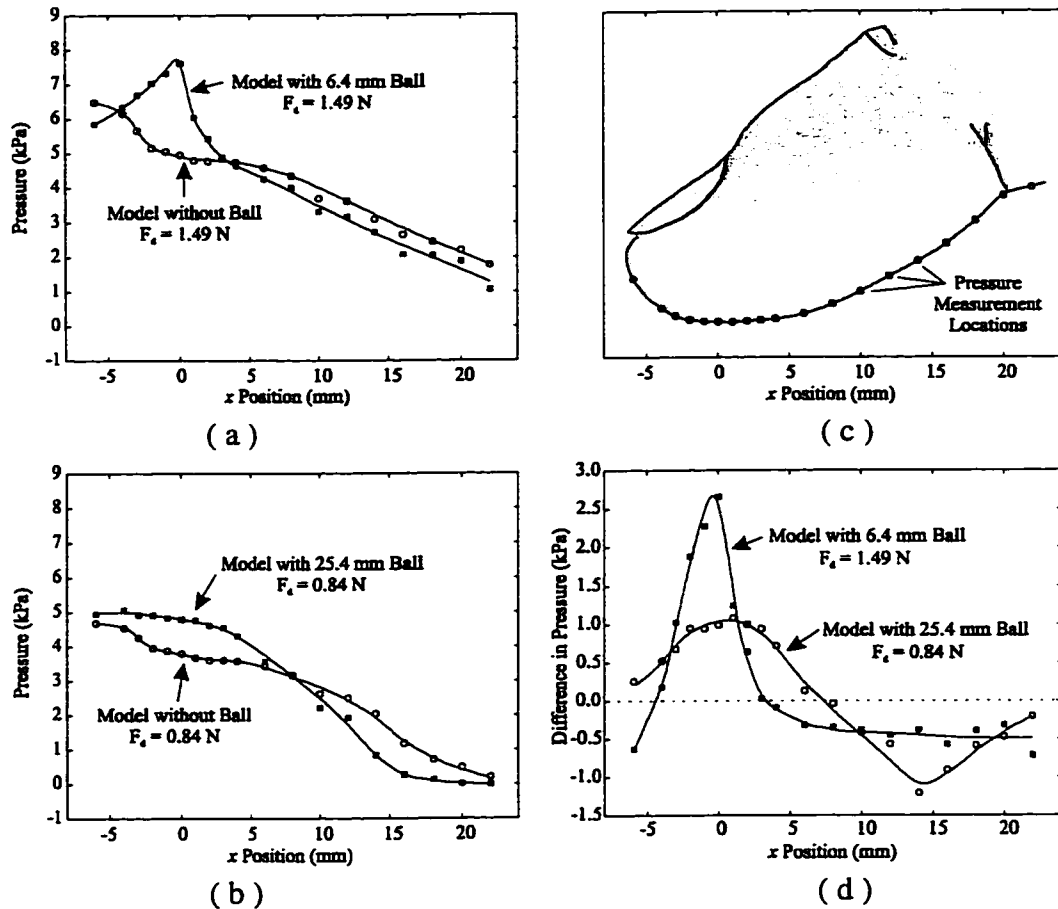


Figure 2.6. Pressure Distribution on Finger at Detection. The solid squares indicated local pressure measurements taken using models with (a) 6.4 mm ball and (b) 25.4 mm ball, and the open circles show pressures using the model without a ball at the same respective detection force levels. (c) The small circles show the locations of the pressure measurements on the wax finger. (d) The difference in the pressure distribution caused by the presence of the ball. The solid squares shows pressure differences due to 6.4 mm ball, and open circles show pressure differences due to 25.4 mm ball.

A similar trend was observed for the other ball sizes and indentation speeds. Figure 2.7 shows the pressures measured on the finger directly above the ball for each of the ball sizes (2.7a) and indentation speeds (2.7b) using the appropriate detection forces contacting models with and without a ball. As with the cases shown in Figure 2.6, the pressures above the ball are higher when the ball is present in the model. As ball size and indentation speed decreased, the pressure concentration caused by the ball increases in magnitude. From indentation tests, it was determined that the viscous properties of the rubber are minimal. This means the change in pressure for the variation in indentation velocity is primarily due to the change in indentation force. Since the integral of the pressure distributions must be the same for the case with and without a ball, the width of the pressure concentration narrows as the magnitude of the difference increases.

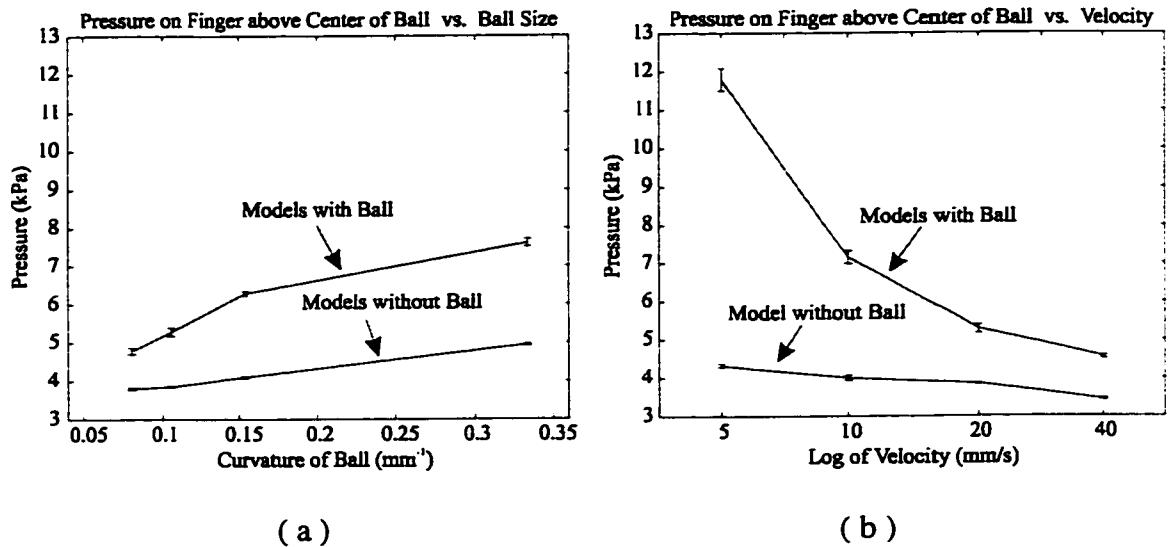


Figure 2.7. Pressure on Finger above Center of Ball. Pressure measurements for variation in (a) ball size and (b) indentation speed. Error bars show standard deviation of five trials for each case.

2.4 Discussion

The primary purpose of this experiment was to determine what physical parameters humans are sensing when they just begin to detect the presence of a hard lump in a soft material. This cannot be answered with absolute certainty, but a good hypothesis can be presented. Our results show the deformation of the fingerpad induced by the presence of the ball was nearly constant for the different ball sizes when the indentation speed was held fixed. This was true even though the indentation forces and pressure distributions were different. This suggests that subjects could detect the ball when the relative deformation of their finger crossed a certain threshold.

Another detection mechanism that explains these results is sensing skin curvature. Subjects could detect a change in the curvature of the skin from the “baseline” level of the finger contacting homogeneous rubber. The shape of the finger (and thus curvature) did not significantly change as indentation force increased when touching the model without a ball. Because the relative deformation of the finger from this state was similar for the different ball sizes, the shape and curvature of the finger was also similar for these cases. Thus, the ball is detected when the change in skin curvature reaches a threshold level. Neurophysiological work has shown a strong relation between changes in skin curvature and mechanoreceptor response [Phillips and Johnson 1981; LaMotte and Srinivasan 1987]. Goodwin and Wheat [1991] performed a psychophysics experiment to measure the ability to discriminate changes in curvature of rigid indentors pressed against the fingerpad. Although the mechanical stimulus to the finger when contacting soft

materials is significantly different, we observed detectable curvature changes of a similar magnitude ($\cong 0.03 \text{ mm}^{-1}$).

One apparent contradiction in the results is that the relative shape change of the finger induced by the ball is similar for the various ball sizes (Figure 2.5a) even though the differential pressure distributions are quite different (Figure 2.6d). To check if this is a reasonable finding, a solid mechanics contact model can be used to predict this relation. The complete interaction between the finger and rubber is too complex for a simple model. Superposition, however, can be used to approximate the problem as the sum of two parts that can be modeled. This technique requires the big assumption that the problem is linear. The first part of the interaction is the finger contacting the homogeneous rubber. This produces the baseline pressure and shape. This contact problem can be well approximated by assuming the rubber is an infinite half-space. The second part of interaction is the changes to this baseline resulting from the presence of the ball in the rubber. This relates the differential pressure (Figure 2.6d) to the relative shape change (Figure 2.5a). Both of these signals were determined by subtracting the baseline from the contact with the homogeneous rubber. This part of the interaction can be modeled using Hertz contact theory.

Hertz contact occurs when two deformable bodies of revolution are pressed together. The shapes of the objects are approximated as parabolas, and the derivation assumes the deformations and contact area are small compared to the size of the object. The theory determines the distributed pressure at the contact area such that the bulk displacements and relative deformations in each body (governed by the equations of elasticity) produce the same local shape in the contact region. The material properties of the objects can be

different, but are assumed to be homogeneous. The general form of the pressure in the contact region that solves this problem is given by

$$p(r) = p_0 \sqrt{1 - \frac{r^2}{a^2}} \quad \text{for } r \leq a \quad (2-1)$$

where r is the radial distance from the center of the contact circle, p_0 is the peak pressure of the distribution, and a is the radius of the circle of distributed pressure [Johnson 1985]. The measured differential pressures caused by presence the ball (Figure 2.6d) are approximately parabolic. Therefore by fitting Hertzian pressure distributions to these curves an estimate on the resulting relative deformation of the finger induced by the ball (as is shown in Figure 2.5a) can be determined. From the Hertz model, the resulting change in shape of a body due to the pressure distribution described above is given by

$$u_z(r) = \frac{1 - \nu^2}{E} \frac{p_0 \pi}{4a} (2a^2 - r^2) \quad \text{for } r \leq a \quad (2-2)$$

where $u_z(r)$ is the deformation of the sphere, and E and ν are the Young's modulus and Poisson's ratio of the sphere's material. The resulting maximum relative deformation (as reported in Figure 2.5) occurs at $r = 0$ and is given by

$$u_z(0) = \frac{1 - \nu^2}{E} \frac{p_0 a \pi}{2} \quad (2-3)$$

Table 5 lists parameters for Hertzian pressure distributions that were least squares fit to the 6.4 and 25.4 mm differential pressure distributions. The fits are reasonable with r^2 values near 0.9 in both cases. Using these values and setting the material properties of the finger to $E = 16 \text{ kPa}$ and $\nu = 0.5$, the resulting maximum deformations predicted by the model for the 6.4 and 25.4 mm ball sizes are very similar, which agrees with our

measured finger deformations. There are other effects about the actual solid mechanics of the finger that are not taken into account by the Hertz model, but these results provide a first order explanation of the findings.

Ball Size (mm)	p_o (kPa)	a (mm)	r^2	Max Deformation $U_z(0)$ (mm)
6.4	2.257	2.696	0.913	0.448
25.4	0.972	6.105	0.890	0.437

Table 2.5. *Least squares fit of pressure difference peaks to Hertz pressure distribution and resulting prediction of maximum relative deformation of finger.*

An interesting finding of this experiment is that the relative deformation of the finger needed to detect the ball remained nearly constant even though the overall contact force and baseline offset pressure varied significantly. Recent monkey neurographic experiments are consistent with this result [Vega-Bermudez and Johnson, 1998]. These experiments show the firing rate of type I mechanoreceptors in the skin in response to indentation by a raised feature was independent of a baseline force offset applied by a flat surface to the fingerpad. This suggests the neural responses from these mechanoreceptors encode a change in local shape or curvature from an offset level rather than the absolute force or pressure distributions. In our experiment, the pressure distribution induced by the homogeneous rubber acts as an offset force. Subjects detected a change in shape or curvature of the finger with respect to this offset stimulus. Thus, the subjects were able to separate the tactile sensations caused by contacting the homogeneous rubber from the changes induced by the presence of the ball. This idea of superposition was used in the contact model described above.

The changes in detection force due to variations in indentation speed can be attributed to the time-dependent response of the mechanoreceptors. Type I mechanoreceptors in the skin are believed to resolve spatially distributed information. The firing rates of these mechanoreceptors are highly dependent on the temporal frequency of the applied stimulus. Higher temporal frequencies induce higher firing rates [Johansson and Vallbo, 1983]. As the indentation speed in our experiment increased, the frequency content of the stimulus of the ball increased. Subjects became more sensitive to changes as this frequency of stimulation increased. This is evident in the decreasing maximum relative deformation as the indentation speed increased. This also explains results presented in chapter 4 where subjects preferred to quickly move their fingers in small circular motions when searching for a lump using natural palpation motions [Peine, Foucher and Howe, 1998]. Moving in quick circles provides a high frequency, repeated stimulus.

This study is in no way is a complete analysis of the palpation process of lump detection in soft materials. There are many other parameters we did not vary in our experiment. It would be interesting to compare our results to the relative deformations created when these parameters are changed. For example, does the maximum deformation change when the surrounding rubber is made stiffer? The logical next step to advance our understanding of what humans are sensing during palpation involves microneurography studies. This will provide insight to what the mechanoreceptors are sensing and how firing rate changes with input stimulus. It would also be of value to determine detection abilities when using natural, active palpation motions compared to the passive case studied here. When determining the shape and size of the ball through

palpation, shape and curvature changes of the finger may become very important. Further experiments are needed to understand this part of palpation.

2.5 Resulting Design Specifications for Remote Palpation Instruments

Understanding the mechanical interaction between the fingers and tissue is important part of determining design parameters for remote palpation systems. Investigations along these lines are useful to determine what aspects of the mechanical stimulus are important for completing a palpation task. Ideally, tactile feedback would provide realistic sensations such that the surgeon feels as if she or he is touching the tissue directly. This requires, at minimum, matching the system's sensitivity to that of the human sense of touch. Based on the results of this experiment (Figures 2.4), the shape display should control the shape output to a high level of accuracy of at least 0.05 mm. This was the minimum shape change induced by the ball that was detected by the subject with the lowest deformation threshold. From the pressure measurements shown in Figure 2.6d, the pressure sensitivity for the distributed pressure sensor should be at least 1.0 kPa. This was the smallest measured pressure difference induced on the finger at threshold. A system with this resolution would allow all of the subjects in this study to feel the lumps embedded in the rubber models at their detection limits. For more robust detection ability at these threshold levels, the resolution of the display and sensor would need to be less than the values reported here.

Chapter 3. Tactile Sensor and Signal Processing

A key hardware component of remote palpation systems is the tactile sensor. It measures distributed contact information as internal tissues are probed. These signals are critical for completing many palpation tasks. A wide variety of tactile sensations can be sensed at the contact surface, including pressure, shape, vibration, temperature, shear, and slip. Sensors capable of collecting these signals have been produced. The majority measure distributed pressure or local contact shape.

The development of these devices has taken place in many research areas, including robotics and teleoperation. The sensors are typically arranged with the sensing elements in a rectangular array. As objects contact the sensor, the local surface shape or pressure distribution can be determined. Many transducers have been proposed to measure distributed pressure, including piezoresistive inks [Hillis 1992], compliant capacitive sensors [Fearing 1990; Pawluk 1998], and optical sensors [Begej 1988]. Other sensing technologies directly measure distributed contact shape [Brocket 1998]. The important performance specifications for tactile sensors include spatial resolution, temporal response, range, accuracy, linearity, and hysteresis. Howe [1994] provides a review of these devices. Previous work on medical application of tactile array sensors (e.g. [Dario and Bergamasco 1988]) was largely aimed at creating autonomous robotic palpation systems.

One of the first design choices that must be made is determining if the sensor will measure pressure or local shape. For the target application of locating lumps in the lung,

a distributed pressure sensor is a better choice than a shape sensor because of the variable compliance of the lung tissue. Lai Fook [1983] determined the stiffness of the lung is linearly related to the inflation pressure. Because the lung has varying levels of inflation during a surgical procedure, the stiffness can change by an order of magnitude. For a shape sensor to detect hard, embedded structures in soft tissue, it would need to have a similar compliance to the tissue. If the sensor were too hard, it would not deform during contact. Conversely, if the sensor were too soft, the tissue would not deform. In both cases embedded structures would not be sensed. The large variation in tissue stiffness would therefore make a shape sensor challenging to develop.

A distributed pressure sensor, on the other hand, can be constructed on a rigid backing. As the rigid sensor probes the tissue, the pressure concentration induced by a lump provides a distinct signal with a good signal-to-noise ratio, allowing straightforward localization. This is true even at the limits of human detection, as was shown in Chapter 3 with the pressure measurements taken with the wax finger replicas.

This chapter describes the prototype tactile sensor developed for the remote palpation instrument. It measures distributed pressure using capacitive array technology developed for robotic applications. In the target application, for example, nodules in the compliant lung tissue can be found by sensing the stress concentration induced by the hard lump as the sensor scans over it. The sensor's construction and specifications are discussed, as well as a signal processing technique specifically designed for locating lumps. A haptic rendering algorithm is also presented to simulate contact with soft materials using a model based technique.

3.1 Prototype Tactile Array Sensor

The remote palpation instrument prototype developed for this thesis uses a capacitive array tactile sensor located at the instrument tip to measure distributed contact pressures as internal tissues are probed. In general, capacitive array sensors consist of orthogonal layers of conductive strips separated by a compressible dielectric. Applying pressure to the sensor's contact surface forces the conductive strips together, increasing the capacitance at the cross-points between the strips. Each cross-point forms one sensing element. The change in measured capacitance of the element is closely proportional to the local pressure above it [Fearing 1990]. Thus, by measuring the capacitance at each element, the distributed pressure can be determined.

Pawluk et al. [1998] describe the design and performance of a flat, eight-by-eight element capacitive array sensor whose construction is very similar to the one used here. Figure 3.1 shows an exploded view of the sensor construction. Rows of copper strips spaced 2 mm center-to-center are mounted to a rigid back support. Thin strips of silicone rubber separated this layer of copper strips from a second layer running perpendicularly to the first. Air between the layers of copper was used as the dielectric. The array was covered with a 2.0 mm layer of rubber (GE RTV 110 Silicone Rubber Adhesive Sealant) to protect it from mechanical damage. A thin layer of gold foil embedded in the rubber was electrically grounded to shield the sensor. Specialized electronics (based on a design by Fearing, 1990) serially scanned the elements by applying a 200 kHz sine wave to the column of an element and demodulating the output from the corresponding row. All unused rows and columns were grounded to reduce cross talk. The resulting element scan rate was 12.8 kHz.

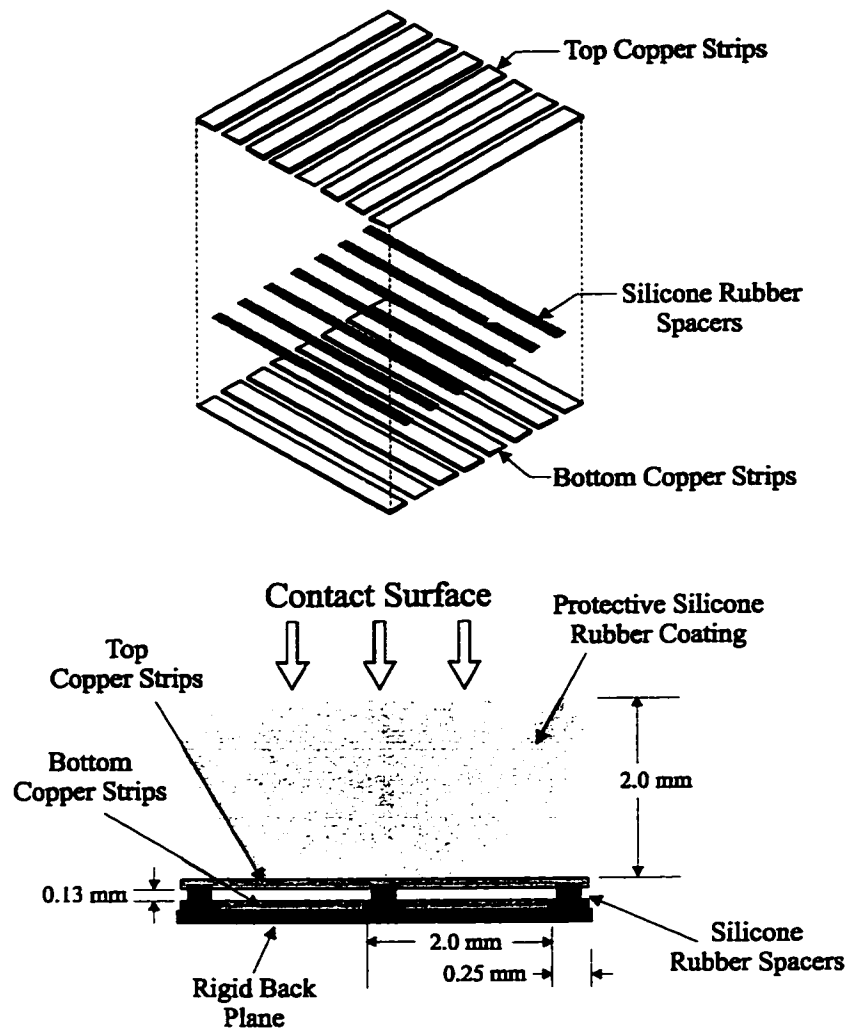


Figure 3.1. *Tactile Array Sensor Construction.* (From Pawluk et al. 1998) Top: exploded view showing the sensor construction. Bottom: side view showing the crossed layers of copper strips separated by silicone rubber spacers. A protective rubber coating is added on the contact surface.

The sensor described above was carefully characterized by Pawluk et al. The noise of the sensing elements was gaussian with a standard deviation of 0.5 kPa. The elements exhibited a linear response with a mean element worst-case squared error (m.s.e.) of 0.4 percent. Hysteresis was below the noise level. The time response for all elements could be described by two time constants, although exact values were difficult to obtain due to sampling rate limitations. The dominant time constant of 2 ms or less accounted for 88

percent of the response. The second time constant was in the range of 300 to 500 ms and accounted for the remaining 12 percent. The spatial resolution of the sensor was limited by coupling between elements and the spatial summation across an element. The proportion of the signal applied to a given element, which is coupled into an adjacent element in the same row and column, was less than 8 percent. Additionally, the linearity of the sensor was confirmed by the invariance of the inter-element coupling with load and successful superposition of two indentations applied to adjacent elements.

One of the benefits of the construction process describe above is the sensor can be formed around a single radius of curvature. This allows cylindrical probes to be wrapped with a sensor. A flat probe would not be acceptable for palpation purposes because the edges would limit the ability to slide along the tissue surface. To demonstrate the sensitivity of these sensors for medical applications, a capacitive array sensor mounted to a 25.4 mm diameter cylinder was pressed against the wrist to sense the pulsation of the radial artery [Peine et al. 1994]. The offset pressure induced by contacting bones and other structures was subtracted from the signal. This allowed the location of the artery to be easily determined from the adjusted signals. Figure 3.2a shows the pressure response from one element located over the artery. Figure 3.2b shows a sequence of pressure images from the 8x8 array.

The tactile sensor used in the prototype remote palpation instrument uses this same construction with a different number of elements on a small cylindrical probe. Figure 3.3 shows a picture of the sensor. A line of ten sensing elements was mounted to a 9 mm diameter aluminum rod, 34 mm in length. Thin strips of silicone rubber separated the bottom layer of ten copper pads from a single copper strip running the length of the

sensor. The first element was 1 mm from the probe tip. Spacing between elements was 2 mm center-to-center. A 2 mm layer of rubber (GE RTV 110 Silicone Rubber Adhesive Sealant) protected the sensing elements from mechanical damage. A 0.02 mm thick layer of metalized mylar covered the rubber layer and electrically isolated the sensor.

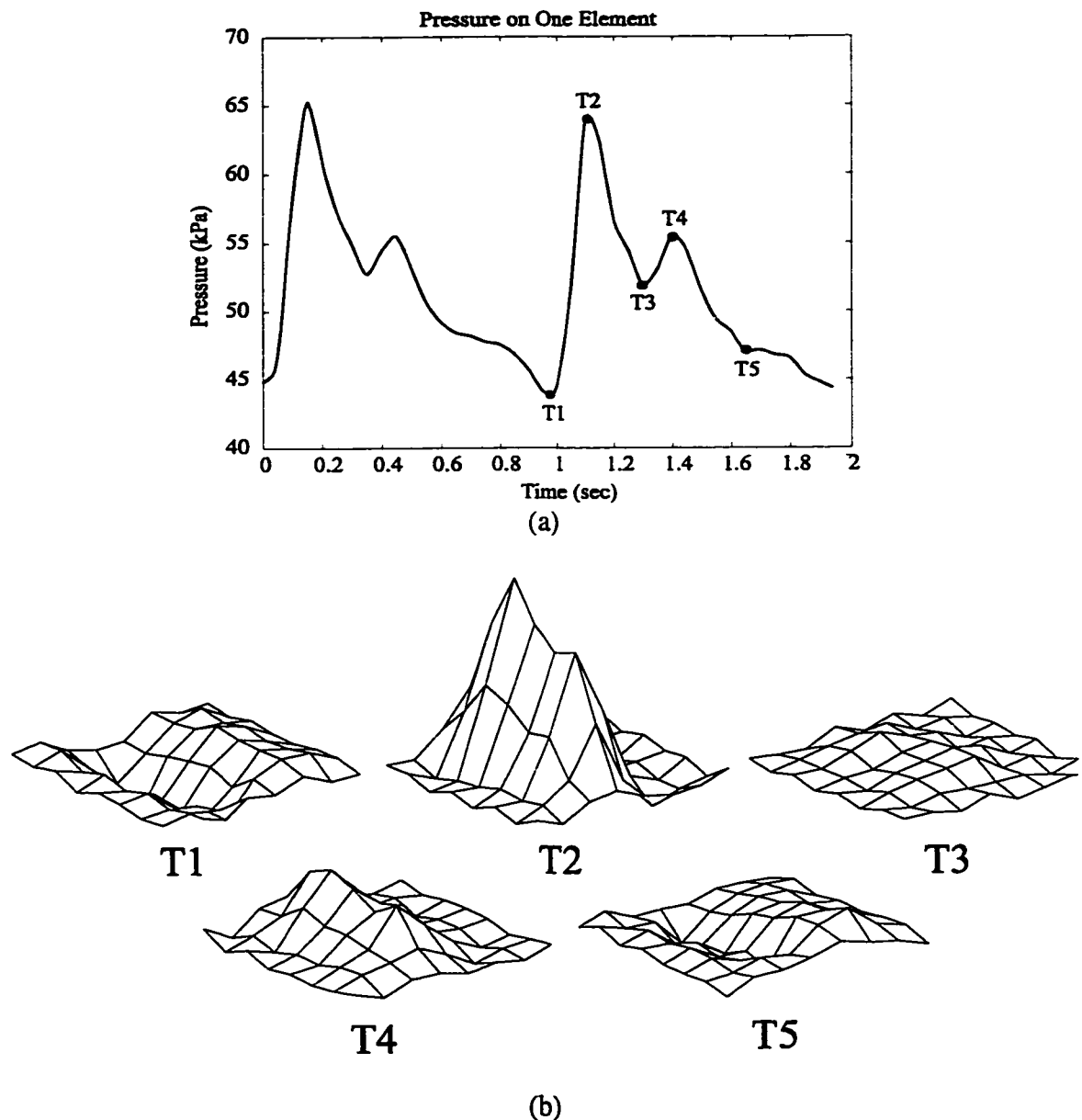


Figure 3.2. *Pressure Signals Measured During an Artery Localization Task.* From Peine et al. 1994. (a) The pressure measured from one element over the artery. (b) Time sequence showing the distribution of pressure measured with the 8x8 sensing array.

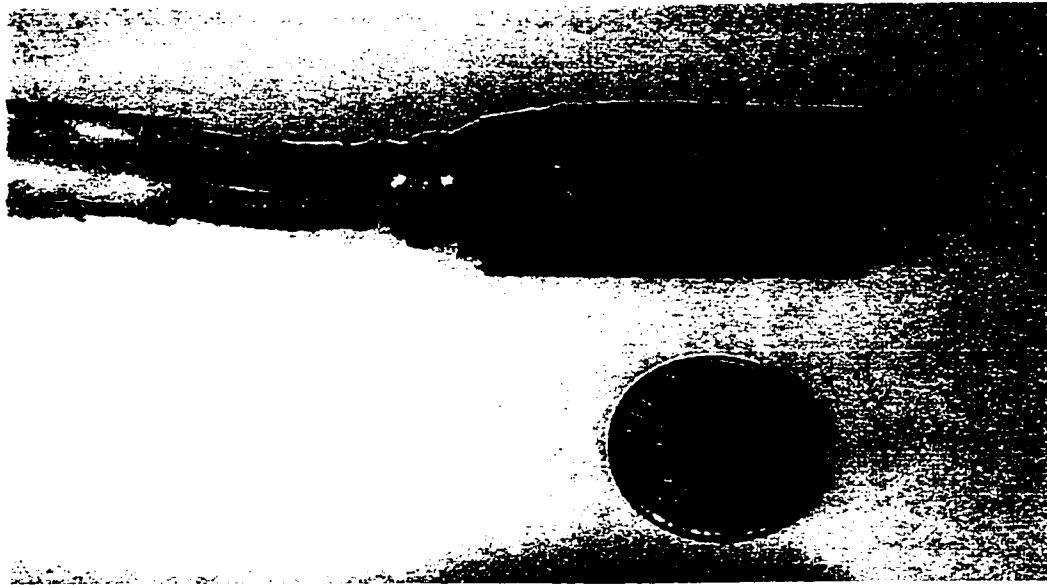


Figure 3.3. *Prototype Tactile Array Sensor Used in Remote Palpation Instrument.* A line of ten sensing elements at 2 mm spacing are placed on a 9 mm diameter rigid probe. A 2 mm thick layer of rubber is added to the surface for mechanical protection. Not shown is a 0.02 mm thick layer of metalized mylar covering the entire sensor for electrical isolation.

Many of the specifications measured by Pawluk et al. are applicable to this prototype sensor. The sensitivity of this sensor was unfortunately lower. The minimum range for the sensing elements was 0-500 kPa and varied between elements depending on the element's initial capacitance. The noise was gaussian with a standard deviation of 2.5 kPa (approximately 1.0 g per element). The sensitivity of this sensor is below the performance specification described in Chapter 2 (1.0 kPa resolution). In order to match the sensitivity of the human tactile system, the performance would need to be improved by a factor of 2.5. Localization of lumps, however, is still possible because normal probing of the tissue occurs well above detection levels. Use of this sensor in lump detection experiments is reported in Chapter 7.

3.2 Signal Processing for Lump Localization

The signal processing determines drive commands for the shape display from the tactile signals collected from the sensor at the instrument tip. Ideally, it would produce sensations the surgeon would feel if contacting the tissue directly. Sensing distributed pressure using a thin, rigid sensor probe complicates this process. Because the shape and stiffness of the sensor is considerably different from the finger, the pressure distributions measured will be significantly different from the pressures generated if the surgeon's finger was contacting the tissue. Achieving a transparent system will require developing a model of the internal tissue from the tactile sensor signals and then computing the sensations the finger would feel if touching this model. The tactile interface could then create these adjusted sensations on the surgeon's finger.

Developing a realistic model of the tissue from the tactile signals is not a trivial task. It involves understanding the relationship between tissue parameters and resulting tactile sensations. With this information, material and structural properties of the tissue can be determined. Spatially integrating these local features relative to the organ's overall shape allows a 3D model of the tissue to be generated. In the prototype palpation instrument, this relative location of the sensor was not measured, making an overall model of the tissue impossible to develop. This section presents a signal processing technique where local features of the tissue are extracted from the pressure signals.

The requirements of the signal processing necessary for the prototype palpation instrument are straightforward due to the simplicity of the target application and hardware constraints imposed by the shape display. Localizing lumps in the lung is primarily a binary task. The system must accurately provide a clean signal that indicates

the presence of a lump as the sensor scans over it. Realistic sensations would provide a more intuitive feedback and speed the learning process, but are not necessary for localization. Determining the properties of a lump (size, depth, hardness, etc.) would most certainly require high fidelity tactile sensations. The needs of the signal processing are also determined by the ability to produce realistic sensation with the current shape display design. The pins of the display are configured in a single line and do not conform to the finger's undeformed shape. The fidelity of the shape feedback is also limited.

The most direct approach to the signal processing is to map measured pressure directly to pin height using an appropriate gain factor. This would require the surgeon to perform the signal processing and determine the presence of the lump from the raw pressure data. This is a reasonable task; however, the fidelity of the prototype tactile shape display (described in Chapter 5) makes this process difficult. Figure 3.4 shows pressure distributions collected with the prototype tactile sensor when probing a rubber model, when the sensor is over an embedded lump and when the sensor is contacting homogeneous material. The dotted line with circles shows the pressure distribution with the homogeneous rubber. The solid line with the squares shows the distribution when the sensor is over a lump. In both cases a similar contact force of approximately 5 N was used. The presence of the lump is quite obvious from these signals.

As was seen with the pressure distribution measured with the wax finger replicas in Chapter 2, the pressure shown in Figure 3.4 consists of two parts summed together. The first is the pressure created when contacting homogeneous rubber. The increase of the signal at the ends of the sensor are due to the edge effects of the finite length probe. The sharp corners of the probe cause stress concentrations similar to a flat punch indenter.

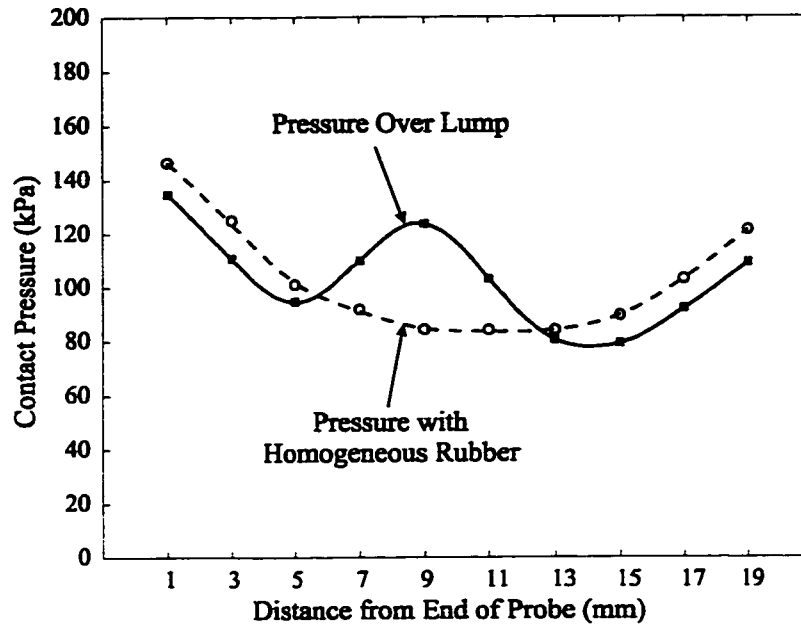


Figure 3.4. *Measured Pressure Distributions when Indenting the Sensor into a Rubber Model.* The dotted lines show the pressure when contacting homogeneous rubber. The circles indicate the actual readings for each element. The solid line and squares show the pressure distribution when indenting the sensor over a lump.

The distribution is not centered because the sensing elements are not centered on the probe. The shape of this distribution scales approximately linearly with overall contact force. The second component of the pressure distribution is the stress concentration induced by the lump. This is seen by the bump in the middle of the pressure distribution. The height of the pressure concentration induced by the lump is of a similar magnitude to the edge effects of the sensor. A low fidelity shape display would therefore make the detection of the lump difficult.

One technique to increase the detectability is to subtract the minimum pressure reading of the ten elements from all the readings. If pin height is mapped to this adjusted pressure signal, at least one of the desired pin positions will be zero. This technique minimizes the motion of the pins by eliminated the large offset and displays the relative difference in pin height to the surgeon. Unfortunately, the edge effects of the sensor

become confusing and can be interpreted as a lump near the ends of the sensor. Eliminating the edge effects so a flat pressure reading is generated while contacting the homogeneous rubber would make the detection process easier.

One solution to removing the edge effects is to change the shape of the sensor. A specific shape can be determined such that a flat distributed pressure is generated. This shape, however, depends on the input force. A second solution is to change the gains on each sensing element to flatten the pressure distribution. This requires lowering the gain for the elements near the edge and increasing the gains for the elements in the middle. Because the shape of the pressure distribution when contacting homogeneous rubber scales with input force, the sensor response when using gain adjustment is flat for varying force levels. Figure 3.5 shows the same pressure readings from Figure 3.4 adjusted using

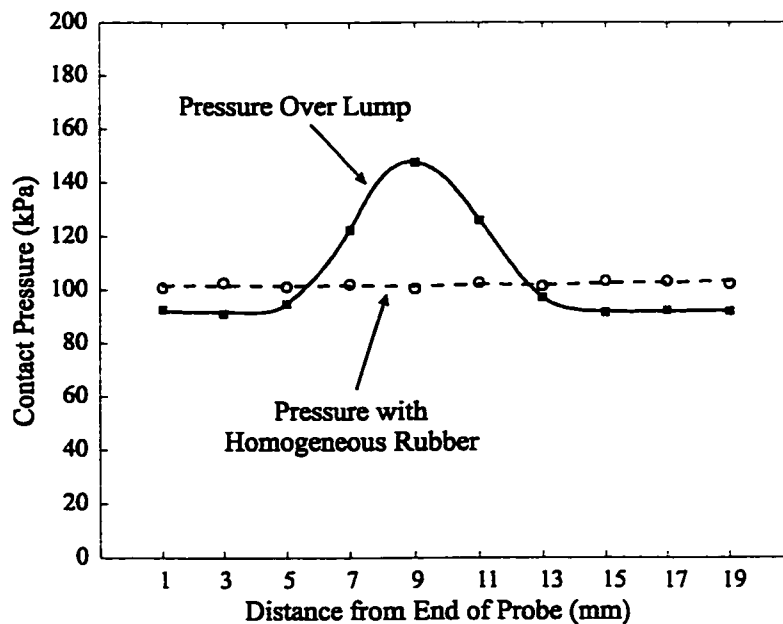


Figure 3.5. *Pressure Distributions After Individual Element Gain Corrections.* The edge effects of the sensor were removed by decreasing the gains for elements near the edge of the sensor and increasing the gains near the middle. This causes a flat response from the homogeneous rubber. This response is flat independent of contact force.

individual gain correction. The pressure distribution is now flat when contacting homogeneous rubber. The stress concentration induced by the ball is added to this flat response. Now by subtracting the minimum reading of the ten elements from all of the elements, a signal is created that clearly indicates the presence of a lump. Figure 3.6 shows the pressure distributions with the offset subtracted. This process eliminates the stress distribution caused by contacting the rubber and only leaves the pressure added by the lump.

Adjusting the individual element gains causes the height of the measured pressure induced by a lump to change depending on the location of the lump under the sensor. Because elements near the edges of the sensor are less sensitive, lumps sensed near the ends will have a smaller signal than lumps sensed near middle – even when the actual

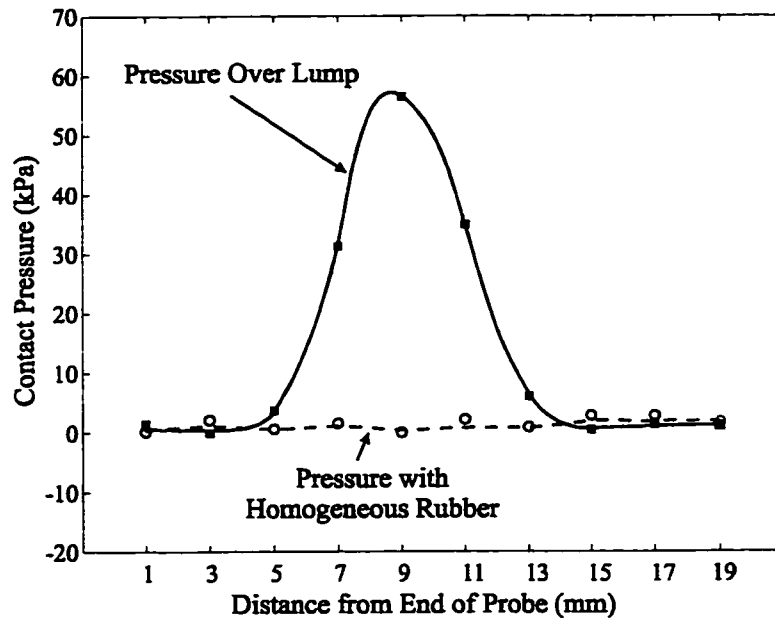


Figure 3.6. *Pressure Distributions after Offset Pressure Subtraction.* By subtracting the minimum pressure reading of the ten elements from all of the elements, the flat response generated from the individual gain adjustment is reduced to a line at zero. The stress concentration of the lump is the only signal left.

stress concentrations are of the same size. Multiplying the pressure distribution (after gain correction and offset subtraction) by the inverse of the element gains can eliminate this problem. Because the signal from the homogeneous rubber is brought to zero, the inverse gain adjustment only changes the signal caused by the lump. As a final step, the processed pressure distribution is multiplied by a gain factor to determine desired pin height. Figure 3.7 shows the resulting desired pin heights determined from the pressure distribution shown in Figure 3.3.

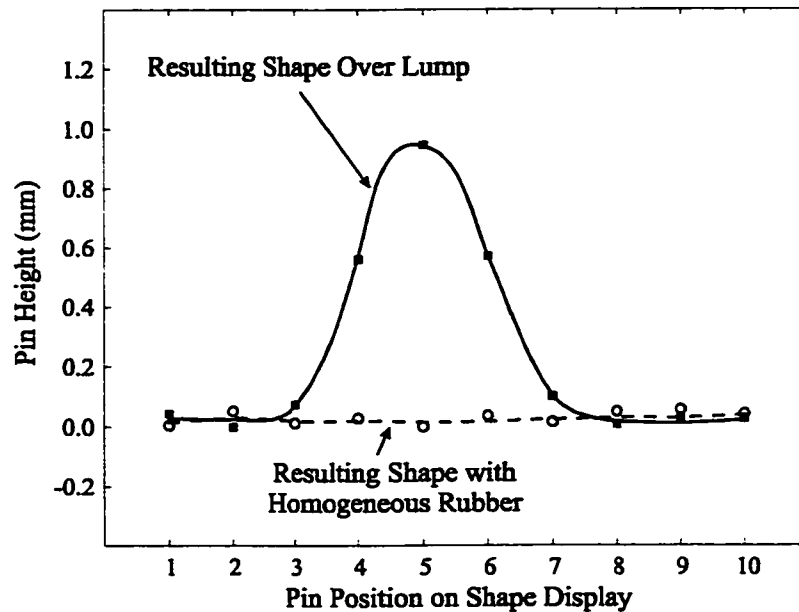


Figure 3.7. Resulting Pin Height. By multiplying the each element by the inverse of the gain adjustment used to eliminate the edge effects, the height of the stress concentration caused by the lump is consistent across the length of the sensor. An overall gain factor of 0.02 mm/kPa was used to transform the pressure to desired pin height.

This signal processing technique can be summarized in equation form. The desired pin height for the i^{th} pin on the n^{th} sample, $y_i(n)$, can be written

$$y_i(n) = \frac{K}{G_i} \left[G_i p_i(n) - \min_{i=1}^{10} \{ G_i p_i(n) \} \right] \quad (3-1)$$

where $p_i(n)$ is the pressure on the i^{th} element on the n^{th} sample, G_i is the gain correction for the i^{th} element, and K is the overall gain to convert the modified pressure reading to mm of pin displacement. This is computationally efficient and simple to implement using computer control. Chapter 7 reports the verification and testing of this technique using the prototype sensor.

This signal processing techniques works extremely well in practice if the sensor is held at a consistent angle with respect to the rubber model surface. If the sensor is tilted so the tip of the sensor digs into the rubber, the pressure distribution caused by the homogeneous rubber changes shape. The stress concentration induced by the end at the sensor tip increases in magnitude, while the trailing edge concentration decreases. If the back end of the sensor digs into the rubber, an opposite shift in the distribution will occur. The individual element gain adjustment technique highly depends on the shape of the distribution remaining constant. This will complicate the interpretation of the signal and confuse the surgeon. This problem is addressed in the instrument design described in Chapter 7. A pivoting sensor head allows the sensor to automatically adjust its orientation to be flush with the rubber surface. This allowed a uniform pressure distribution to be consistently obtained.

3.3 Haptic Rendering Model to Simulate Soft Tissue Contact

Once features of the remote organ's structure and material properties have been determined from the measured tactile sensations, models are needed to predict the mechanical interaction between the surgeon's finger and sensed tissue. Appropriate stimuli can then be applied to the finger such that the surgeon feels as if he or she is touching the tissue directly. These modeling techniques must be computationally efficient and take into account the complexities of the shape and mechanics of the fingerpad.

As a step in this direction, a haptic rendering algorithm has been developed in collaboration with Pawluk and Wellman [Pawluk et al. 1997] to produce the realistic feel of compliant tissues. This requires understanding how the finger would have interacted with the compliant tissue if it were in direct contact, and then how to relay this information through a haptic display system. The principle behind the simulated tissue interaction is that the surgeon imparts the desired contact force to the haptic interface. The stiffness display system, consisting of a shape display mounted on an instrumented linear actuator, then produces the correct deformation profile and rigid body motion, corresponding to the expected result for the real tissue. The shape display provides the necessary tactile information, while the linear actuator provides the kinesthetic (force-displacement) relationship and measures the total force exerted by the surgeon's finger. For this task, it is important to produce both tactile and kinesthetic sensation. Srinivasan and LaMotte [1995] have shown, in direct manipulation experiments, that kinesthetic (force-position) sensing alone is also insufficient: their subjects were unable to determine

the difference between even the hardest and softest rubber samples used in the absence of the distributed skin sensation of surface deformation.

In order to predict the response of the fingerpad to a remote object, we need a good model of the finger-tissue interaction. Experimentally, Pawluk and Howe [1996] have begun to examine this issue by considering the dynamic contact of the human fingerpad with a flat, rigid surface. They have found that the quasi-static pressure response of the fingerpad can be successfully approximated by Hertzian contact [Johnson 1995] modified to allow for a nonlinear variation of the modulus of elasticity. Approximating the fingerpad as a sphere, the contact pressure distribution, $p(r,x)$, can be described by

$$p(r,x) = \frac{2 E_f^*(x)}{\pi R_f} [a(x)^2 - r^2]^{\frac{1}{2}} \quad (3-2)$$

where r is the radial distance from the center of contact, x is the maximum fingerpad deformation (i.e., at $r = 0$), E_f^* is the modulus of elasticity of the fingerpad, R_f is the radius of curvature of the fingerpad, and $a(x)$ is the radius of the contact area. From Hertz theory, the radius of contact, $a(x)$, is given by

$$a(x) = (R_f \delta)^{\frac{1}{2}} = \left(\frac{3 P R_f}{4 E_f^*(x)} \right)^{\frac{1}{3}} \quad (3-3)$$

where P is the total contact force, and δ is the rigid body indentation. The nonlinear varying modulus of elasticity is assumed to be

$$E_f^*(x) = \frac{2b}{m} [e^{mx} - 1] \quad (3-4)$$

where b and m are parameters of the model fit to experimental data [Pawluk and Howe 1996]. In reality, the stiffness increase is a local effect and does not change the bulk properties as this approximation does.

We can generalize this model to interactions between the fingerpad and objects of varying radii and compliance by making the following substitutions in equations (3-2) and (3-3)

$$1/R_f \Rightarrow 1/R = (1/R_f + 1/R_t) \quad (3-5)$$

where R_t is the radius of curvature of the tissue, and

$$\frac{1}{E_f^*} \Rightarrow \frac{1}{E^*} = \frac{1-\nu_t^2}{E_t} + \frac{1}{E_f^*} \quad (3-6)$$

where E_t is the modulus of elasticity and ν_t is the Poisson's ratio for the tissue. Although this generalization has not been verified experimentally, it provides a preliminary estimate of the expected interaction between the fingerpad and compliant surface.

To display the estimate of the object's compliance on a shape display, we need to know the deformation profile of the fingerpad to provide the appropriate position command to each of the pins of the display. From the Hertz model, the deformation of the fingerpad, referenced to its undeformed shape $F(r)$ is

$$u_z(r) = \frac{1}{E_f^*} \left(\frac{3PE^*}{32a^3R^2} \right)^{1/3} [2a^2 - r^2] \quad (3-7)$$

where

$$x = u_z(0). \quad (3-8)$$

There is also an overall rigid body motion of the finger which occurs upon contact, δ , described by Equation 3-3.

To simulate tissue interaction we must measure the contact force P which the surgeon applies to the display. We then must produce the desired motion: both the fingerpad deformation $u_z(r)$, which can be represented using the tactile shape display, and the rigid body motion δ , which can be provided by the linear actuator. In order to do this,

we must solve for $u_z(r)$ and δ using equations (3-2) through (3-8). In these equations, the parameters describing the fingerpad, R_f , b , m , are assumed to be measured a priori, and the parameters describing the tissue, R_t , E_t and ν_t , are assumed to be measured from the environment. Knowing the applied force P , $u_z(r)$ and δ can be calculated in real-time. If the Young's Modulus of the finger and tissue are constant, a closed-form solution exists. When the modulus depends on the deformation, x , numerical techniques are required.

Figure 3.8 shows the response of the model at an applied force of 3 N, using parameters measured for a typical fingerpad data [Pawluk and Howe 1996] in contact with a flat compliant surface ($E_t = 15$ kPa, $\nu_t = 0.5$). The solid line shows the overall fingerpad motion, whereas the dotted line shows that component (the rigid body motion)

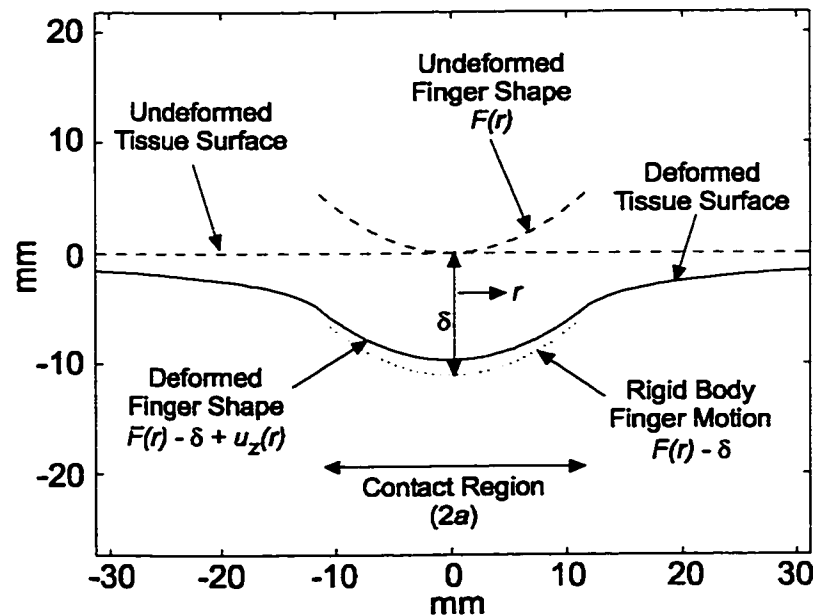


Figure 3.8. *Response of Haptic Rendering Algorithm.* The solid line shows the overall motion of the tissue surface. The dotted line shows the rigid body motion applied with a linear actuator. The difference between these two curves is produced by the tactile shape display.

which would be provided by a kinesthetic feedback mechanism; the difference between these two is the deformation to be provided by the tactile shape display.

The maximum deflection $x = u_z(0)$ and rigid body motion δ of the fingerpad for contact with flat surfaces of various linear compliance as a function of contact force are shown in Figure 3.9. The logarithmic effect in both responses is due to the shape of the

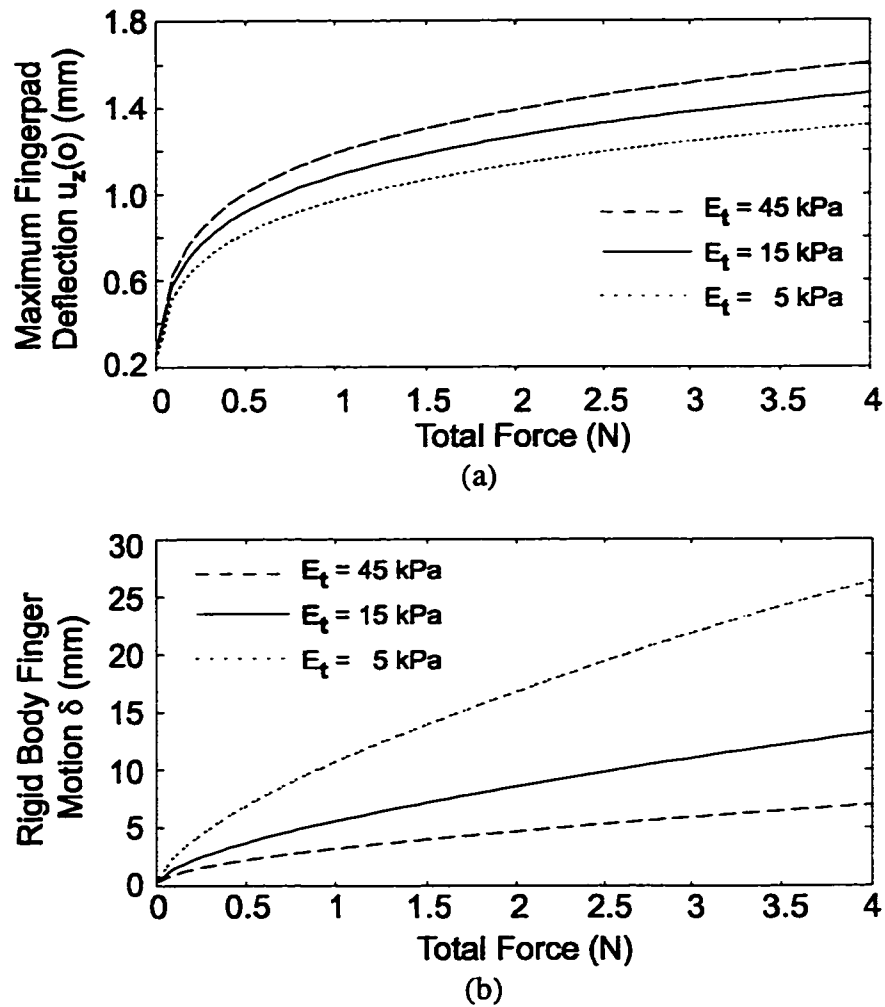


Figure 3.9. *Fingerpad Deflection and Rigid Body Motion of Finger for Specific Values of Tissue Modulus.* (a) The maximum deflection of the fingerpad exhibits a logarithmic trend due to the exponentially increasing stiffness of the finger and its curved geometry. (b) The rigid body motion behaves nearly linearly after the initial contact between the finger and tissue.

finger and the exponentially increasing modulus of elasticity (E_f^*), which causes the fingerpad to become stiffer at increasing forces and therefore more difficult to deform.

There are many aspects of the contact interaction this model does not capture. The large deformations produced and inhomogeneous structure of the finger would change the induced pressures and deformations. Modeling techniques of this nature do provide a start on adequately determining drive commands for remote palpation instruments so they provide more realistic sensations of the remote tissues. More advanced algorithms are needed to simulate contact with more intricate tissue structures. Some of the key issues involved in the development of these processing techniques are discussed at the conclusion of this thesis.

Chapter 4. Finger Speed during Lump Localization

The development of effective remote palpation systems requires matching the performance of the instrument to the methods and capabilities of human haptic perception. This chapter reports measurements of finger speed during a lump localization task. This is part of an ongoing series of studies aimed at characterizing pertinent aspects of haptic sensing [Pawluk and Howe 1996; Hajian and Howe 1997]. Finger speed is particularly important because it determines the required temporal bandwidth of the remote palpation system: as the finger speed increases, the sensor and display must respond more quickly to the variation of pressure at the instrument tip.

Adequate pin speed is also critical for correctly correlating tactile and kinesthetic sensations. If the display is too slow, tactile features will not be perceived in the correct location. Figure 4.1 shows this problem graphically. When quick finger motions are used, the desired shapes for the display to create contain high frequency information. Temporal filtering, due to low temporal bandwidths, causes the actual shape created to be lower in magnitude, more spread out, and time delayed. This causes the operator to sense the position of the feature some time after it has been past. The faster the finger moves, the more pronounced this problem becomes. Localization is then more complicated because the tactile feature will appear to move relative to the object depending on the direction and speed of the scanning motion of the finger. This is why slow feedback systems often require a move-and-wait strategy.

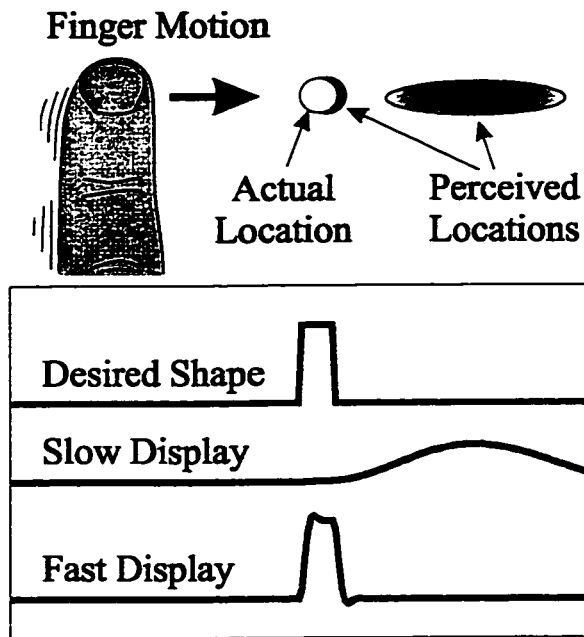


Figure 4.1. *Effects of a Low Temporal Bandwidth Display.* Slow pin speeds cause the sensation of a tactile feature to be lower in magnitude, more spread out, and delayed in time. This causes the location of the feature to be incorrectly perceived.

The main purpose of this study is to find typical finger speeds in single-digit lump localization. A secondary goal is to determine if there is a major difference in palpation speed between surgeons, for whom palpation is a frequently used professional skill, and the general population. The absence of such a difference may permit the use of a more accessible subject group for subsequent studies of palpation methods and for testing remote palpation technology.

The experimental design draws upon the fundamental work of Pennypacker and colleagues, which is unique in its systematic approach to the study of palpation [Adams et al. 1976; Saunders et al. 1986; Pennypacker and Iwata 1990]. These studies quantified the main psychophysical parameters for lump detection in breast self-examination, including the roles of lump size, stiffness, depth, background nodularity, search pattern, and training. In the experiments reported here, we measured fingertip position and

applied force as subjects located hard lumps in rubber models that emulate soft tissues. To determine if the gross mechanical properties of the tissue have a major effect on finger speed, we used three different types of rubber model. The measurements of finger location were analyzed to determine mean and average maximum speeds for each model type.

4.1 Experimental Methods

4.1.1 Apparatus and Experimental Setup

The rubber models used here had mechanical characteristics similar to soft tissues commonly palpated during medical procedures. They were constructed by filling a plastic petri dish (88 mm diameter, 15 mm deep) with a soft silicone rubber (General Electric RTV6166, Young's modulus \cong 2.5 kPa). To simulate tumors or hard lumps in the rubber models, 4 mm steel balls were glued to the bottom of each dish before the rubber was added. Pilot studies indicated that 4 mm was large enough that subjects could locate every ball and small enough that it required thorough searching to find them. This accords with the results of Adams et al. [1976] who found that the ability to detect 4 mm lumps in more complex simulated silicone breasts averaged over 90 percent.

To determine if alterations to the thickness and stiffness of the model caused large variations in palpation strategies, we modified the "reference" version described above (15 mm thick homogeneous rubber) in two ways. The first "thicker" variation consisted of a homogeneous 25 mm layer of the same rubber. The second "skinned" variation added a 1 mm thick skin of stiffer rubber (General Electric RTV108, Young's

modulus \cong 600 kPa) on top of the softer 15 mm layer. Three rubber models were created for each type with 2, 3, or 4 embedded ball bearings to ensure that subjects searched the entire model carefully. All of the rubber models were powdered with talc to limit the stickiness of the surface of the rubber; however, significant friction was still present between the rubber and human fingertip ($\mu \cong 1.2$ at 1 N normal force, increasing at higher forces).

Indentation tests were conducted on each of the three types of rubber models to compare their stiffness to tissues of interest. Figure 4.2a shows force-displacement plots for normal indentation using a 19 mm hemispherical probe. Figure 4.2b shows force-displacement curves for lateral motion when the probe was indented with a constant normal force of 5 N. Also plotted are similar measurements for lung [Lai-Fook et al. 1976] and breast tissue [Madden et al. 1978]. The stiffness of each of the rubber models is of the same order as these tissues.

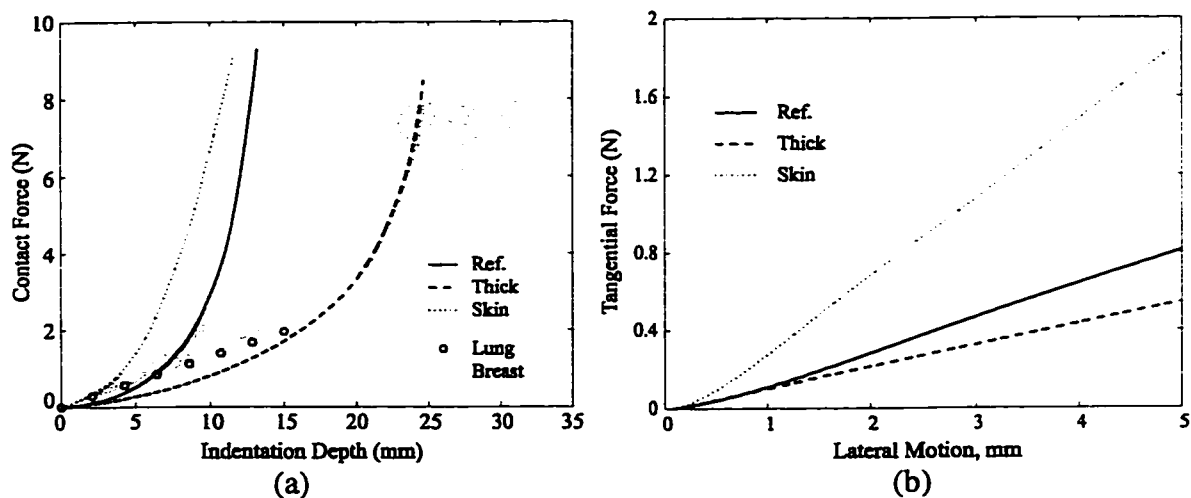


Figure 4.2. Rubber Model Stiffness. (a) Force-displacement curves from normal indentation tests of the three types of rubber models using a 19 mm spherical probe. Similar data for breast [Madden et al. 1978] and lung tissue [Lai-Fook et al. 1976] are also plotted. (b) Force-displacement curves from tangential motion at a constant normal force of 5 N.

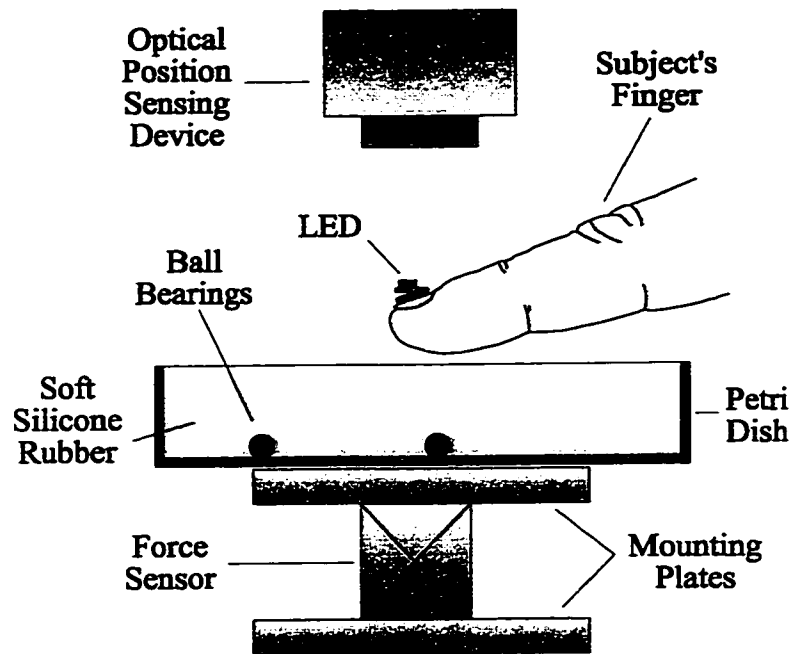


Figure 4.3. *Experiment Apparatus.* Force sensor measures normal force subject applies to the rubber model, and optical position sensing device (approximately 70 cm above) measures x and y position of the light emitting diode (LED) glued to the subject's fingernail.

The experimental apparatus is shown in Figure 4.3. For each trial, the experimenter placed a model on top of a strain-gauge force sensor, which measured the normal force applied to the model by the subject's finger. An optical position sensing device (models OT-3210/OT-3001, On-Trak Photonics Inc., Lake Forest, CA, with 50 mm lens) located 70 cm above the model measured the position of a light emitting diode (LED) glued to the subject's finger nail. This system measured the x and y coordinates of the fingertip within the plane parallel to the top surface of the model. The peak-to-peak noise amplitude of the force sensor and position sensor was approximately 0.013 N and 0.05 mm respectively. To avoid aliasing, the output signals from the force and position sensors were hardware filtered using four-pole low-pass filters with corner frequencies at 20 Hz. These signals were digitized to 12 bits at a sample rate of 100 Hz. The

nonlinearity of the position sensor was corrected using a least-squares fit to data collected from a calibration grid. The absolute maximum deviation from linearity was less than 0.5 mm after calibration.

To smooth the signals for velocity estimation, the measured signals were filtered in software with a six-pole low-pass filter with a corner frequency of 15 Hz. Pilot studies indicated 95 percent of the measured signal power was below 3 Hz. To ensure that all motions of interest were preserved, a filter corner frequency five times the 95 percent level was selected; this value also accords with results showing that voluntary finger motion frequencies are under 7 Hz [Keele 1986]. Velocities in the x and y directions were found by numerical differencing of adjacent samples of the filtered position data. Finger speed was then calculated by finding the magnitude of the velocity vector.

4.1.2 Experimental Procedure

A total of 12 subjects, naive to the purposes of the study, voluntarily participated in the experiments (8 male, 4 female). To determine the effect of professional experience on palpation technique, we divided the subjects into two groups: 'experts' and 'novices.' The experts consisted of five surgeons (ages 35-45, mean 39) with an average of 13 years surgical experience. The novices included seven individuals with no medical training (ages 19-54, mean 27). Each subject completed 18 trials. A trial consisted of locating all of the lumps in one of the models. Each of the 9 models (3 types, each with three different lump counts) was presented twice. A partial latin squares presentation order based on model type and number of lumps was used to minimize learning effects.

For each trial, the subject was instructed to wait for a beep from the data acquisition computer and then probe the model with the index finger of his or her dominant hand. An opaque screen precluded visual observation of the rubber model. When a lump was detected, the subject centered the finger over the lump and pressed a button with the other hand. The subject then continued searching the model until satisfied that all the lumps had been detected. After finishing the search, the subject removed his or her hand from the screen and told the experimenter the trial was completed. To discourage exceeding the force sensor range, a buzzer sounded when applied forces exceeded an acceptable level ($\cong 15$ N), a realistic limit for palpation of tissues in vivo.

At the beginning of the session, subjects were informed that the objective of the experiment was to examine the methods people use when searching for a lump in soft tissue with the index finger. The experimenter then read instructions detailing the experimental setup and procedure. Subjects were instructed that localization accuracy was important and that finding the lumps quickly was not important, and told to use the finger tip rather than the flat of the index finger to probe the model. No advice on search strategy was given. A practice period allowed subjects to become familiar with the three types of models and let them develop an overall search strategy. Several practice trials using the experimental protocol followed, until the subject felt comfortable with the experiment, then the 18 trials commenced. The time to complete one trial varied from 15 to 90 seconds, and the total time for all trials for one subject was approximately 45 minutes.

4.2 Experimental Results

The position and force data collected during the experiment revealed that all of the subjects used the same basic palpation procedure when searching for a lump. This consisted of pressing the finger into the model, making a small circular motion around the contact point while indenting the rubber, retracting the fingertip out of contact with the model, then moving to a new contact location. This simple motion was repeated many times, with the contact points following one of three systematic and consistent search patterns. Six subjects used a spiral pattern starting with the outside edge and circling in to the center; five used a vertical strip pattern with a series of lines scanned from top to bottom; and one used a spoked wheel pattern with lines radiating from the center. These patterns are consistent with the patterns observed by Saunders et al. [1986]. All subjects combined found over 95 percent of the lumps.

Using the force data, each trial was segmented into a series of contact intervals. Figure 4.4 shows the force record from part of a typical trial with a thicker model containing three lumps. (This same data is used in Figures 4.5 through 4.8.) The force record consists of a series of peaks separated by periods where no force is applied. Each interval corresponds to one of the probing motions described above. The bottom trace in the plot shows when the subject pressed the button, indicating a lump had been located. The trial was segmented using a threshold of 1 N to find the starting and ending points for each contact interval. A plot of the x and y position data along with the location of the lumps is shown in Figure 4.5. The circular motions that occur when the finger is pressed against the model can be distinguished from the translation used when moving to a new contact point.

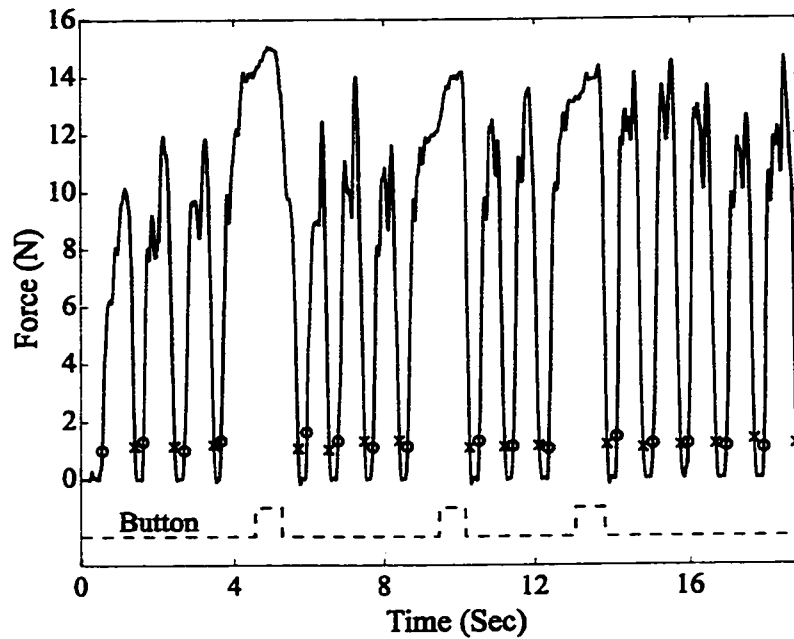


Figure 4.4. *Force Data from Part of a Typical Trial.* Solid line shows force, dashed line indicates when subject pushed button after locating a lump. Trials are segmented into a series of contact intervals using a 1 N threshold to find the starting and ending points, shown by O's and X's respectively.

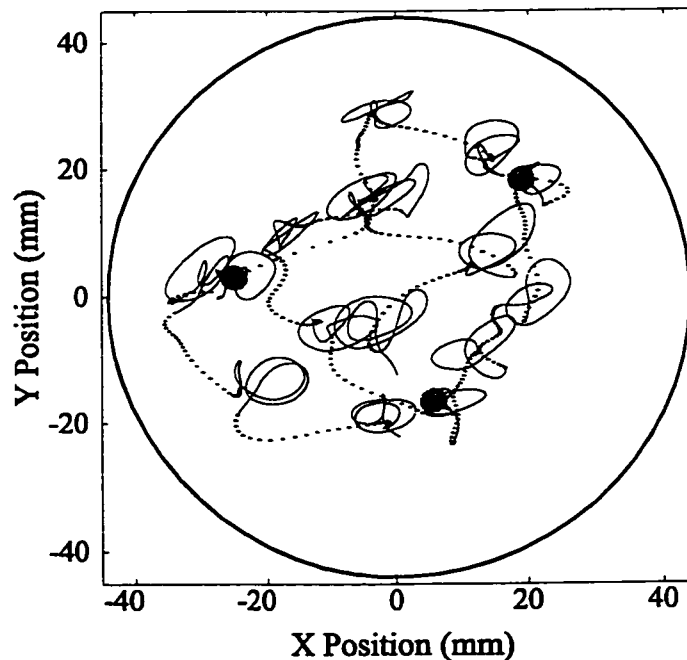


Figure 4.5. *Segmented x and y Position Data.* (Same trial shown in Figure 4.4.) Solid lines show finger path during contact intervals, dotted lines show path between contact intervals (force below 1 N), and three small shaded circles indicate the position and size of the lumps found by the subject.

Finger velocity may depend on whether a lump can be felt during a contact interval. We therefore classified each interval into one of three categories. In the first category, the finger position was not near a lump, so the subject had no opportunity to feel one. In the second, subjects possibly detected a lump as they moved within half a finger width of it, and then on the next interval indicated that they found it. In the third category, subjects homed in on the lump during the interval and then pressed the button. Figure 4.6 shows the position, force, and speed during a typical example of each of these categories. For each contact interval of each trial, we then calculated the mean, standard deviation, and maximum of the speed during the interval. Figure 4.7 shows these values for all of the intervals in this typical trial. The average speed during the intervals when a lump was located is much slower because subjects were instructed to hold the finger over the lump while pressing the button.

Once all of the trials for one subject had been segmented and each contact interval classified, we concatenated intervals of the same model type and category into groups. The average speed for each group was calculated by finding the mean of the group. The average maximum speed for the group was the mean of all the maxima measured during each interval in the group. The mean and average maximum speed used between contact intervals was calculated similarly. Figure 4.8 shows a histogram of the speeds in one group from one subject. The mean and maximum speeds for each subject showed no significant difference between the first and second category for all three model types ($t_{11} < 1.49$, $p > 0.2$). The speeds measured for the third category were skewed by the instruction to hold the finger over the lump while pressing the button. We therefore used only the results from the first contact interval category for the following analysis.

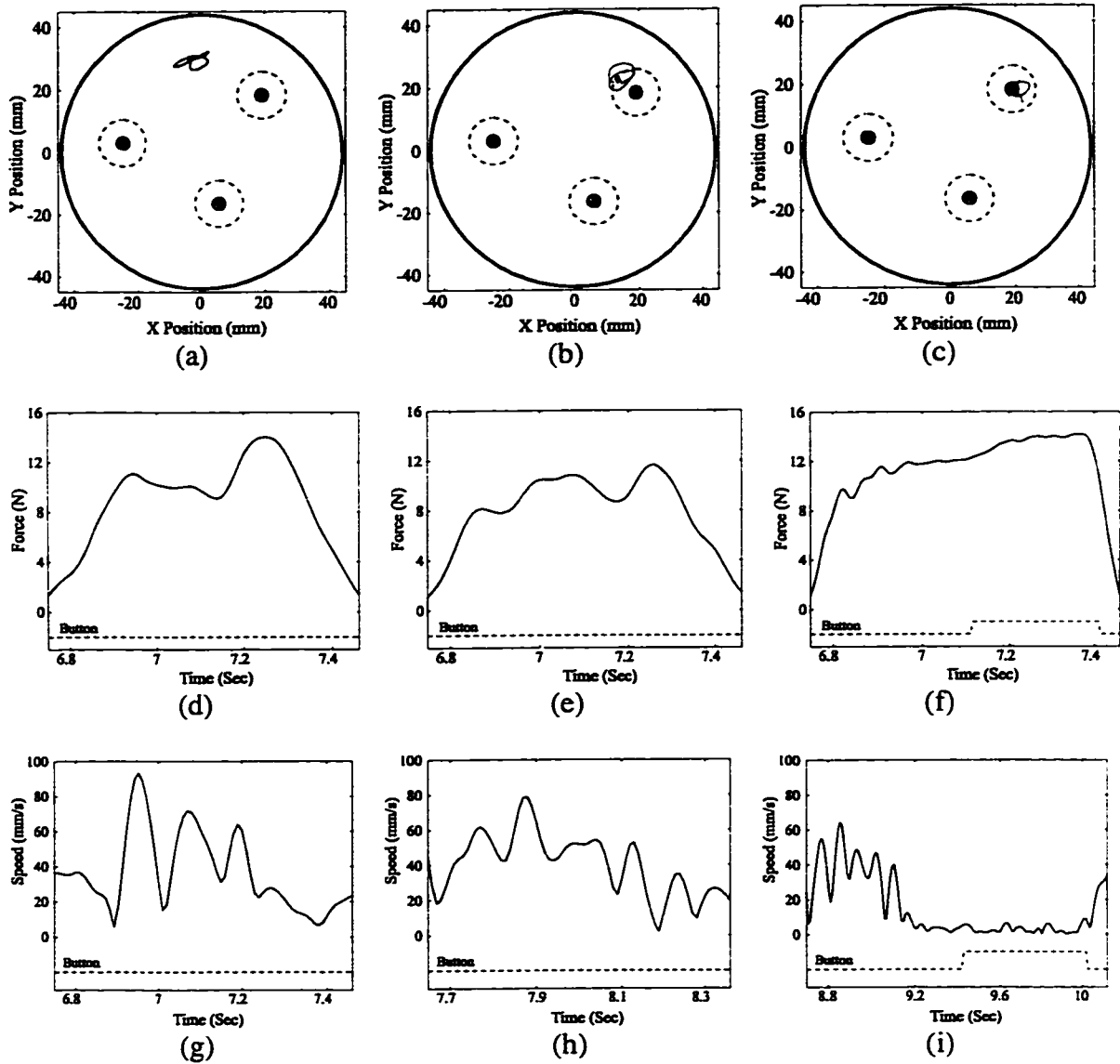


Figure 4.6. Categories of Contact Intervals. (Data from the sixth, seventh, and eighth contact interval of the trial shown in Figures 4.4 and 4.5.) Plots (a)-(c) show position, (d)-(f) force, and (g)-(i) speed. The solid line indicates finger path, small circles are the lump locations, and dashed circles indicate a distance equal to half the subject's finger width from the inclusions. First column (plots a, d, g) shows the first type of interval, where the subject had no opportunity to feel a lump; second column shows the second type, where the subject was within half a finger width of a lump and then found it on the next interval; and third column shows the third type, where the subject indicated locating the lump by pushing the button. Dashed line indicates the status of the button.

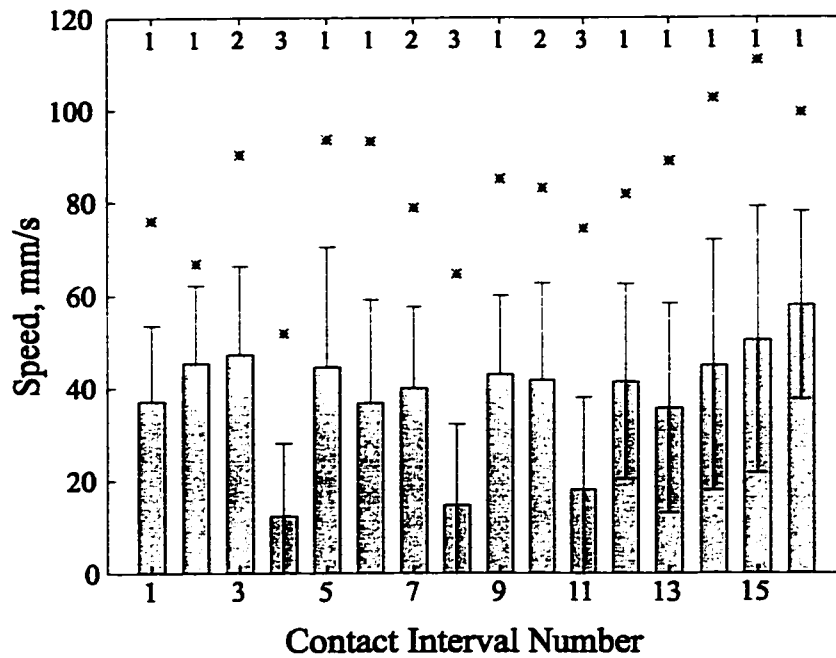


Figure 4.7. *Finger Speeds.* (Same trial shown in Figures 4.4 – 4.6.) Bar height indicates average speed for each contact interval, error bars the standard deviations, and asterisks the maximum speeds during that interval. Numerals at top indicate contact interval category.

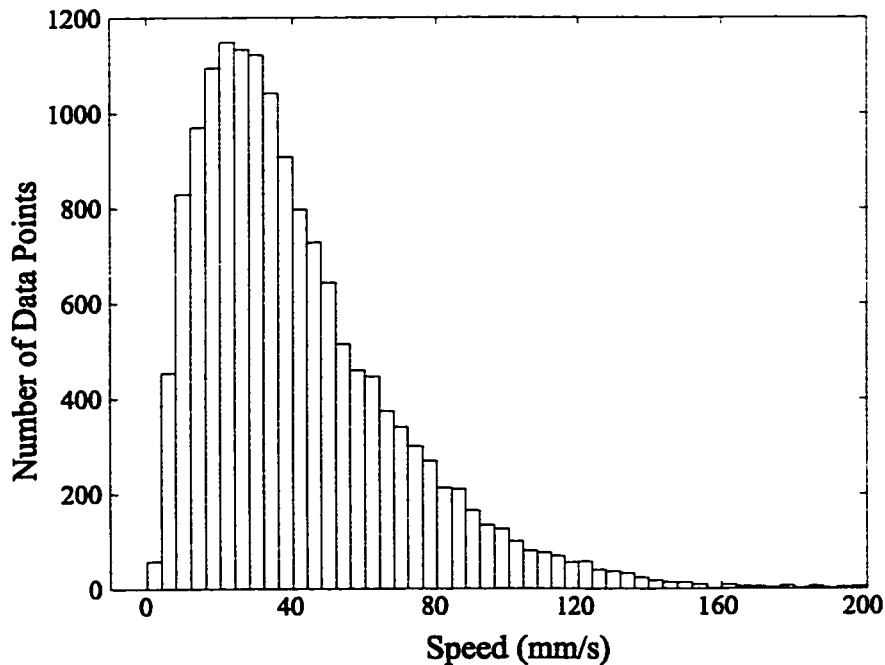


Figure 4.8. *Histogram of speeds.* All trials for a typical subject are shown with thicker rubber model and first category of contact interval.

Figure 4.9 shows cumulative distribution functions of the mean and maximum speeds for the first category. Separate plots are presented for each of the three model types and for non-contact motion with all models; each plot shows separate curves for expert and novice subjects. The curves all follow approximately sigmoidal shapes. Table 4.1 shows the means and standard deviations of the average and maximum speeds for the three model types and for non-contact motion. Matched pair t test comparisons of these results are shown in Table 4.2. Although some of these variations attained statistical difference, the means for the contact motion for the thicker and skinned model types are within 15 percent of the reference model. When contrasting these speeds to the non-contact speeds used between contact intervals, however, the difference is approximately a factor of two. For level of expertise, we found no significant difference between experts and novices (average speed: $t_{5,7} = 0.022$, $p > 0.9$; maximum speed: $t_{5,7} = 0.603$, $p > 0.5$).

<i>Rubber Model Type</i>	<i>Mean Average Speed, mm/s</i>	<i>Standard Deviation</i>	<i>Mean Maximum Speed, mm/s</i>	<i>Standard Deviation</i>
<i>Contact Motion:</i>				
Reference (15 mm)	39.2	18.0	83.9	31.1
Thicker (25 mm)	42.1	18.3	97.7	36.1
Skinned (15 mm with skin)	33.7	13.1	87.7	27.0
<i>Non-contact Motion:</i>				
All model types	76.1	18.6	146.4	36.9

Table 4.1. Mean and standard deviation for average and maximum speeds used for the three model types and for non-contact motion.

<i>Rubber Model Type</i>	<i>Average Speed</i>		<i>Maximum Speed</i>	
	t_{11}	p	t_{11}	p
<i>Contact Motion:</i>				
Thicker (25 mm)	2.782	0.018	5.185	0.002
Skinned (15 mm with skin)	3.161	0.009	0.844	0.390
<i>Non-contact motion:</i>				
All model types	6.036	0.001	6.016	0.001

Table 4.2. Results from matched pair t tests comparing speeds used for the reference model to the speeds used for the other two model types and for non-contact motion.

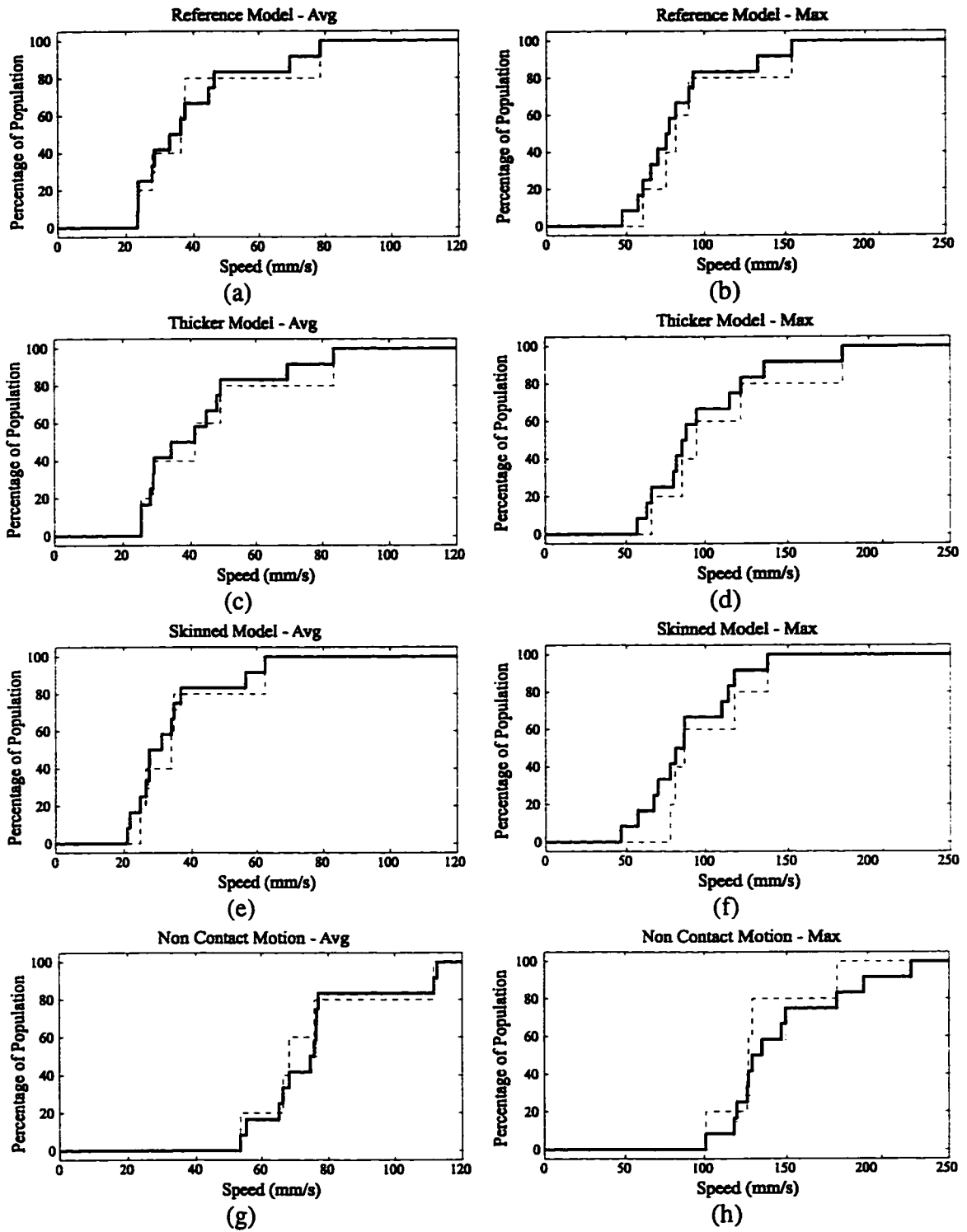


Figure 4.9. *Cumulative distribution functions.* Curves indicate the fraction of the population with a mean or average maximum speed below that level. Dashed lines indicate the distribution of experts, dotted lines indicate the distribution of non-experts, and solid lines indicate experts and non-experts combined.

4.3 Discussion

These results suggest that people use a consistent, stereotyped palpation technique for single-finger lump localization. The separation of the palpation technique into a global search strategy and local contact motions is essential for explaining the observed behavior. The search strategy varied but had the common result of providing a systematic search pattern that covered the entire model. The local contact motion was an invariant component of the detection and localization process. All subjects consistently used small circular motions although the experimenter provided no instruction.

Analysis of the mechanical interactions between the finger and rubber model may provide insight into why this basic motion was always used. As the finger is pressed into the soft rubber, a near-uniform high stress is created on the finger pad. As the finger moves over the lump, an additional local stress concentration moves across the finger pad. Presumably the coherent relative motion of the low amplitude local concentration with respect to the high stress near-uniform background allows subjects to localize the lump. Chapter 2 of this thesis and other previous studies present simple mechanical analyses that support this explanation [Dario and Bergamasco 1988]. An additional factor may be that circular motions used during contact increase each contact interval's search area and therefore decrease the overall number of intervals necessary to search the entire model.

Another important aspect of the contact interaction is that subjects did not slide over the surface of the model during a contact interval. The lateral motions the subjects used did not create tangential forces that exceeded the surface friction of the models used in this experiment; these frictional conditions are realistic for a subset of surgical

procedures. Under these conditions it may be advantageous to avoid slips because sliding causes irregular shear forces on the finger which can mask the stress concentration induced by the lump [Lederman 1978]. In addition, remaining in contact with a fixed point on the surface may make it easier to correlate kinesthetic and tactile information. In some surgical procedures, however, the tissue of interest may present a relatively regular and slippery surface where smooth sliding is possible. Further experiments are planned to determine palpation strategies and finger velocities under these conditions.

Finger speed measurements may also help elucidate the relationship between tactile sensing and motor control in perceptual tasks. Many studies have demonstrated that neural response and perceptual thresholds vary greatly with the frequency content of the stimulus [Boff and Lincoln 1988]. In particular, perceptual thresholds are far lower for dynamic than for static stimuli. The circular motions used during contact intervals would therefore have the benefit of providing a repeated, time varying input to the mechanoreceptors. This suggests that subjects pressed deeply into the compliant “tissue” to increase the amplitude of the stress concentration, and moved in quick circles to provide higher-frequency stimuli.

Moving quickly may enhance the sensation of the lump; however, this comes with a price. The higher the finger speed, the more power required to make a given lateral excursion from the contact point, and the more energy expended per contact interval. Also, as finger speed increases, motion control becomes less precise and unwanted variations in the pressure on the finger can mask the sensation of the lump. The magnitude of lateral motion involves a similar trade-off: as the distance from the contact point increases, the area covered grows, as does the force required to achieve that

displacement. Subjects probably choose a finger speed and motion amplitude that balances energy expenditure, stimulation amplitude, and search time.

These results indicate that in a simple palpation task the finger speeds used by surgeons are not significantly different from speeds used by individuals with no medical training. Harris et al. [1994] found no significant differences in psychomotor skills of surgeons compared with other medical specialists. The similarity of speed across training level also supports the conjecture that speeds are optimized for the limitations of the human sensory-motor system. It should be noted that this experiment used a straightforward detection task that largely involved motor and perceptual faculties. Differences between surgeons and novices are more likely to be evident in complex tasks that require higher level functions such as discrimination and diagnosis.

4.4 Resulting Design Specifications for Tactile Displays

A main motivation for this study was to determine design parameters for tactile display devices used in remote palpation instruments. Ideally, these instruments will feel completely transparent to the surgeon, allowing the use of natural, unrestricted palpation techniques. The speed at which a tactile display must recreate shapes or pressures depends directly on the speed at which the sensor is scanned across the tissue. For this purpose, the velocity values in Table 4.1 and the distribution functions in Figure 4.9 provide estimates of the required parameters.

The observed velocities suggest that effective tactile display devices for palpation will require surprisingly high bandwidths. Based on task resolution requirements, the prototype shape display uses an array of actuated pins spaced 2 mm apart. The maximum

spatial frequency the display can create (i.e. the Nyquist limit, with pins alternating up and down) is then 0.25 cycles/mm. Using the cumulative distributions for the reference model in Figure 4.9, the average maximum finger speed for 90% of the population tested is approximately 120 mm/s. If the maximum spatial frequency is scanned across the display at this rate, each pin must travel up and down at a temporal frequency of 30 Hz. Figure 4.10 shows this idea conceptually. This bandwidth specification, in combination with displacement, force, and packaging requirements, is difficult to achieve with current actuators, as discussed in the following chapter. Further experiments should be directed at determining the effects of restricted speed or bandwidth on palpation efficacy and efficiency.

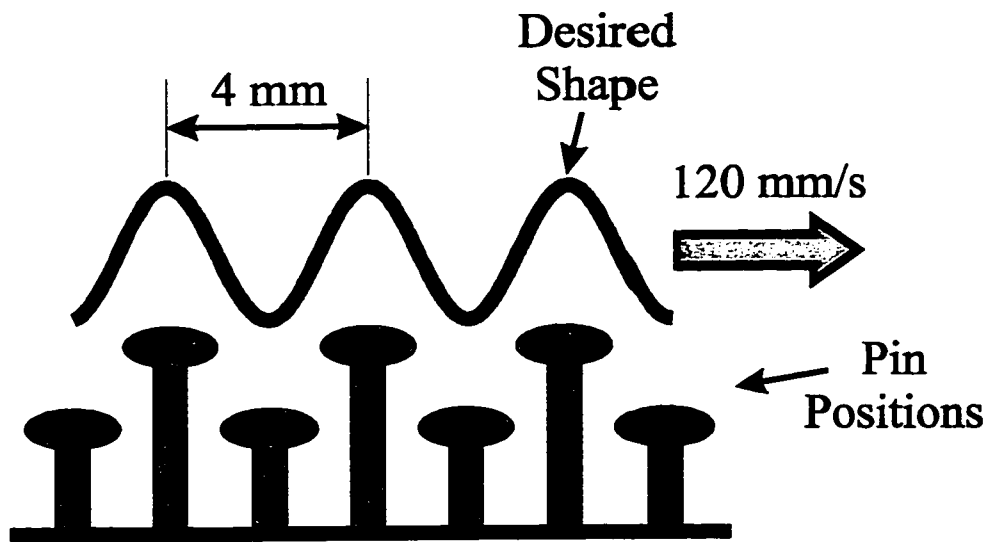


Figure 4.10. *Temporal Bandwidth Requirement Based on Measured Finger Speeds.* The maximum spatial frequency the display can generate is 0.25 cycles/mm by alternating the pins up and down. If this pattern is scanned across the array at 120 mm/s the resulting pin motion is 30 Hz.

This initial experiment concerned lump localization using a single finger, and there are many other palpation techniques that involve factors that have not been included in this experiment. In particular, surgeons must often operate near the limits of detection

and locate structures masked by anatomical irregularities and nodularity in the tissue. The number of fingers used as well as hand position are also varied depending on the task. Considerable additional work will be required to better understand how these variations affect finger speed and palpation technique.

Chapter 5. Tactile Shape Display

Tactile display devices typically consist of an array of individually actuated pins that can be raised and lowered against the fingertip. The goal is to recreate skin deformations that are produced during actual palpation tasks. Development efforts have been slow due to the numerous design challenges. Minimal pin spacing is required to produce sensation with high spatial frequency. Humans are able to distinguish two points spaced 0.9 mm apart. This implies that pins in a display should be spaced as closely as 0.9 mm in order to convince users that they have a shape pressed into their fingerpad, rather than an array of pins. Large pin displacements (approximately 3 mm) are needed to match the maximum deformation of the fingerpad. If the display is creating shape, the pins must produce large forces and be stiff enough to deflect the fingerpad. If the display is to move with the finger, a small and lightweight construction is required. As discussed in the previous chapter, the display must also have high temporal bandwidth. Slow actuator speeds cause tactile information to be poorly correlated with gross motion of the finger, making it difficult to quickly and accurately locate tactile features. This specification is of particular interest because many of the prototype displays described in the research literature have fallen far short of the 2 mm spacing and 30 Hz requirement determined from the finger velocity experiment in Chapter 4.

This chapter presents the design of a high bandwidth shape display for use in the remote palpation instrument. The prototype was used in an experiment to measure the relation between display bandwidth and performance in a simple lump localization task. First, a description of prior research efforts on tactile displays is presented.

5.1 Previous Research on Tactile Displays

Much of the work on tactile display devices has focused on “sensory substitution” aids for the blind. The most familiar of these, the OPTACON, is a commercially available camera-tactile display system [Bliss 1970]. Vibrating pins represent the intensity pattern as the device is manually scanned across a printed page. A few devices for presenting static (non-vibrating) shape information have been developed, but progress is slow due to the numerous design challenges.

Cohn et al. [1992] implemented a tactile pressure display using a 5x5 close-packed array of pneumatically actuated pins. The design was compact, but forces were limited to 0.2 N and pulse-width modulated air valves limited temporal bandwidth to 8 Hz and induced unwanted vibrations. Hasser and Weisenberger [1993] describe a 5x6 array using shape memory alloy (SMA) wire actuators configured in a flexure design. This display provides the high density required for mounting in surgical instruments, but force levels are limited to 0.2 N per element, restricting the ability to represent shapes with high curvature under force reflection loads. Kontarinis et al. [1995a] describe a 6x4 pin shape display with 2 mm pin spacing. Small mechanical levers actuated with SMA wires produces approximately 1 N of pin force with 3 mm of displacement. Temporal bandwidths are limited to 6 or 7 Hz. Finally, Fisher et al. [1998] describe a shape display with a 8x8 array of pins spaced 1.6 mm apart actuated with SMA wires shaped as springs. The high density of the design provides excellent spatial resolution and adequate pin forces (> 2.5 N), but temporal bandwidths are low due to the thermal effects of the SMA.

The prototypes described above are limited in performance and suffer from low bandwidths and poor reliability. The high-density packing makes it is especially challenging to keep the large number of actuators functioning properly. At present, remote palpation systems using these displays are only useful for aiding simple palpation tasks where high fidelity tactile signals are not necessary. The development of faster, more robust displays is needed. The next section describes a prototype display developed in conjunction with Wellman [1997] for use in remote palpation instruments that meets these requirements.

5.2 Mechanical Design of Prototype Shape Display

5.2.1 Configuration Design

Incorporating the shape display into the remote palpation surgical instruments requires a compact design. Using a single row of pins simplifies packaging and mechanical design constraints, yet retains the functionality of a matrix of pins because textures can be easily perceived along the line of the pins. The user can also sweep the display to perceive curvature perpendicular to the line of pins. There is clearly a trade-off between perception of two dimensional curvatures and temporal bandwidth, and we have chosen to concentrate on the latter. Figure 5.1 shows that the line of pins runs along the finger pad rather than across it. The size of various available components limits the pin spacing to 2.0 mm on center. In order to cover the length of most finger pads, we have chosen to use ten pins.

The small pin-to-pin spacing, compact size and the extremely high force and stiffness requirements, led us to choose shape memory alloy (SMA) wires to actuate each of the

pins. This material is more suited to this task than electromagnetic actuators because of its high force-to-weight ratio and high intrinsic stiffness. It also provides much larger displacements than piezoelectric or magnetostrictive materials. There is a price to be paid for these benefits and SMA has its own set of design challenges which must be addressed.

Shape memory alloy shortens when it undergoes a phase transition from the Martensitic to the Austenitic phase. This reversible phase transition can be produced by heating the wire above its transition temperature using electric current. It is well known that SMA exhibits hysteresis when cycled through this transition [Ikuta 1990]. It is also a relatively slow process because it can take a long time for the wire to cool and lengthen. Previous authors have suggested that it is possible to increase the bandwidth and account

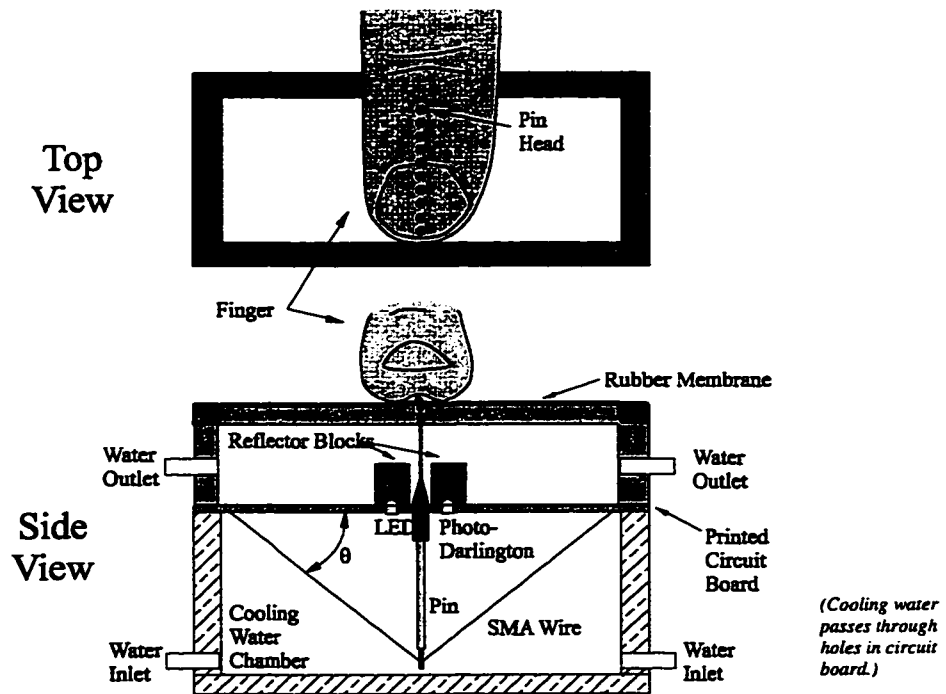


Figure 5.1. *Prototype Tactile Shape Display.*

for the hysteresis by developing a model of the process and incorporating this in the controller [Ikuta et al. 1990; Grant and Hayward 1997]. While this undoubtedly will work to some degree, we have chosen to increase the bandwidth through careful thermal design and have minimized the hysteresis through position feedback control of the display.

5.2.2 Mechanical Design

SMA typically undergoes less than 5% strain during the phase transition. In order to compactly package the display we have configured the wires in a V shape, as shown in Figure 5.1. Kinematic analysis reveals that if the original length of the wire is $2L$ then the displacement of the pin, δ , is

$$\delta = L \sin(\theta) - \sqrt{L^2 \sin^2(\theta) - \{1 - (1 - \gamma)^2\} L^2} \quad (5-1)$$

where γ is the maximum strain of the wire. The stiffness of the pin, K , is related to the angle, θ , also shown in Figure 5.1, and the stiffness of the wire, K_w , by the equation

$$K = 2 \sin^2(\theta) K_w \quad (5-2)$$

K_w is a function of the phase of each wire, its length and its diameter, which should be chosen to maximize heat dissipation. These two equations make it clear that there are trade-offs between compactness, the displacement of each pin, and the stiffness of each pin. Thus, they can be solved to determine the required wire length to produce a minimum stiffness, displacement and desired compactness.

In order to facilitate the construction of the display, it uses a layer based modular design that includes all electrical connections on a single printed circuit board. This also

minimizes the number of parts that are required and makes for an overall size of 78 mm by 35 mm by 57 mm. Preliminary testing revealed that nickel-titanium shape memory alloy wire can be cycled at 4.8% strain with a 2N load for tens of thousands of cycles with no appreciable loss in performance. Thus, as an extra margin of safety, we chose to limit the SMA to 4.5% strain, which provides the required 3mm displacement when each V in the display is 60 mm wide by 20 mm deep. The usual number quoted to achieve millions of cycles is 2% strain. We have sacrificed life-span for compactness in this prototype.

During assembly, the SMA wires are first electroplated* with copper over a small portion of their length near the end, soldered to the board at one end, and then passed through the pins and the board, where they are tied off. Each knot is electroplated and then soldered to the board to complete the electrical connection. This electroplating and soldering process produces high strength, high-conductivity connections to the SMA wires, which is a difficult challenge.

The position of each of the pins is measured using an infrared light-emitting diode (LED) and photo-Darlington transistor pair. As can be seen in Figure 5.1, the pair is mounted in the printed circuit board, and the light from the LED is reflected past the pin to the photo-Darlington by a pair of specially designed reflectors. Dividers separate each pin to prevent crosstalk. Each pin has a tapered shoulder so that the amount of light it blocks varies with its position, which causes the collector current in the photo-Darlington to vary as a monotonic function of pin position.

* We use a solution of water and copper sulfate mixed in a 25:1 (H₂O:CuSO₄) ratio by weight, and a 5 mA plating current per wire. Each wire is plated for 5 minutes.

The circuit board also serves as a bearing surface for one end of each pin, while the top block on the display provides the second bearing surface. Together these constrain the pins to move linearly with minimal side loading. The top of each pin is recessed into the surface of the top block to provide a nearly flush surface for the user's fingertip to press against. Finally, the necessary spring return force for each pin is provided by a latex rubber membrane, which also serves as a seal.

5.3 Thermal Design

In this application, the phase transition of SMA is thermally driven, and because it is always possible to apply more electrical current to cause the wire to contract faster through resistive heating, the fundamental limitation is cooling. Because the rate of heat transfer depends on the ratio of surface area to volume, we use two small (75 micron) wires rather than one larger one to actuate each pin. We also use SMA wire with a transition temperature of 90 °C because the rate of cooling is linearly related to the temperature difference between the wires and the cooling medium.

In previous work, we found that ambient air cooling resulted in a bandwidth of perhaps 1 Hz, while forced air cooling increased this to 5-6 Hz [Ikuta 1990]. To obtain the required 30 Hz bandwidth, the present design uses a slowly recirculating bath of water. Water has been chosen as a cooling fluid because of its high thermal conductivity and tremendous heat capacity which allows for a low recirculation rate within the display. This ensures more uniform cooling of all of the wires in the display, and thus more uniform pin-to-pin performance.

5.4 Controller Design

Because of the success of the mechanical and thermal design of the display, a simple linear controller has proved adequate to drive each pin. To obtain maximum performance, it is desirable to always keep the wires operating between the minimum transition temperature and the maximum transition temperature. We use a proportional controller with a constant offset current. The current offset is used to heat the wire to near the transition temperature and its magnitude and the gain are determined experimentally. For the experiments reported here they were 0.5 amps and 4 amps/mm, respectively.

In order to achieve maximum performance, the desired positions of each of the pins are always kept slightly above zero to ensure their temperature remains at approximately the transition temperature. In addition heating the wires to more than their highest transition temperature has no effect on their length, but does require more heat to be dissipated before expansion begins, which slows the response of the display. Therefore we restrict the maximum displacement of the pins to 4.5% strain. Finally, current is limited to 2.5 amps per pin in the display to ensure that wires will not be destroyed by overheating.

5.5 Display Performance Characterization

The optical sensors were calibrated by placing a potentiometer with a lever arm attached to it on top of each pin. A 50 gram weight was placed on the lever arm and a triangular current wave drove each pin. A cubic spline was used to linearize the feedback for each pin. Figure 5.2 shows the results of the calibration for a representative pin.

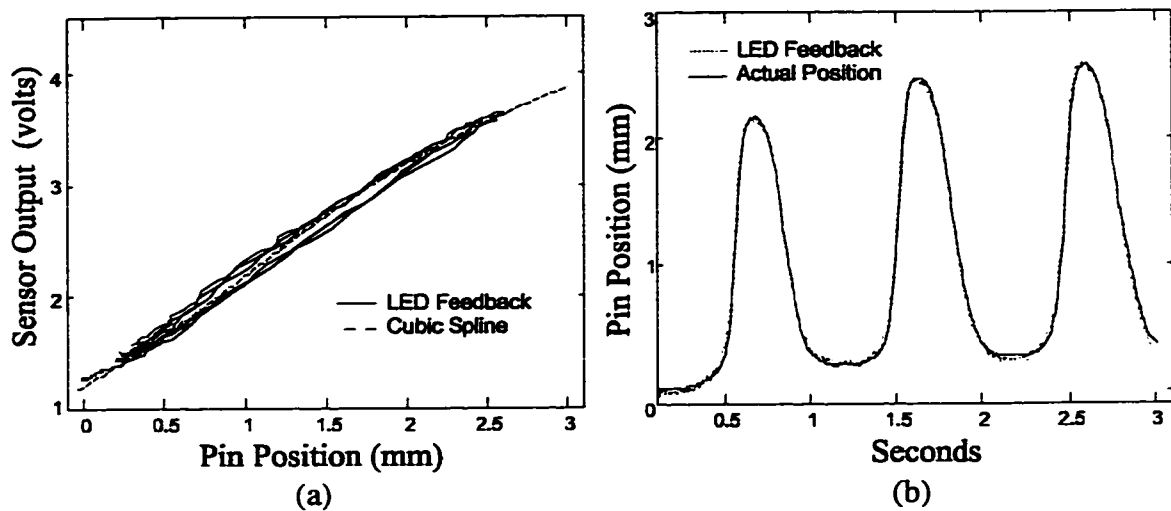


Figure 5.2 - (a) Output of the optical feedback plotted against the actual position of a pin; (b) output of the optical sensing after fitting cubic spline (dotted line) and actual position (solid line).

Figure 5.3 shows the response of a representative pin to a 1 Hz triangle wave command with 3 mm of displacement. Figure 5.3(a) shows the response under two loading conditions: no load, and when the experimenter was pressing on the entire display with finger tip force of at least 10 N. This data is replotted in Figure 5.3(b) to show the relationship between commanded and actual position; the hysteresis is well under 0.1 mm. Figure 5.3(c) shows the controller current required for each load. In the loaded case, peak current approached 2 Amps while in the unloaded case the current reached a more modest level of 1.6 Amps. Together, these figures show that the simple proportional controller ensures good performance across the entire range of anticipated load impedance.

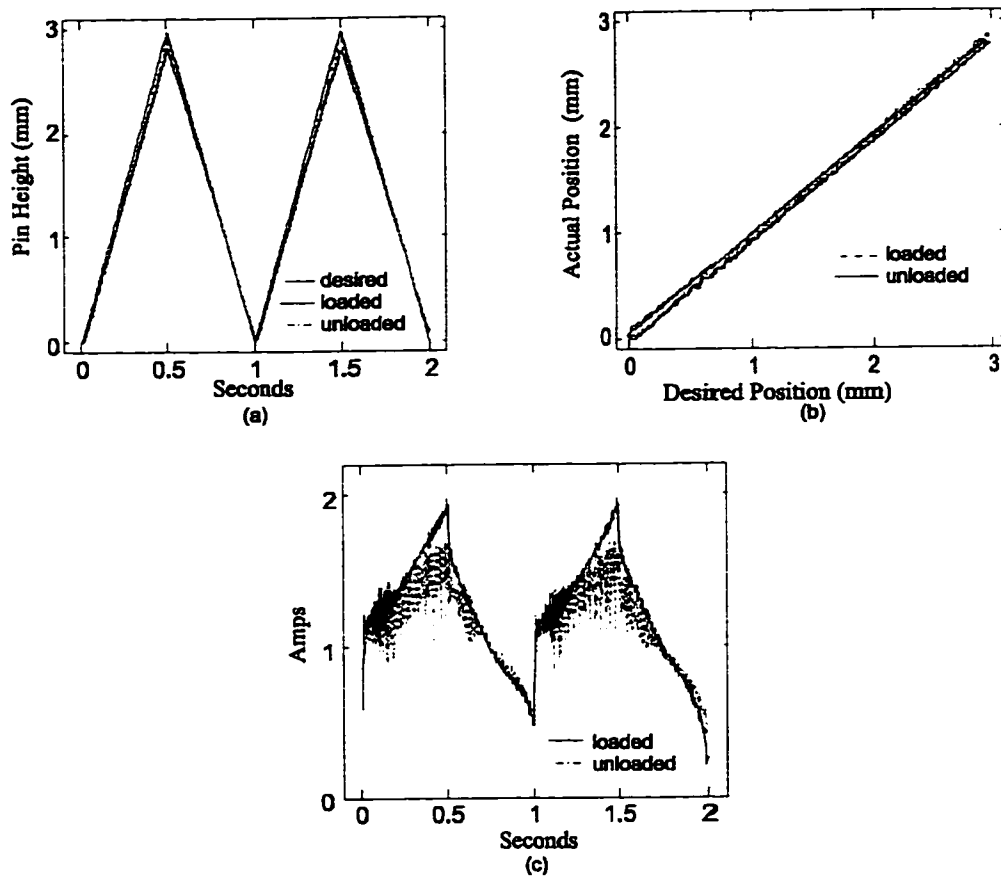


Figure 5.3 - (a) Desired and actual position of a representative pin under unloaded and loaded (finger pressing at 10 N total force) conditions, (b) the same data plotted as desired versus actual position (note minimal hysteresis) and (c) the current required under loaded and unloaded conditions.

Characterizing the bandwidth of this nonlinear system is problematic because the fall time is effectively slew rate limited by the wire cooling rate. One useful performance measure is the output amplitude at each frequency, in response to a triangle wave command at the maximum static displacement. Figure 5.4 shows the frequency response of the display when driven with a 3 mm triangle wave position command for one second with a finger pressed firmly (total force approximately 5 N) against the display. The frequency at which the output amplitude is 3 dB below the commanded input amplitude is approximately 40 Hz. Although the maximum frequency shown in the figure is 100

Hz, output can be felt at frequencies approaching 150 Hz, suggesting that the display can be used for vibrotactile feedback [Kontarinis and Howe 1995; Wellman and Howe 1995] as well as shape feedback. Table 5.1 summarizes the design targets and measured performance of the display.

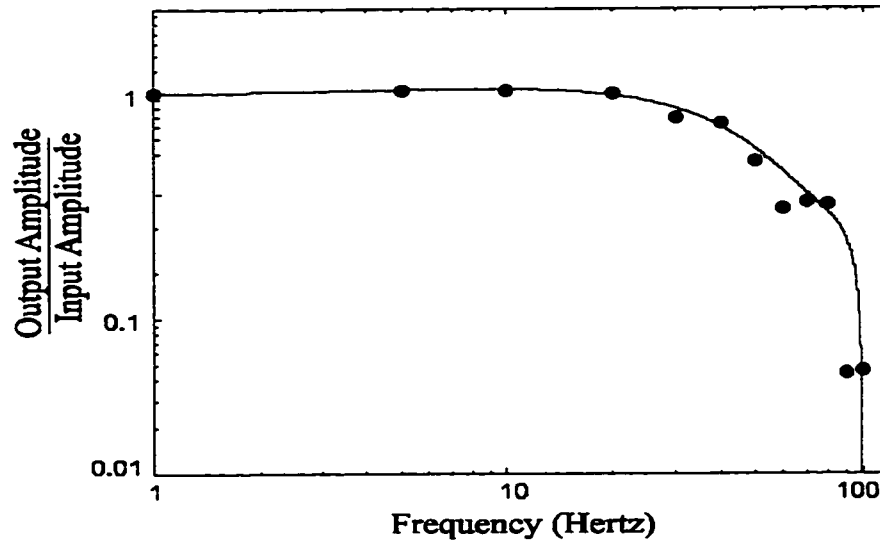


Figure 5.4. Frequency Response of the Shape Display.

Parameter	Design Goal	Achieved Performance
Pin Displacement	3.0 mm	3.0 mm
Pin Force	1.2 N	>1.5 N
Pin Stiffness (at maximum displacement)	Rigid	>35 kN/mm
Pin-to-pin Spacing	0.9 mm	2.0 mm
Frequency Response	30 Hertz	40 Hertz (-3dB point)

Table 5.1 - Design targets and measured performance of the shape display.

5.6 Effect of Bandwidth on Performance of Lump Localization

To quantify the effect of high bandwidth of the shape display on task performance, we asked subjects to perform a prototypical search task while a digital filter with a cutoff frequency of 1, 5 and 30 Hz was applied to the commanded positions for the display. These frequencies were chosen because they correspond to approximately the frequency response reported for shape displays cooled with still air, forced air and water respectively.

The display was mounted to the mouse pointer of a digitizing tablet. Subjects grasped the display with the dominant hand and rested the index finger tip on the pins. The tablet measured finger position as subjects moved within a test area. The computer sampled the display location and raised and lowered the display pins to represent virtual small-scale shapes at fixed locations. Subjects were asked to search a 150 mm diameter circle as quickly as possible to find two small dots (3 mm diameter by 2 mm height cylinders). They were asked to locate each dot in the search space and center the display on the dot and press a button. Once they found both dots, they were asked to press a second button to end the experiment. The time subjects took to search the space and their average velocity while searching were recorded.

Five subjects (three male, two female, 24 to 29 years of age) were asked to search each of eight virtual environments with two randomly placed dots as described above for the two highest bandwidths, and four virtual textures for the slowest bandwidth. Each subject was presented with the same eight (or four) virtual textures as the other subjects, and these were presented in random order. Subjects were told only that some of the

parameters of the display had changed when the frequency bandwidths were altered. Each subject was allowed two, three-minute practice periods each time that the frequency response of the display was altered in order to minimize the effect of practice on the results. They were given a maximum of three minutes to complete the search, although this limit was only reached during testing with the 1 Hz filter.

Figures 5.6 and 5.7 show the results of the experiment. The average search velocity more than doubled, going from 18 mm/sec to 55 mm/sec when the filter cutoff frequency was increased from 1 Hz to 5 Hz. The effect of going from 5 Hz to 30 Hz was somewhat less pronounced, as the velocity only increased to about 90 mm/second. The search times showed a steady decrease from approximately 150 seconds, to 50 seconds, to 25 seconds when the filter cutoff frequency was changed from 1 to 5 to 30 Hz, respectively.

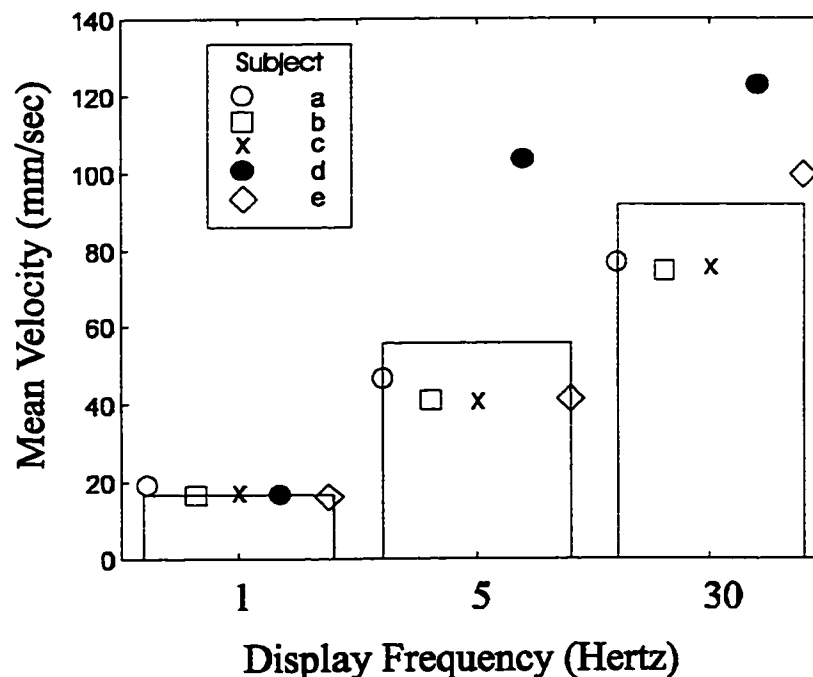


Figure 5.6 - Mean finger velocity during search for all trials at each test frequency (bars) and mean search velocities for each individual subject for each test frequency (symbols).

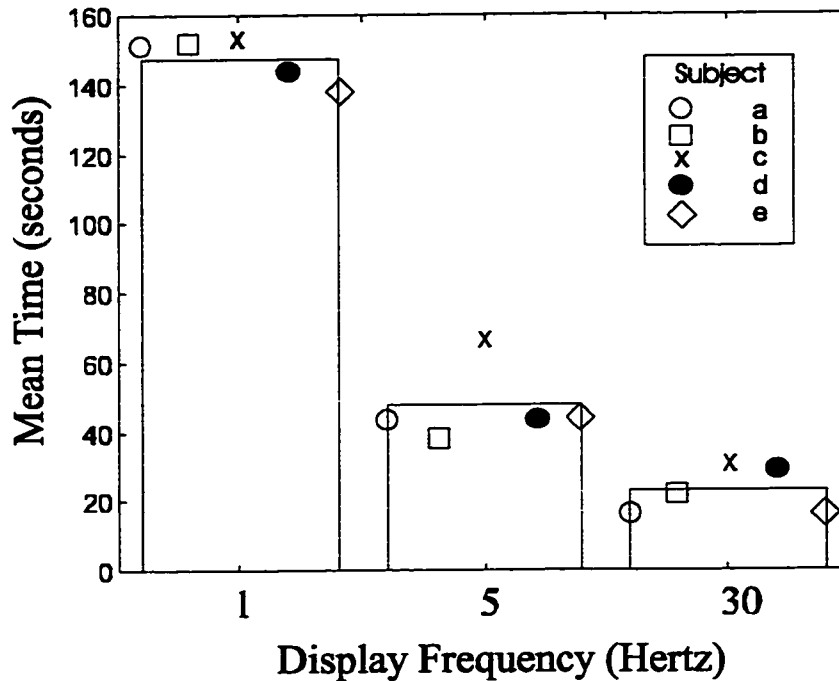


Figure 5.7 - Mean search time to find both dots (bars) and the mean search time for each of the subjects (symbols).

5.7 Discussion

This prototypical experiment shows that at least for some tasks, high bandwidth is essential for good task performance. Subjects described “extreme frustration” when using the display to search the space with the filter set at the lowest cutoff frequency. It is interesting to note that although subject *d* moved at a much higher average velocity than any of the other 4 subjects during the 5 Hz frequency trials she took nearly the same amount of time to complete the task as the other subjects. This suggests that she did a large amount of wasted searching at high speeds when the display could not move the pins up and down quickly enough. During experimentation she was observed to pass directly over the top of the dots, apparently without noticing, on more than one occasion.

This is a real concern in tasks like tumor localization where finding tumors accurately and quickly is a priority, because it will be very difficult to maintain a regular search pattern and ensure that no tumors will be missed. Thus, it is important that any tumors that may be encountered are felt the first time.

An interesting subjective result of our first studies with this display is that it is relatively easy to perceive curvature along the line of the display, but extremely difficult to perceive curvature perpendicular to it by sweeping the display. It may be necessary to compare two points on the finger pad at the same time in order to have an impression of curvature. Rotating the orientation of the line of pins can provide curvature information in other directions, but this makes sensing shape information about tactile features difficult. A two-dimensional array of pins is needed for tasks that require more realistic sensations.

Chapter 6. Taxonomy of Palpation

One of the most important aspects of a remote palpation instrument is the mechanical design of the surgical instrument itself. It physically links the tactile sensor to the tactile display and allows the surgeon to scan the sensor over internal tissues. This couples the surgeon's finger motions (kinesthetic feedback) with the small-scale shape information (cutaneous or tactile feedback). Ideally, the instrument would permit the surgeon to use hand and finger motions typically used in traditional palpation. This would provide a transparent interface so the surgeon feels as if he or she is palpating the internal tissues directly. This is a formidable task.

The human arm, hand, and fingers are an amazing mechanism with a large range of motion and high level of dexterity. Palpation relies heavily on the superb human ability to control the position and orientation of the hand and fingers. As a surgeon palpates an organ, the fingers scan over the irregularly curved tissue in a consistent manner. The fingers are orientated normal to the surface, keeping the fingerpad in a uniform contact state with the tissue. This allows control of contact in both normal and tangential directions with respect to the tissue surface. Developing a surgical instrument with this level of movement is an immense challenge. At best, a few degrees of freedom are possible. The design challenge is further complicated by the mechanical constraints imposed by the minimally invasive surgical technique. The instrument must fit through a 5-15 mm diameter entry port.

Due to these limitations on the mechanics of the instrument, it is essential to incorporate the most important aspects of natural palpation motions into the design. This requires a detailed knowledge of natural palpation motions and an understanding of how hand configuration and finger motions are chosen for a specific palpation task. This chapter presents a taxonomy of palpation. It categorizes palpation techniques based on hand configurations and finger motions. Implications of these observations for the surgical instrument design are also discussed.

6.1 Taxonomy of Palpation: Hand Postures and Finger Motions

Palpation is a broad term used to describe any medical procedure where the hands and fingers are used to probe tissue to determine mechanical properties or occluded structure. It includes a wide variety of procedures from many different medical disciplines (for example, [Chodak et al 1986; Naylor 1994; Slaton 1993; O'Reilly and Keogh 1992]). In all cases, palpation is a combination of arraying the hand and fingers in a given configuration while moving the fingers to probe the tissue. Just as there is a wide variety of palpation tasks, there is an equally diverse set of hand configurations and finger motions used during each of these palpation tasks. Because of the consistency between medical practitioners, it seems reasonable there is some logic behind why a specific motion and posture are chosen for a given palpation procedure. In light of this, it is useful to formulate a "taxonomy of palpation," with the goals of understanding the range of palpation styles, determining important parameters about the mechanics in each case, and classifying the different styles based on these key parameters.

To a large degree, this study was inspired by the work of Lederman and Klatzky [1987] on classifying motions used during haptic exploration and the work of Cutkosky and Howe [1990] on a taxonomy of manufacturing grasps. Lederman and Klatzky observed that people use a particular hand and finger motion when looking for specific information about an object that can be learned through haptic exploration. They correlated different motions with different types of exploratory procedures. For example, lateral motions are used to sense texture, pressure is used to sense hardness, and unsupported holding is used for sensing weight. Cutkosky observed machinists working in a machine shop and developed a taxonomy that classified hand configurations used during manipulation and grasping of various objects. They divided the taxonomy based on two main types of grasps: power grasps, where security and stability are emphasized, and precision grasps, where dexterity and sensitivity are important. Each type of grasp is then structured based on the complexity of the object's geometry (flat, round, small, long, etc.), and the requirements of the finger positions (prehensile using the thumb, contact with the palm, wrapping of the fingers, number of finger, etc.).

Palpation relies on the combination of hand configuration and finger motion. To adequately describe and classify palpation, it is then necessary to look at both aspects. To this end, I have developed a table of typical palpation motions and parameters that can be sensed using these motions, and a taxonomy classifying hand and finger configurations used for palpation. This required attending many surgical procedures to carefully observe surgeon's palpation motions and analyzing my personal palpation style.

Surgeons select finger motions for a palpation procedure according to the information to be learned. Table 6.1 describes some of the most frequently used palpation motions, the corresponding parameter being sensed, and typical procedures that use the motions. The finger motion has two components: normal forces/displacements into the tissue, and tangential motions caused by sliding or pushing along the surface of the tissue. The amount of normal pressure mainly depends on the type of tactile sensation associated with the task. Localizing objects embedded deep in a soft tissue requires high forces, while feeling texture requires low normal forces. The extent of lateral motions depends on whether the tactile signals are spatially distributed. Following a contour of a bone, for example, requires scanning with the fingers over relatively large distances. Sensing tissue stiffness, on the other hand, is primarily a local sensation and does not require any lateral motion.

<i>Finger Motion</i>	<i>Parameter Being Sensed</i>	<i>Example Procedure</i>
Steady applied pressure No lateral motion	Time varying pressure or temperature	Locating arteries during dissection
Varying applied pressure No lateral motion	Tissue stiffness	Detecting necrosis of the liver
Light applied pressure Fast lateral motion	Surface texture	Evaluating a rash on the skin
Heavy applied pressure Small lateral motion	Localization of hard occluded objects in soft tissue	Detecting lump during a clinical breast exam
Heavy applied pressure Large lateral motions	Contour following	Following a rib to determine location for an incision
Moderate applied pressure Differential motion between thumb and finger(s)	Function test	Sensing the thickness of an artery wall by rolling it between the fingers

Table 6.1. *Basic palpation motions.*

Because finger motion is a key aspect of palpation, finger mobility and range of motion are important parameters to characterize hand configurations. Figure 6.1 shows a taxonomy of hand configurations structured according to finger mobility. A primary determination of hand configuration is whether grasping is necessary to support the tissue. The taxonomy is divided based on this parameter.

Configurations 1-11, on the left side of the tree, show hand positions using an opposing thumb to grasp and support the tissue. In these configurations, the palpation motions primarily result from holding the hand steady while moving the fingers. In many cases this finger-based motion is desirable because kinesthetic and tactile sensations are enhanced due to the thumb and fingers probing the same tissue simultaneously.

Configurations 12-20, on the right side of the taxonomy, show hand positions where a rigid backing supports the tissue. In these configurations, the motion primarily results from holding the fingers steady while moving the whole hand. This allows palpation of large areas or organs too thick to grasp with the fingers. It should be noted that in both finger-based and arm-based motions, all of the palpation motions listed in Table 1 are possible, with varying degrees of success. The finger-based motions, for example, have limited ability for lateral motion and cannot be used to palpate internal regions of large organs.

The hand configurations in the taxonomy are arranged vertically by the amount of finger mobility possible with a configuration. For example, when using a power grip or restricted by space constraints, finger motions are very limited. When squeezing a thin layer of tissue near the edge or probing a surface with the fingertips, the fingers have a

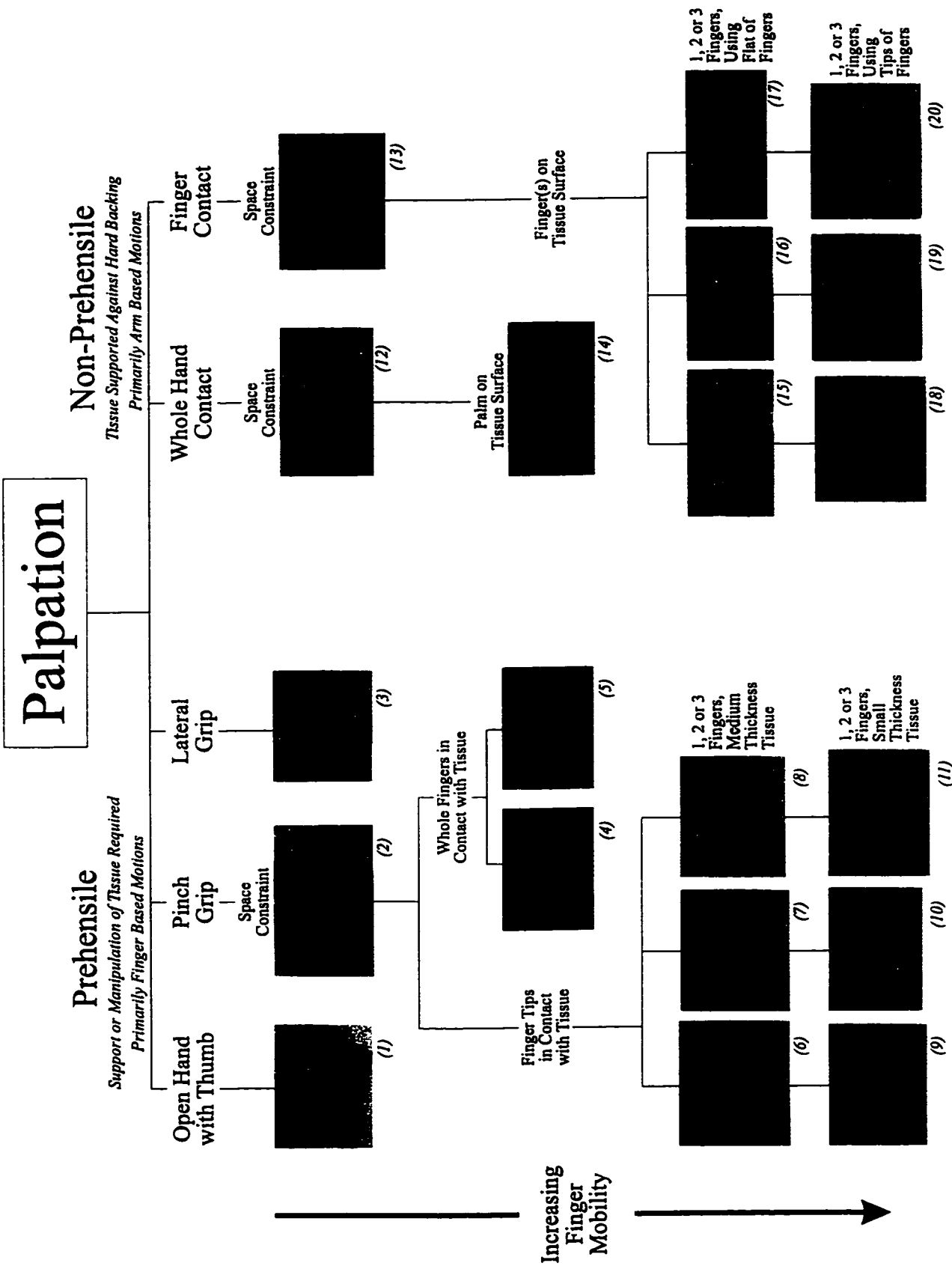


Figure 6.1. Taxonomy of Palpation Hand Configurations.

great deal of mobility. The ability to move fingers freely is crucial for maintaining a consistent contact between the fingerpad and the tissue. If the orientation of the finger cannot be adjusted or normal force cannot be controlled, the mechanical stimulus to the fingerpad is more complex and requires more concentration to perceive the desired tactile sensation.

Choosing a palpation style for a given medical procedure largely depends on maximizing finger mobility. In general, a hand configuration is used that gives the most finger motion while meeting the basic mechanical needs of the situation (i.e. Does the tissue need supporting?, Will the fingers fit in the space?, etc.). Other considerations also influence palpation. If large areas need to be scanned quickly, the whole palm or flat of the fingers may be used. If the tactile sensations are difficult to perceive, a pinch grasp may be chosen for its enhanced sensitivity.

It should be noted this is not an exhaustive description of palpation. Many other palpation techniques are used, often for a specialized task. [Baum et al. 1995] This taxonomy is based on limited observations, but it successfully classifies some of the most common and important aspects of palpation.

6.2 Resulting Design Specifications for Remote Palpation Instrument

Developing a surgical instrument that allows natural palpation motions is challenging due to the wide variety of palpation techniques. It is therefore necessary to determine the important aspects of palpation motions and incorporate these into the design. Often this will depend on the specific surgical application. From my observations, there are three main considerations. First, it must be determined if the tissue needs to be

supported by the instrument. Second, it is important to control the contact between the tactile sensor and the tissue in a consistent way. And third, ergonomics and human factors issues are critical for extended use of the instrument.

When designing a remote palpation instrument, one of the first considerations that must be addressed is determining if the instrument needs to support the tissue through grasping. This is important for the overall structure of the instrument. If the instrument must support the tissue, a gripper of some sort must be incorporated. If there is sufficient support behind the tissue (either naturally or through the use of additional tools), direct probing on the surface is possible and a gripper is not needed. These two design approaches fall into the two hand configuration categories described above. The gripper would encourage finger-based motions, while the probe would use arm-based motions. Both designs have advantages and disadvantage depending on the needs of the surgical procedure.

Maintaining a uniform contact configuration between the sensor and tissue is another important design criteria for the instrument. In normal palpation, finger mobility is a key aspect of choosing a palpation technique. The ability to freely move the fingers allows good control over the interaction between the fingers and tissue. This provides a regular input stimulus, or baseline, to the tactile sensory system. If the interaction is not well controlled, and the force and orientation of the finger is significantly varied during the palpation motion, the baseline sensation will change. A steady baseline causes the tactile sensations of interest (for example, the pressure concentration indicating the location of an embedded object) to more clearly stand out against the sensations felt from contacting normal tissue.

Similarly, the success of a remote palpation instrument largely depends on the surgeon's ability to scan the tactile sensor over the surface of an internal organ in a consistent manner. This involves maintaining a uniform contact force while keeping the sensor normal to the organ's surface. The tactile sensations measured by the sensor will be much easier to interpret due to the consistency of the baseline sensations. As was shown in chapter 3, this greatly simplifies the necessary signal processing.

A final consideration for the instrument design is ergonomics. Current minimally invasive surgical techniques have many ergonomic problems [Berguer 1996; Berguer et al. 1996]. Typically, surgeons rigidly stand in the same position and do not shift their weight for long periods of time. They concentrate on a video monitor located slightly above eye level on the other side of the patient. The tools are awkward to use and often require elbow and wrist joints to rotate outside of comfortable limits. Surgeons often feel fatigued after performing a minimally invasive procedure. At times, the surgical tools can cause pain. During retraction, a surgeon may apply excessive force to a scissors grip handle for extended periods. This causes high stress concentrations on the fingers, cutting off circulation and cramping muscles. There is evidence that minimally invasive surgery causes repetitive stress injuries [Berguer and Beckley 1996]. A tool that causes pain or injury is unacceptable. An effective remote palpation instrument design should not cause any of these problems and should coordinate well with the surgeon's natural arm, hand and finger motions.

Chapter 7. Remote Palpation Instrument

The prototype of the remote palpation instrument draws the components discussed in the previous chapters together by incorporating the tactile feedback system into a surgical instrument. The key hardware components include the tactile sensor at the tip, the shape display on the handle, and a linkage connecting the surgeon's hand and finger motion to the sensor's motion. In order to be usable in minimally invasive thoracic surgery, the sensor and distal portions of the instrument must fit through a 5-15 mm diameter entry port. The design should also implement the ideas outlined in the previous chapter. It must work with natural hand and finger motions, allow consistent contact interactions between the sensor and tissue, and minimize ergonomic problems.

Analysis aiding the design of these mechanisms is often too difficult. Building and testing prototypes, on the other hand, is an excellent way to understand which aspects of a design are crucial for a successful device. Often, ideas that look great on paper are fundamentally flawed. This quickly becomes apparent when testing the prototype. The opposite is also true – ideas that seem unworkable are later perceived as elegant solutions after a prototype is constructed. Rapid prototyping provides valuable feedback that is difficult to obtain any other way. In light of this, the development of a working prototype of a remote palpation instrument will greatly contribute to the process of understanding the design space for these devices. This chapter presents the evolution and testing of a prototype I developed. It involves the integration of many of the ideas and hardware previously discussed in this thesis.

7.1 Design Approaches

One of the first design considerations that must be addressed is choosing the type of palpation motion the surgeon will use with the instrument. This will determine if the instrument acts as a grasper or a probe. From the taxonomy presented in Chapter 7, there are two main types of motions: finger-based and arm-based palpation. The choice is often determined by whether grasping is necessary to support the tissue. If finger-based motions are incorporated into the instrument, a mechanism is needed to link the surgeon's finger motion to the sensor motion. By using a supporting plate under the sensor, tissue can be grasped and palpated. This is advantageous because the tissue does not need to be rigidly backed. On the other hand, if arm-based motions are used to move the instrument, the tissue needs to be well supported as the sensor probes the tissue surface. There are advantages and disadvantages for both of these designs.

The material stiffness of lung tissue is proportional to the lung's inflation pressure [Lai Fook 1976]. In minimally invasive thoracic surgery, the lung is partially deflated to make room for manipulating the tissue and viewing the pleural cavity. This causes the lung to be extremely compliant and pliable. The ribs in the chest wall can provide a rigid support for probing the lung, but often the lobes are not against the chest wall. This is especially true when the surgeon continually moves the lung with a grasper while searching for a nodule. Since adequate support of the tissue may not be available, a finger-based motion design was chosen.

7.2 Finger-Based Motion Design

One configuration for a finger-based motion instrument is intended to grasp the tissue between the sensor and a rigid support plate. The motions of the sensor are controlled through a linkage connected to the surgeon's finger. As discussed in Chapter 7, palpation uses two main types of finger motion: indentations normal to the surface into the tissue, and lateral motions sliding along the surface. During a pinch grasp with the index finger held straight, most of the rotation of the index finger occurs through the metacarpal-phalange (MCP) joint. Normal forces are applied by squeezing with the thumb and finger together, and lateral motions are produced by moving the index finger side-to-side. The linkage connecting the surgeon's finger to the sensor should synchronize with these natural motions.

The finger-based motion prototype design is shown in Figure 7.1. Mechanical construction of this prototype was done by Emans [1996]. It consists of a two degree of freedom cable driven linkage. The surgeon controls the position of the sensor by moving his or her finger, allowing remote tissues to be grasped between the sensor and rigid support plate. The up and down movements of the finger control contact force between the sensor and tissue. The mechanism also reflects these forces back to the surgeon's finger, which is important for assessing tissue stiffness. Lateral motions of the finger slide the sensor across the tissue surface. Tactile sensations produced during sliding are measured by the sensor and recreated by the shape display. The linkage extends over the index finger and holds the shape display against the fingerpad. This causes the whole shape display to move with the finger, which is important for correlating tactile and kinesthetic sensations.

To permit natural finger motions, a gimble placed the center of rotation of the linkage at the MCP joint of the index finger. The sensor attached to the main instrument shaft through a universal joint. This permits horizontal and vertical rotation about the joint. Four cables running inside the instrument shaft force the orientation of the sensor to match the finger's orientation. A consistent contact interaction between the sensor and tissue is possible if the tissue thickness remains constant across its width.

Figure 7.1 shows a drawing and picture of the prototype. To simplify construction, this version was slightly oversized. The main shaft and support plate are 20 mm wide, which would not pass through a 15 mm diameter surgical entry port.

At the Center for Minimally Invasive Surgery at the Harvard Medical School, tests were conducted with our prototype in a pig thoracic cavity – with little success. Both kinesthetic and tactile sensations through the instrument were unusable. Compliance in the cable drive mechanism made the sensor hard to control and provided confusing force feedback. Another problem resulted from the size of the support plate. At large rotation angles, the sensor would fall off the edge of the plate. Additionally, the position feedback of the pins in the shape display was not working and control was purely open loop. This caused tactile sensations to vary significantly with time. This was all complicated by the crescent shaped chest cavity of the pig, which greatly reduced valuable operating space.

The design of the linkage was also lacking. The area of tissue that could be palpated was limited because the tissue needed to be in line with the sensor and support plate. The orientation of the support plate was fixed and remained in line with the instrument shaft.

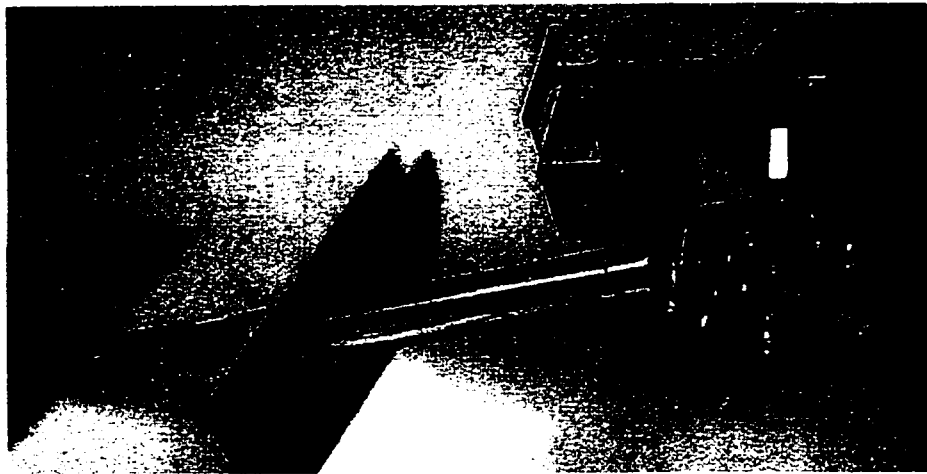
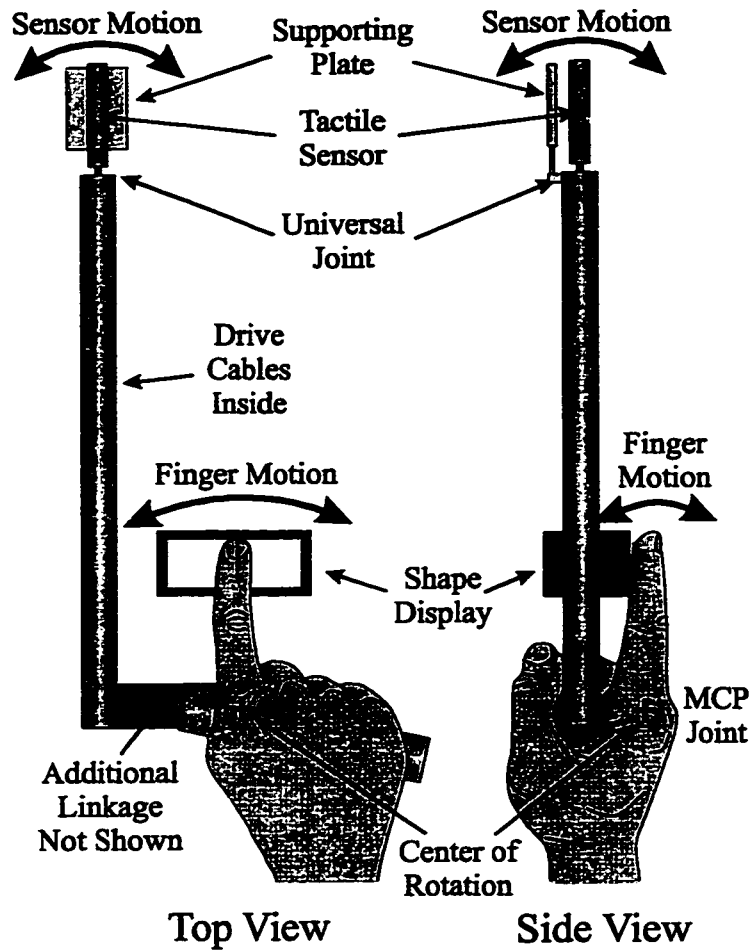


Figure 7.1. Finger-based Motion Prototype. The sensor follows the surgeon's finger motions by means of a two-degree of freedom cable drive linkage. Forces against the sensor are reflected back to the finger. A gimble places the center of rotation at the MCP joint of the index finger.

The addition of a wrist would increase the amount of tissue that could be reached; however, tissues away from the edge of the lung would still be difficult to palpate due to the limited size of the gripper. It was also observed that the lateral motions of the finger became fatiguing. The weight of the shape display also impeded palpation. In fact, a counterweight was needed to support the display in the normal direction.

7.3 Arm-Based Motion Design

The disappointments of the previous prototype taught many lessons. Designing a satisfactory two-degree of freedom linkage into a minimally invasive tool is challenging. The palpation motions used by the design were fatiguing and unsatisfactory because of the limited search area. The next prototype investigated the alternative approach, arm-based motion design. With this technique, a rigid shaft transmits the motions of the surgeon to the sensor by pivoting about the fixed rotation point imposed by the surgical entry port. The design provides excellent position and force transmission through the rigid shaft. Arm-based designs also allow more tissue to be palpated due to the large angles that can be swept out. Because the probing motions with the sensor are similar to single finger palpation, the tissue must be supported by some other means. This could be a problem in surgery. However, after observing minimally invasive procedures, it became clear to me that support for the tissue can be achieved by carefully positioning the lung against the ribs or by using other tools to provide a rigid backing.

7.3.1 Sensor to Instrument Shaft Joint Design

A major challenge of using this design is determining how to make a consistent contact between the sensor and tissue. A passive or actuated joint is necessary to align the sensor with the tissue surface. A consistent contact interaction allows signal processing to be simplified. As shown in Chapter 3, rocking the sensor causes confusing signals to the surgeon. If the ends of the sensor dig into the tissue, the pressure distribution caused by the homogeneous tissue will not be uniform. Because the prototype shape display has relatively low fidelity, it is necessary to have a high signal-to-noise ratio between the sensations of the tissue and the pressure concentration caused by the lump. Surgeons would have difficulty differentiating varying baseline signals from the pressure concentrations induced by the presence of a lump. The design must therefore work to eliminate this rocking motion by connecting the tactile sensor to the instrument shaft with a passive joint. The orientation of the sensor could then adjust to the contour of the tissue surface.

Because there are so many factors, initial analysis is not always practical. Therefore, a “cut and try” approach was used to determine the correct type of passive joint to utilize. Many simple prototypes were constructed and tested on rubber models. This was an interesting process with many surprises along the way. With some designs, it took only 30 seconds of playing with the prototype to reject the idea. This was true with the first sensor joint prototype constructed. It used a universal joint between the sensor and instrument shaft. It was chosen because it allows the sensor to completely orient itself to the tissue by forcing the torque about the joint to be zero. This would ensure a uniform contact pressure distribution. After trying the prototype on a rubber model, we realized a

planar contact surface is needed for this to work. The round sensor design flopped to the side as lateral forces were applied to the joint. This made sliding the sensor across the surface impossible.

In the next prototype, a pin joint perpendicular to the length of the sensor was used. This allowed rotation in only one direction and held the sensor upright. Once again, a valuable lesson was learned from the prototypes. If the pin joint is located a significant distance above the interface between the tactile sensor and tissue, the ends of the sensor would dig into the tissue as the sensor was slide forward and backward. Figure 7.2 shows the situation. The force imposed on the instrument shaft on the pin joint can be split into forces in the directions normal and tangential to the surface of the tissue in contact with the sensor. To maintain a force balance, the tissue imposes an equal and opposite force on the sensor surface. Friction between the sensor and tissue causes a torque to be generated about the pin joint. The amount of torque is proportional to the coefficient of friction and the distance between the sensor surface and pin joint. This torque causes the sensor to rotate and digs the edges into the tissue when attempting to slide in the direction parallel with the sensor axis. This rocking motion would create a non-symmetric baseline pressure on the sensor. Reducing the distance between the pin joint and the sensor surface can minimize these effects.

Moving the center of rotation of the sensor to the surface is difficult with a pin joint because the pin would need to be located on the sensor's surface. It is possible to move rotation point to the surface artificially using a four-bar mechanism. Figure 7.3 shows a possible mechanism configuration. The sensor is attached to the instrument shaft through two links. The remote center of rotation for the mechanism is shown with an arrow. This

point remains fixed as the sensor rotates. This would cause frictional forces to act through the center of motion and not create a rocking torque. Unfortunately, this design is impractical for a minimally invasive tool due to the limited range of rotation and added size. It would be difficult to fit the device through the 15 mm entry port.

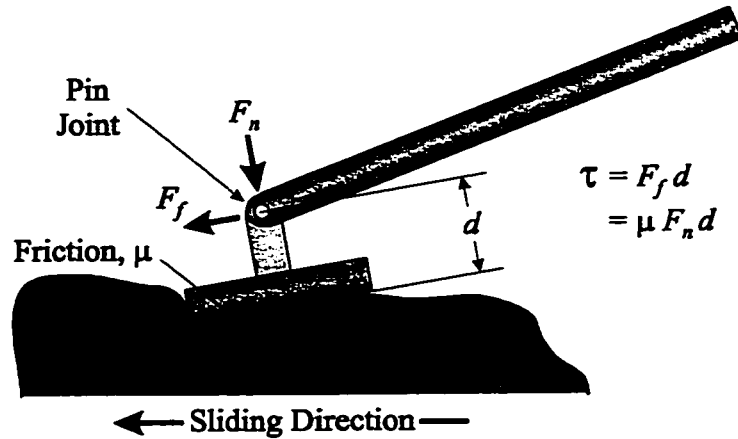


Figure 7.2. *Tactile Sensor with Pin Joint Digging into Tissue.*

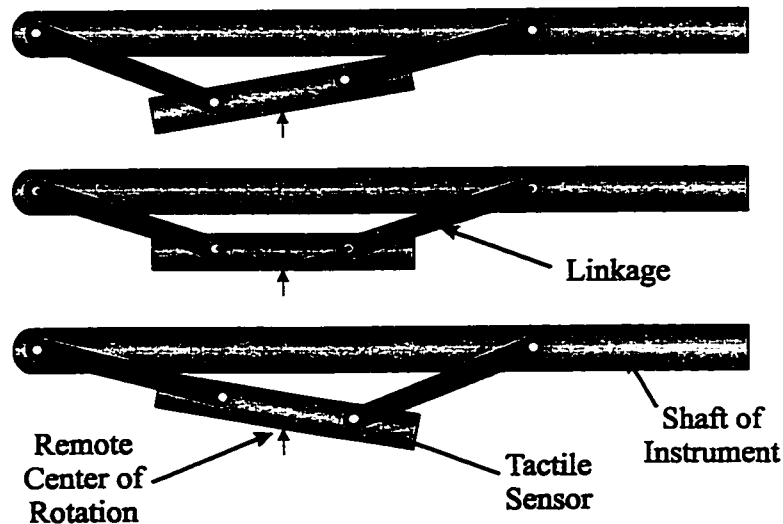


Figure 7.3. *Remote Center of Rotation 4-Bar Mechanism.*

The final configuration for the joint connecting the sensor and instrument shaft is shown in Figure 7.4. A pin joint was located as close to the sensor surface as possible. The figure shows the sensor in a consistent orientation with respect to the surface while following the contour of the lung. There will be some rocking induced by the friction, but this should be minimal because the lung's surface is extremely slippery. An additional benefit of this configuration is the sensor can be rotated into alignment with the instrument shaft, allowing the sensor to easily pass through the entry port.

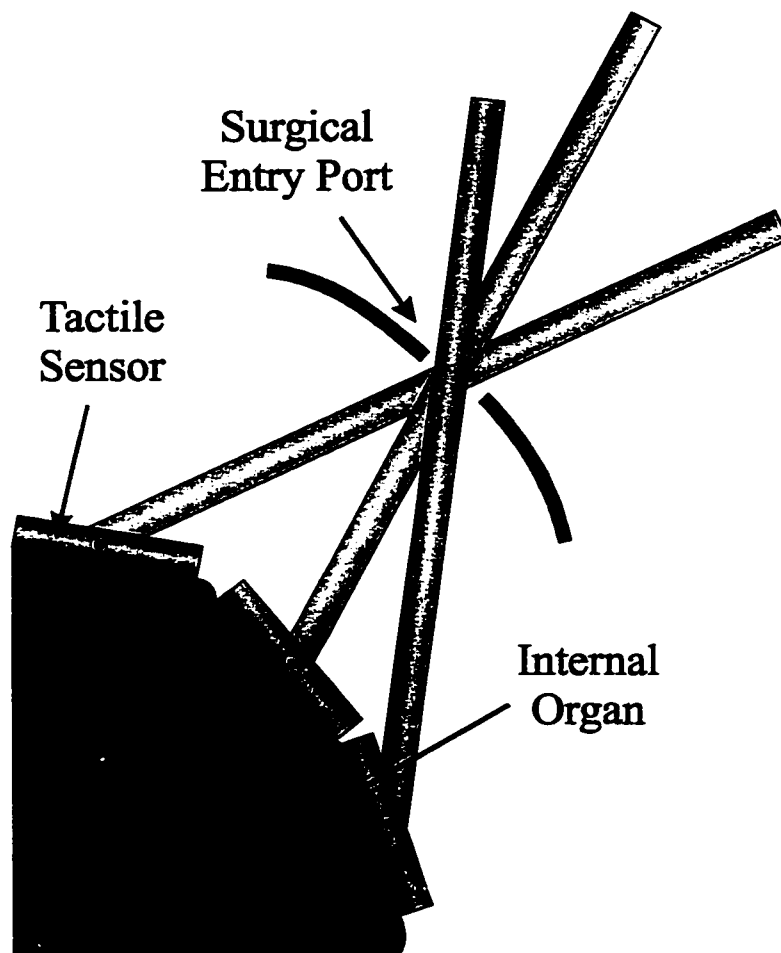


Figure 7.4. *Contour Following with Passive Pin Joint.*

7.3.2 Handle to Instrument Shaft Joint Design

The next aspect of the instrument design investigated concerned connecting the handle and shape display to the other end of the instrument. It was determined a joint was needed at this end as well to prevent ergonomic problems. If the display is rigidly aligned with the instrument shaft, awkward hand and arm motions are needed to probe the internal tissue. If large angles are traversed with the instrument, the wrist may be forced to hyperextend.

The first prototype constructed incorporated a pin joint connecting the instrument shaft to the handle and shape display. The pin was perpendicular to the axes of the finger and instrument shaft. This allowed the hand to remain horizontal as the sensor was scanned side to side. Figure 7.5 shows the hand motions necessary with this design. It is obvious from the drawing that the wrist rotates significantly during the palpation motion.

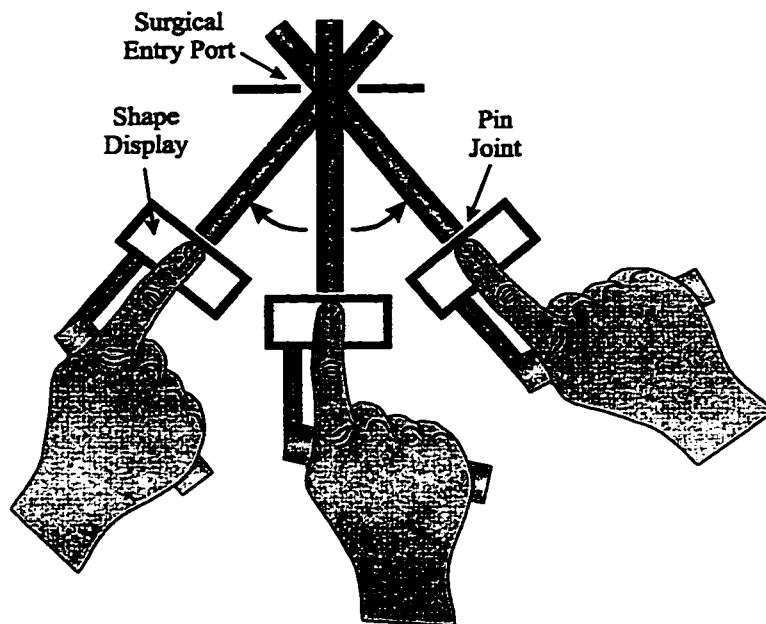


Figure 7.5. *Hand Motions Necessary with Pin Joint at Handle.* (Note: the axis of the pin is in the plane of the paper.)

The second prototype design used a universal joint to connect the handle and display to the instrument. Figure 7.6 shows the hand motions used during a palpation motion with this design. As can be seen, the hand and wrist remain in a near constant orientation. The instrument is maneuvered using more natural motions of the whole arm. One problem with this configuration is the sensor would roll during lateral movement when the angle between the sensor and instrument was near 90 degrees. If a single line of sensing elements is used, as in our system, this can cause the active area of the tactile sensor to roll off the tissue. This problem can be overcome by putting tactile sensing elements around a larger fraction of the sensor circumference.

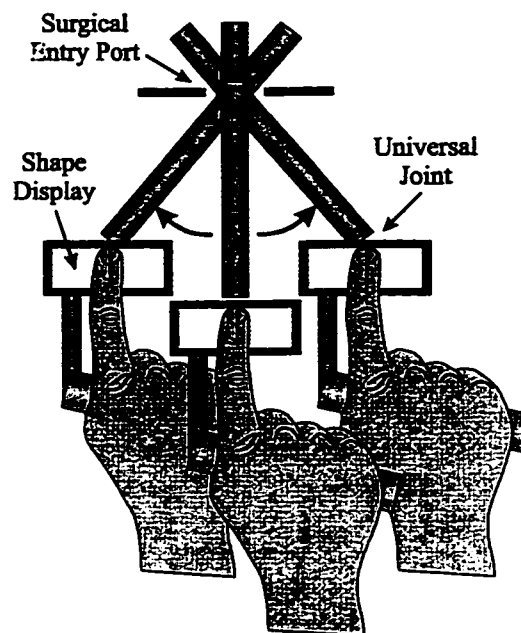


Figure 7.6. *Hand Motions Necessary with Universal Joint at Handle.*

The center of rotation imposed by the surgical entry port creates problems with an arm-based design. The mapping between the motions of the surgeon's finger and the motions of the sensor can be confusing as there is mirroring between these two motions.

As the surgeon moves his or her finger left, the sensor moves right, and vice versa. In our prototype system, this reversal of left and right is not a problem because we use a line of sensors and pins. If a 2D array of pins were used, the small-scale shape would need to be mirrored so tactile and kinesthetic sensations would be correlated.

If the angle between the sensor and instrument shaft is near 90 degrees, motions along the axis of the sensor cause a mirroring as well. In the target application of thoracic surgery, the angle is often around 30 degrees. In this configuration, motion along the axis of the sensor is accomplished by sliding the instrument in and out of the entry port. This does not mirror the motions. An additional problem the mirroring effect causes is normal forces into the tissue are created by lifting on the handle. This causes the kinesthetic force-displacement sensations of the finger to be in a different direction from the tactile sensations. Often, the more the handle of the instrument is lifted, the higher the pins on the display are raised.

7.4 Final Prototype Performance

The combination of the pin joint at the sensor and the universal joint at the handle produced a workable instrument design. Many of the specifications previously describe were accomplished. A consistent contact interaction between the sensor and tissue can be maintained while using natural hand and finger motions. The fixed rotation point created by the entry port does cause difficulties, but these obstacles can be overcome through training.

Figure 7.7 shows a picture of the working version of the arm-base motion prototype. This is the culmination of the design portion of this thesis. The specifications of the array

sensor are described in Chapter 4. The shape display is described in Chapter 6. The signal processing technique uses baseline subtraction (as described in Chapter 4) to determine drive commands for the display from the sensor readings.

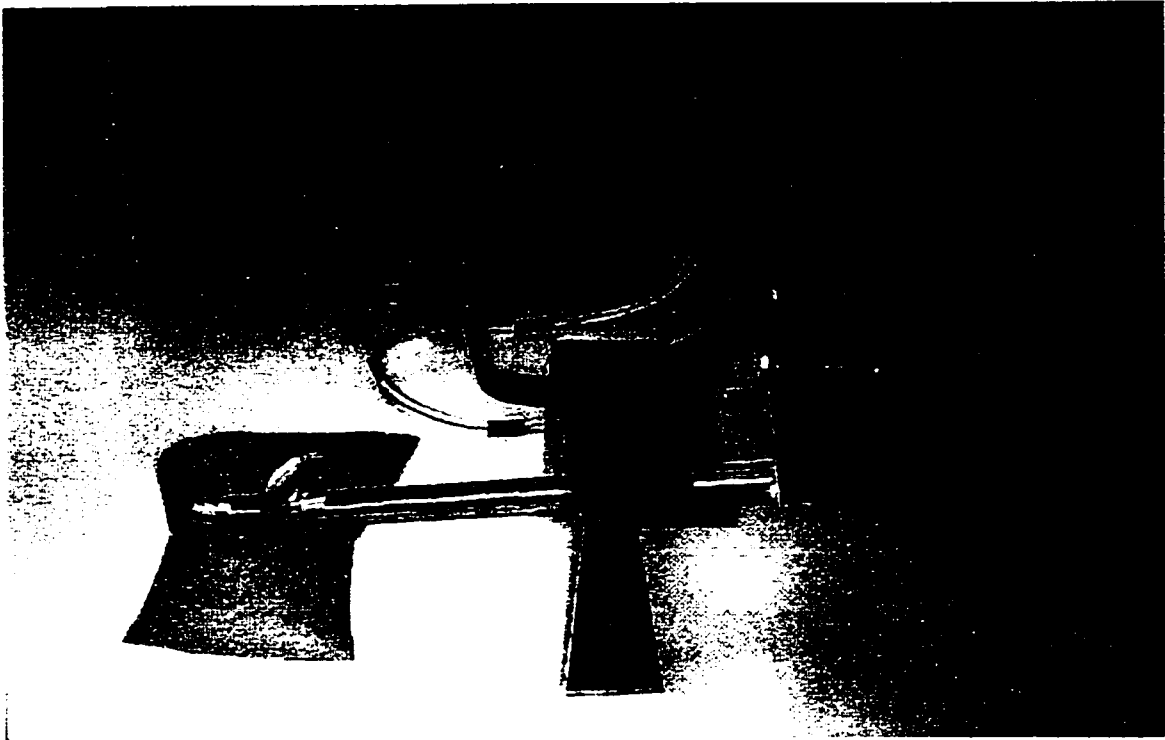


Figure 7.7. *Working Prototype of Arm-Based Remote Palpation Instrument.*

As with the finger-based motion design, the prototype was slightly oversized to simplify construction. The instrument shaft is 16 mm in diameter. The pin joint through the sensor rotated enough to align the sensor with the instrument shaft for insertion through the surgical entry port. After insertion, the sensor can rotate out and scan the tissue. The cabling for the tactile sensor are looped to lower torsional stiffness. As shown in Figure 7.2, it is important to minimize the torque about this joint.

The performance of the tactile feedback is adequate to locate lumps in rubber models using the instrument in a minimally invasive configuration. The signal processing technique described in Chapter 3 works well and only provides a major stimulus when a lump is located. The baseline subtraction successfully removes sensations created when normal, homogeneous parts of the rubber model are palpated. (Results from a typical palpation trial will be presented below.) Informal experiments showed lumps near the surface of a rubber model could be located with the prototype instrument, but could not be detected without the tactile feedback present. In this case, kinesthetic information alone was not enough. Only the stress concentration induced by the lump during contact made localization possible.

The controllers for the shape display used in the prototype are not set for peak performance as was demonstrated in Chapter 6, as this causes the SMA wire actuators to break often. The resulting control reduces the fidelity in the small-scale shape information, but the performance is still reasonable for completing a localization task. Figure 7.8 shows one of the pins (randomly chosen) tracking slow triangle and square waves. The position error during this motion was less than 0.1 mm for the triangle wave. The rise times of the pin for the square wave are less than 0.45 msec with a steady-state offset of 0.07 mm. The fall times are less than 100 msec with a steady-state offset of 0.04 mm.

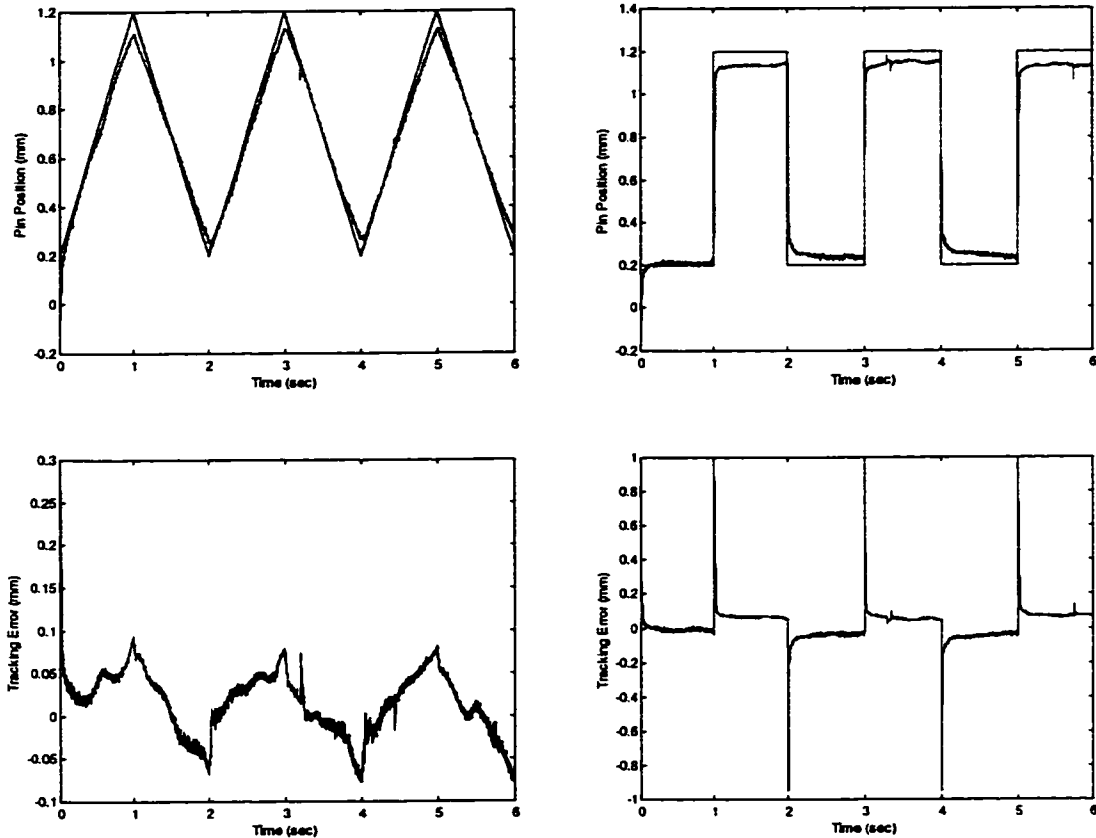


Figure 7.8. *Pin Motion Tracking a Triangle and Square Wave*

7.5 Lump Localization Experiment using the Remote Palpation Prototype

After initial tests with the remote palpation instrument prototype, many important questions arose about the requirements of the location and weight of the shape display. The weight of the display is approximately 350 g when the water-cooling tubes and electrical wires are included. After using the instrument for a time, this became tiresome to support this weight and apply the additional upward forces (5 to 10 N) used to indent the sensor into the rubber model. In one test, I tried taking the shape display off the instrument and used my other hand to feel the tactile feedback. This resulted in the

tactile sensations being felt in one hand while the kinesthetic sensations were sensed with the other. Surprisingly, this caused little deterioration in the ability to detect and localize lumps. In fact, the instrument became easier to control due to the decrease in mass. If the display can be taken off the instrument, its design can be greatly simplified. Relaxing space and weight requirements would permit the use of actuators that provide higher fidelity positioning while maintaining fast pin motion. In light of this, I performed an experiment to measure how localization times and palpation techniques are effected by these parameters.

7.5.1 Experimental Methods

In this experiment, subjects located hard plastic balls embedded in rubber models. The setup and experimental technique is similar to the finger velocity experiments presented in Chapter 6. Figure 7.9 shows the setup used for this experiment. Rubber models 25 mm thick were created by pouring a soft two-part silicone rubber (GE6166) into a 12 cm diameter glass petri dish. The thickness of the rubber exceeded the height of the sides of the dish by 10 mm so the hard edges would not be perceived as lumps. In each model, three 9.5 mm diameter plastic balls were embedded 1 mm from the model surface. Placing the lumps near the surface provided a large tactile signal when the sensor scanned over them. The location of the lumps could not be determined using kinesthetic sensations alone while using reasonable force levels. The surfaces of the rubber models were covered with a 0.15 mm thick sheet of latex rubber for protection. This also visually occluded the location of the lumps in the model. A hand lotion was used to lubricate the surface of the latex to minimize friction with the sensor.

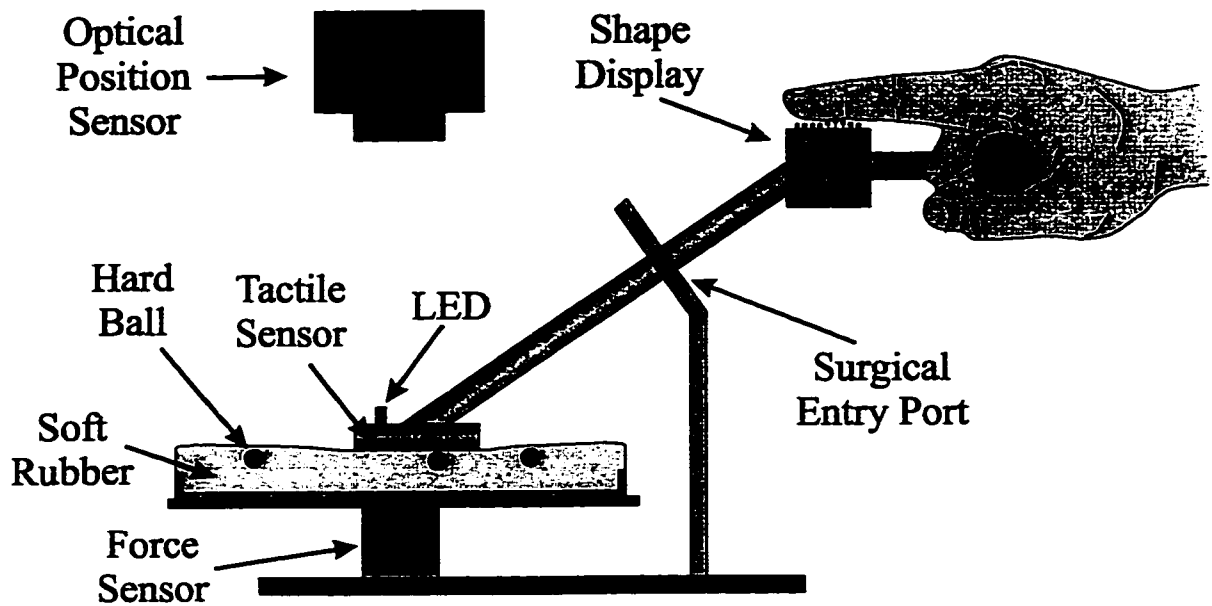


Figure 7.9. *Setup for Minimally Invasive Lump Localization Experiment.*

An important aspect of prototyping and testing is to mimic the surgical situation as closely as possible. For this reason, a video camera and monitor were used for the subjects to view the model during a palpation trial. A screen blocked the direct view of the model and instrument tip. This increased the difficulty of the task because subjects were forced to look at the monitor and could not view their hands. The camera's viewing angle was approximately 30 degrees off from viewing angle of the subject. Because the camera was close to the model, relative sizes of objects were distorted. Objects near the camera appeared larger than objects away from the camera. These are realistic problems in minimally invasive surgery and increase the difficulty of smoothly controlling the sensor.

A rigid support with a hole simulated the ribs and chest wall. The hole acted as the surgical entry port with instrument passing through it. The physical layout of the entry

port, camera, and model were based on real measurements taken in thoracic surgery. To assign a coordinate frame, the y direction is perpendicular to the entry port and the x direction lies across the model as shown in the figure. The center of the rubber model was aligned in the x direction with the entry port and located 15 cm away in the y direction with 6.5 cm of vertical spacing. The resulting angle between the model surface and the instrument is realistic for thoracic surgery. The camera lens was 11 cm away from the entry port in the x direction, 11.5 cm from the center of the model in the y direction, and 7.5 cm above the model surface. The monitor was located slightly above eye level approximately 1.5 m from the subject.

To measure the palpation motions used by subjects during the experiment, contact force and the location of the instrument tip were recorded. A force sensor located under the rubber models (RMS noise 0.013 N, range 20 N) measured normal forces between the tactile sensor and the rubber model. The location of an LED glued to the top of the sensor was tracked using an optical position sensor located 70 cm above the surface of the model (RMS noise 0.05 mm, range 150 mm). The signals were sampled using the same computer running the control for the tactile feedback. The signals were filtered in hardware using a 2 pole low-pass filter with a cutoff frequency of 25 Hz. The data was recorded at a 100 Hz sampling rate. In software, the signals were filtered again with a 4 pole low-pass filter with a cutoff frequency of 20 Hz. A finite difference method was used to calculate the instantaneous velocities in the x and y directions. The speed of the sensor during the trial was found by computing the magnitude of the velocity vectors.

For this experiment, subjects were asked to locate all three lumps in the rubber model with the instrument as quickly as possible. When one of the lumps was located, the

subjects were instructed to center the sensor over the lump and verbally indicate a lump had been found. A button was pressed to indicate the perceived location. Three types of trials were included in the experiment. In the first type, subjects located lumps with the shape display mounted on the instrument. In the second type of trial, the shape display was removed from the instrument and held in the opposite hand from the one used to control the motion of the instrument. The third type was similar to the second in that the display was off the instrument, but a dummy weight of 350 g was added to instrument to simulate the weight imposed on the instrument by the display. In all three types of trials, the instrument was running the tactile feedback system using the same control parameters.

A total of six voluntary subjects (4 male, 2 female, mean age 22 years) completed five trials for each of the three trial types. The same five models were presented for each type and the order was randomized to prevent subjects from learning the location of the lumps in the models. To minimize learning effects in the data, the subjects were given extensive practice times to become familiar with the setup for each trial type. Preliminary studies showed the practice time used was adequate. All five trials for each type were taken consecutively. The order of type was the same for all subjects. The shape display on the instrument was done first, followed by the display off the instrument and finally with the display off and the dummy weight on the instrument. Localization time for a trial was determined from the time the contact force crossed a 1 N force threshold until the third button press. The average sensor speed for the trial was calculated by taking the mean of the speeds during the localization time period. Maximum speeds were measured by taking the third highest peak during this same time

period. This technique was chosen arbitrarily, but had the goal of minimizing possible errors induced by occasional noise peaks in the data.

7.5.2 Results

The sensor position during a typical trial is shown in Figure 7.10. The results from this same trial are shown in Figures 7.10 through 7.16. The dotted line shows the path of the sensor. Some indication of sensor velocity can be seen because the dots are spaced at equal 100 msec time intervals. The large outer circle shows the boundary of the rubber model. The small circles indicate the locations of the lumps as indicated by the subject. Figure 7.11 shows the contact force between the sensor and rubber model and the state of the button used to signal a lump was found. All subjects used contact forces between 3 and 10 N. The speed of the sensor during this trial is shown in Figure 7.12. In this trial, the mean speed was calculated at 41 mm/s and the maximum speed was 120 mm/s.

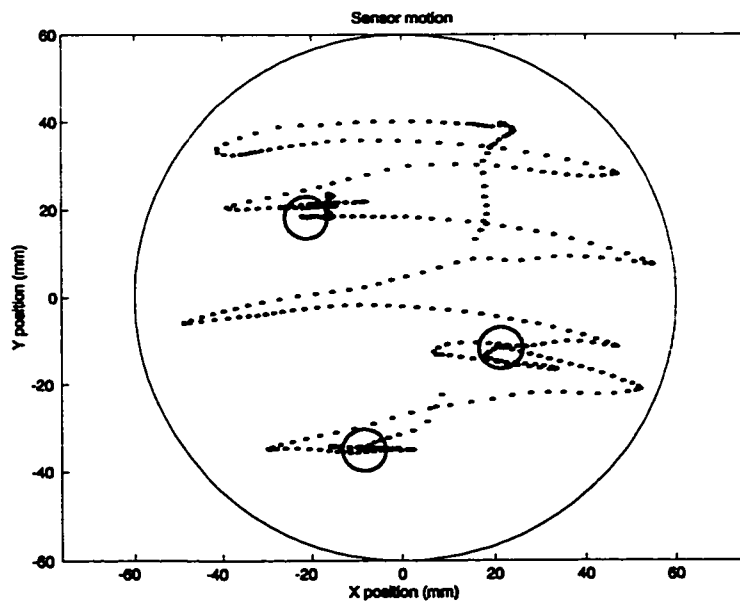


Figure 7.10. *Position of Sensor during Typical Trial.*

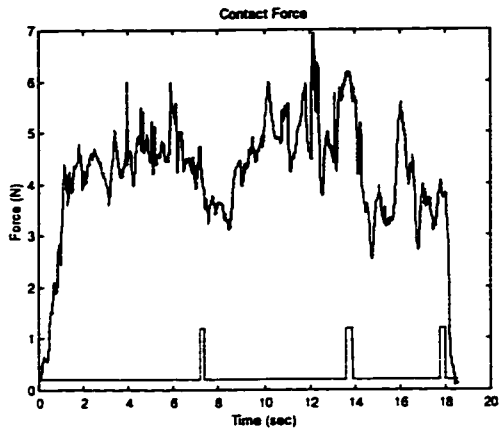


Figure 7.11. *Contact Force during Typical Trial.*

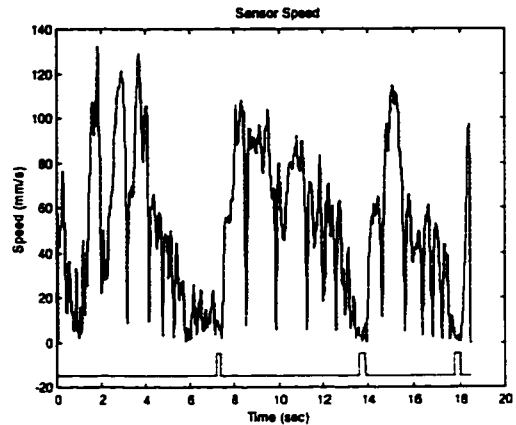


Figure 7.12. *Sensor Speed during Typical Trial.*

The desired positions versus time of all ten pins of the shape display are shown in Figure 7.13a. Figure 7.13b shows the spatial distribution of these desired positions versus time. As can be seen, when the sensor passes over the top of a lump, a quick spike was generated in the command position, forcing the pins up. The distribution of the lump covered approximately 5 to 6 mm or 3 tactile elements. When the subject held the sensor over the top of the lump a sustained position command was generated.

Figure 7.14 shows the actual position of the pins versus the desired command positions during a typical trial. This gives an indication of the fidelity of the display during actual experimental conditions. The solid line in the plot shows the ideal one-to-one correspondence. Perfect pin control would result in all of the data points falling on this line. For this data, the dotted lines show the bounds that include 95% of the points.

The signal processing algorithm described in Chapter 3 was implemented in the display controller. This involved scaling the actual pressure readings to produce a flat response when contacting homogeneous rubber and then subtracting off the minimum

reading. Figure 7.15 shows the desired position of the pins when the baseline that was subtracted is added back to the signals. The baseline varies with contact force. The signals away from the spikes caused by the lumps are actually 10 curves closely on top of each other. These uniform readings from the sensor are accomplished through a combination of the pivoting sensor head and the adjusted gain correction described in Chapter 4. Figure 7.16 shows signals collected from the sensor if the gain adjustment is not included and each element reports true pressure. Determining the lump location using these desired position commands could be difficult, especially with the current fidelity of the shape feedback.

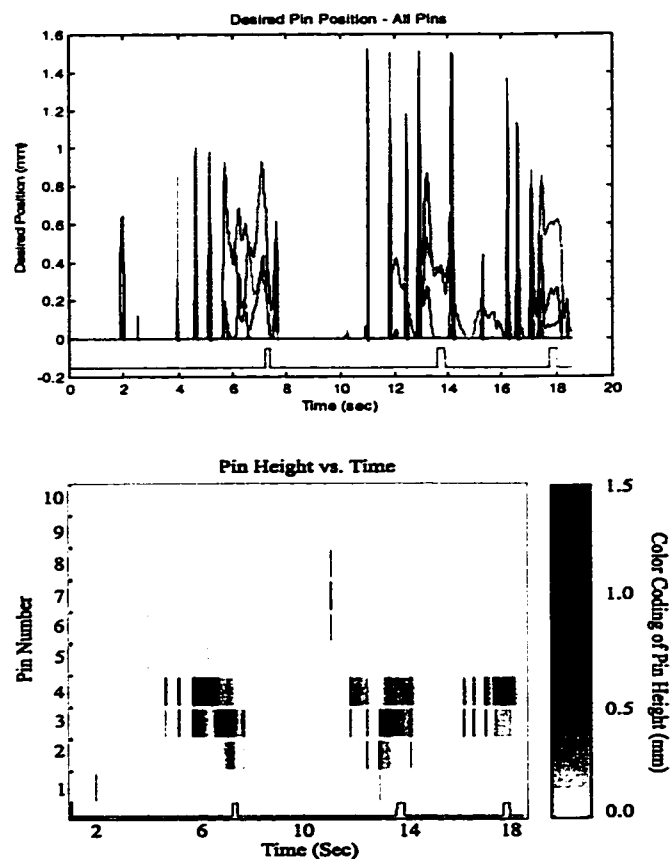


Figure 7.13. *Desired Position of Pins during Typical Trial.*

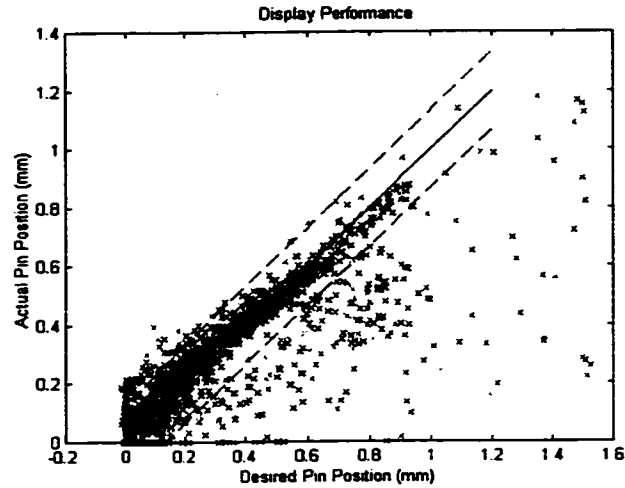


Figure 7.14. *Actual versus Desired Position of Pins during Typical Trial.*

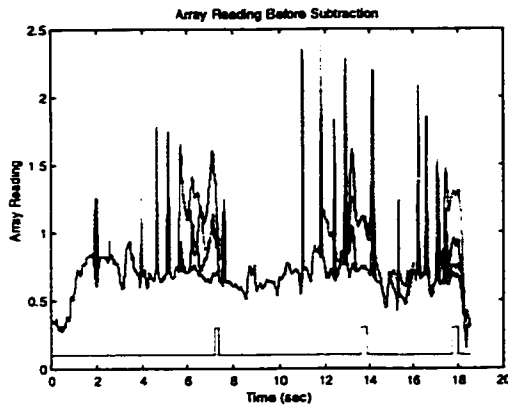


Figure 7.15. *Desired Position of Pins with Baseline Added Back.*

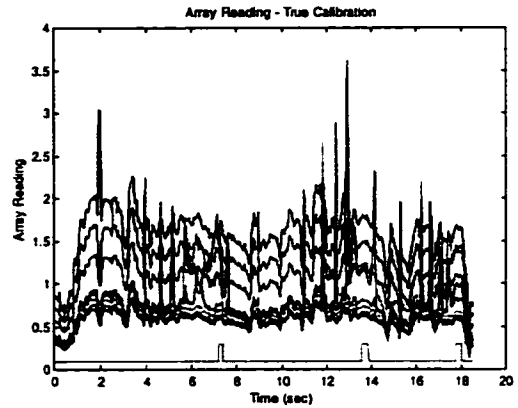


Figure 7.16. *Desired Position of Pins Using Unscaled Pressures.*

The results for all subjects are plotted in Figure 7.17. Figure 7.17a shows the search times needed to find the three lumps. The gray bars indicate the mean of the subject means. The thicker error bars indicated the standard deviation of the subject means. The markers in the plots (circle, square, etc.) show the mean of the each subject and corresponding standard deviation. The same symbols are consistently used for the same subject in all of the plots. The search time did not show a significant variation for each of the different types of trials. Table 7.1 reports the actual values of means and standard

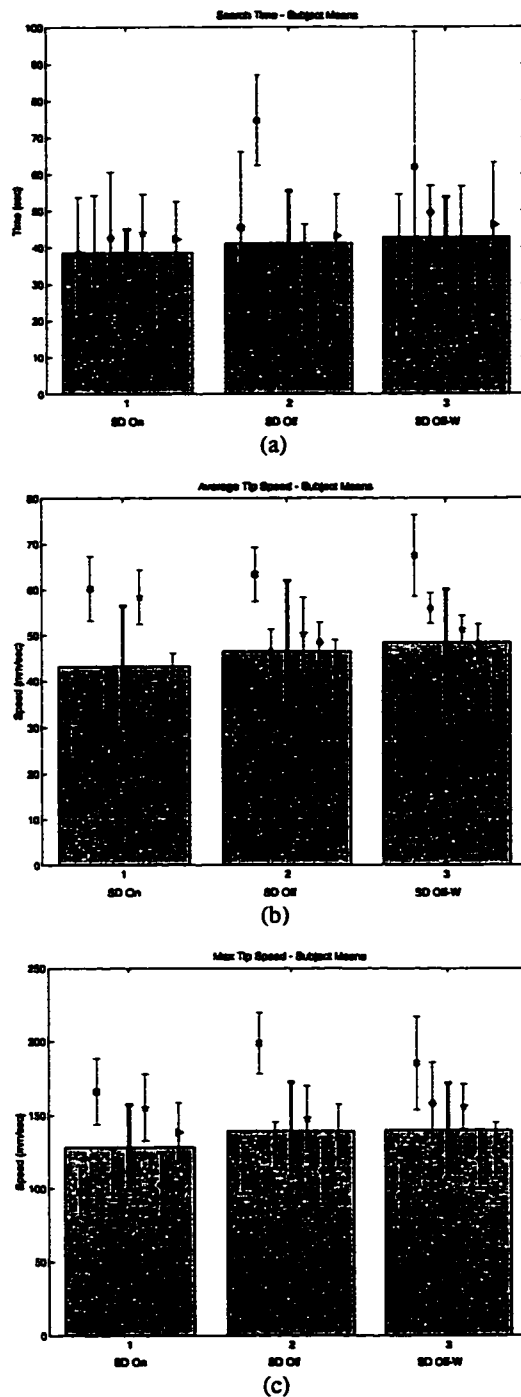


Figure 7.17. Results of MIS Lump Localization Experiment. (a) Average search times, (b) mean sensor speed, and (c) maximum sensor speed for the three trial types. Trials with the shape display on the instrument are labeled SD On. Trials with the display off the instrument and no counterweight are labeled SD Off. Trials using the counterweight are labeled SD Off-W. The height of the shaded bar show the mean of the subject means, and the dark lines indicate the standard deviation of these means. Individual subject means and standard deviations for each measurement and trial type are also shown. The symbols for subjects are consistent throughout.

deviations. Figures 7.17b and 7.17c shows the average and maximum sensor speeds used during the palpation tasks, respectively. The means and standard deviations are as in Figure 7.17a. The scanning speed of the sensor did not show any significant variation between the different types of trials.

	Search Time (sec) Mean \pm (std)	Mean Speed (mm/s) Mean \pm (std)	Max Speed (mm/s) Mean \pm (std)
Display On	38.55 \pm (6.39)	43.23 \pm (13.25)	128.30 \pm (28.86)
Display Off	41.11 \pm (18.50)	46.54 \pm (11.39)	139.56 \pm (31.94)
Display Off w/ Weight	42.81 \pm (12.15)	48.45 \pm (16.49)	140.07 \pm (38.22)

Table 7.1 *Experimental Results from Localization Experiment.*
(Means are shown for all subjects.)

7.5.3 Discussion

The experimental results validated the preliminary observations from using the prototype. The lumps were located even with the shape display located off the instrument. Based on subjective comments, reducing the weight of the instrument by removing the display was helpful, but not significantly enough to effect the aspects we investigated in this experiment. In part this shows the remarkable adaptively of the human sense of touch. Through a brief training period, subjects overcame obstacles and performed at a consistent level.

Although the results of this experiment lie within the realm of the null hypothesis, they still provide useful and interesting information. First, the system was functional and

multiple subjects found the minimally invasive localization task straightforward with the instrument design and tactile feedback. The pin joint at the sensor and universal joint allowed the subjects to use natural hand motions and maintain a consistent contact with the rubber models. The tactile sensations were vital to the subjects finding the lumps.

Another important aspect of these results is the finding that the shape display does not need to be integrated into the instrument for this task. This may not be true for more complex tasks where tactile and kinesthetic sensations are more intricately linked. Relaxing the size and weight constraints on the display would change the complexity of the display design problem dramatically. More reliable actuators could be used and packed into a 2D array that still provide the necessary requirements of the pin motion. Integrating the display into the instrument does have advantages. If the display is off the instrument, both hands of the surgeon are occupied. Also, a single instrument could take up less space in the overcrowded operating room [Alacron and Berguer 1996].

One of the most beneficial aspects of this experiment was getting the feedback from subjects about the palpation instrument. After 60 to 90 minutes of use, subjects understood the good points and bad points of the instrument design. Subjects commented that the passive joints and handle made the instrument felt natural to use and did not require awkward motions. Some, however, found the universal joint annoying because it made the rolling orientation of the sensor hard to control. Others wanted the handle turned 90 degrees. The weight of the display was heavy enough that a strap running perpendicular to the finger across the knuckle was needed to help hold the index finger against the display.

Subjects initially wanted the display on the instrument. They felt most comfortable with the correlation of feedback onto one hand. After getting used to the display in the other hand, all the subjects found the localization task straightforward for both configurations. Most subjects found the instrument easier to control with the weight of the display removed. One subject said adding the dummy weight made it feel terrible, but she was still able to complete the task with the same skill. The weight caused fatigue and often subjects used their other hand to support the display when it was on the instrument. The kinematics of the arm-based design caused some frustration. Many commented it felt strange to apply a downward force on the tissue by lifting, especial since the finger was facing down.

The video feedback also drew many comments. Some felt the most challenging part of the task was manipulating the sensor over the model surface using the visual feedback. This is a difficulty for surgeons as well, and many hours of practice are necessary to learn the complex mapping caused by the off-axis viewing angle of the camera [Tendick et al 1993]. The size change of objects as they moved away from the camera also caused problems. Areas of the model near the camera were often searched more thoroughly because they seemed bigger. To a large extent, the variations between subjects in search time was largely determined by the efficiency (or lack thereof) of their search strategy. Subjects with consistent search techniques missed fewer areas of the model and searched the space more quickly. It should also be noted that just as with the virtual reality lump localization experiment presented in Chapter 6, speed did not correlate with search time. Subjects who moved quickly often passed over the top of a lump without detection.

Subjects felt the tactile sensations generated by scanning over a lump were obvious to detect. One observation especially insightful about the signal processing technique involved the inability to accurately gauge applied contact forces. The baseline sensations measured by the sensor are largely determined by the amount of contact force. When this information is subtracted out, the subject could not use tactile clues to estimate contact force. The weight of the display made force-displacement information of the whole hand difficult to perceive. This makes sense based on the distributed pressure measurements taken in the lump detection experiment presented in Chapter 3. The tactile sensation to the finger consisted of an offset distribution proportional to contact force and the local pressure bump added by the presence of the ball.

Chapter 8. Conclusions and Future Work

Minimally invasive techniques are an exciting frontier of surgery. The ability to operate inside the body through a few small incisions brings tremendous benefits to patients. Currently, surgical tools used for these techniques deprive the surgeon of directly touching internal tissue. This causes simple palpation tasks to become frustrating and time consuming. The development of remote palpation systems would rectify this problem and allow tactile information to be effectively used for localization and diagnosis. Ideally, these systems would provide a transparent interface between the surgeon's hands and internal tissues. Developing hardware capable of doing this is difficult because palpation is a complex sensory-motor process. A detailed understanding of the design space for these devices is needed.

The research in this thesis primarily focuses on remote palpation instruments for locating hard nodules in the lung. Hardware designs and palpation experiments were tailored to this target application. This provides a glimpse at only a small corner of the design space, but the results obtained reach far beyond the scope of product development for these simple devices. The ideas are useful for more ambitious schemes to provide more transparent palpation feedback for surgical robots and advanced instruments.

This chapter discusses some of the future work needed to advance this research. It is divided into two parts. The first section discusses improvements necessary to make the prototype system useful in surgery. This involves advancing the hardware components and conducting more investigations to understand single finger palpation for lump

localization. The second section discusses advanced signal processing techniques necessary for transparent feedback. This provides an excellent framework to show how the application specific research in this thesis fits into the larger goals of remote palpation systems.

8.1 Improvement for Prototype System

The localization of nodules in the lung during minimally invasive thoracic surgery is an application where remote palpation systems can make a significant improvement. The tactile sensations created as the sensor scans over the lump are easy to detect, thus simplifying the signal processing and reducing the requirements of the tactile feedback system. The prototype instrument described in Chapter 7 is functional and successfully located lumps in rubber models; however, many more improvements are necessary for the device to be of value in a surgical environment. A number of these are product development issues that this thesis did not address. There are many more fundamental questions to answer to provide a solid scientific foundation for design. This section discusses some of the specific issues related to the target application and prototype instrument. It is divided into sections based on the major hardware components.

8.1.1 Tactile Sensor and Signal Processing Design

There are several improvements necessary for the tactile array sensor. The first is increasing the sensitivity to match the design specification set by the detection experiment in Chapter 2. The technology is available to do this and the performance could greatly be enhanced. It is also possible to increase the number of rows of sensing

elements. The current design only uses a single row. This is a problem when large angles were swept out with the instrument because the sensor elements would lose contact with the tissue. Multiple rows could alleviate this problem.

The signal processing can be improved in many ways as well. By changing the shape of the sensor and introducing a large radius curve along the length, the stress concentrations induced by the edge effects could be diminished. It would also be of value to introduce some information about overall contact force in the tactile output. With the current instrument design contact force is hard to estimate. Tactile clues could make this easier.

There are many more experiments and studies needed to improve our understanding of tactile stimuli generated during palpation. These results will help determine other important design specifications. One of the most interesting research areas involves expanding the work of the palpation experiment described in Chapter 2 by investigating active palpation. In the experiment presented, detection limits were determined. Normal sensation levels during unrestricted palpation are of interest as well and would provide insight to other facets of the palpation process, such as how edges are used during a detection task. Further investigations are needed to understand the relation between properties of the remote tissue and measured tactile sensations. This could lead to signal processing that conveys properties of the lump as well as location.

8.1.2 Tactile Shape Display Design

Designing tactile shape displays is an immense challenge. Fitting so many actuators in a small space introduces many complexities. Many improvements in the prototype

display described in Chapter 5 are needed. One of the biggest drawbacks is the lack of fidelity in pin motion control. The optical feedback technique was complicated due to the water filled environment. Bubbles and electrical conduction through the water were problems. The water allowed the high bandwidth of pins, but limited performance in other ways. The weight of the device was significant due to the large tubes necessary for the recirculating cooling.

Another major limitation of the display was the configuration of the pins. Although a single line of pins does allow an area to be searched by sweeping, important information about the lump could not be detected. It was possible to sense curvature along the length of the pins, but sensing curvature in the other direction by combining pin motions with finger motion across time was extremely difficult. A two-dimensional (2D) array of pins is thus necessary to provide realistic sensations of a lump. The line also limited search ability by reducing the time the sensation of the lump was present on the finger. If the sensor was moving quickly, it was challenging to stop the sensor while maintaining the sensation of the lump. Usually, the lump would be passed by and backtracking required guessing the sensed location. A 2D array would improve performance by increase the time the sensation was present.

The design of tactile displays is such a challenging task that specifications, such as temporal bandwidth requirements, are important and necessary for proper development. More experiments are needed to determine these specifications based on performance during palpation tasks. Questions concerning which sensations should be produced, how much fidelity is necessary, and how many pins are necessary are fundamental questions worth addressing.

8.1.3 Surgical Instrument Design

Improvements to the instrument design constitute the majority of changes necessary to make the prototype palpation instrument described in Chapter 7 a usable product for surgery. The end design was functional but suffered from many flaws. For starters, it was too big. Packaging is critical for success and must include features such as easy sterilization. The cabling was also less than optimal. The bulky wires created unwanted torque on the pivoting sensor head causing variations in the baseline stress distribution. Improvements in the ergonomics are also necessary. The handle design and excessive weight of the display made extended use of the system tiring.

The structural layout of the instrument used the fixed rotation point imposed by the surgical entry location to its (mechanical) advantage. This had the benefit of simplifying the design, but caused confusion by reversing motions and forces required to move the sensor. Lifting the handle to apply downward forces with the sensor was the most unnatural of these problems. More advanced mechanisms are needed to transmit the motions of the surgeon's hands to the sensor. A possible solution is to combine the mechanism used in the finger-based design with the pivoting sensor head used in the arm based design. This would eliminate the mirroring problem while maintain the benefits of using arm based motions. There is room for tremendous creativity in designing these mechanisms. Quantifying hand configurations and finger motions used during palpation tasks will aid this process.

One of the more profound findings from the localization experiment using the prototype instrument described in Chapter 7 was the fact that performance did not significantly drop when the display was not on the instrument. This brings many

questions to the forefront as to the necessity of tactile feedback at all. What are tasks that require close coupling between tactile and kinesthetic information? Possibly the tactile information measured with the sensor could be displayed visually or by sound, thus dramatically reducing the complexity of the palpation instrument. But how distracting is sensory substitution? And what range of procedures can be accomplished without tactile feedback? These questions are critical to the development of useful products.

It should also be noted that the prototype palpation instrument developed in this research is useful for other applications that utilize single finger palpation. Some of these tasks include sensing the stiffness of internal organs or locating arteries during dissection. Chapter 3 demonstrated feasibility of measuring the pressure sensations of the artery using the tactile array sensor. Investigations to where single finger palpation is used will provide more applications for these devices.

8.2 Advanced Signal Processing Techniques

Many of the experiments, results, and discussions in this thesis have concentrated on design specifications for the hardware components of remote palpation devices. This is because kinesthetic feedback mechanisms and tactile displays are the primary limiting factors in the development of these systems. It should be noted that hardware is only one part of the design space and other issues are equally important to the advancement of remote palpation instruments. One of the most significant of these issues is signal processing. It determines drive commands for the tactile feedback devices from signals collected from the sensors inside the patient's body. Sophisticated signal processing is needed to determine what sensations the surgeon would feel if touching the tissue

directly. This section describes a framework to accomplish this task and shows the relation of the research presented in this thesis to this grand scheme.

One technique to achieve transparent feedback for a remote palpation system is to match perfectly the properties of the sensor to the surgeon's finger. This causes the contact interaction between the sensor and tissue to be identical to the interaction that would occur if the surgeon's finger were touching the tissue. The kinesthetic and tactile sensations measured by the sensor could then be directly reproduced, requiring no signal processing. However, developing a sensor that matches the compliance, shape, and sensitivity of the finger is a formidable task. And even if this were possible, the approach is impractical due to the wide variations in finger properties between surgeons. A more realistic method is to use a simple sensor design and transform the contact information collected to appropriate sensations produced if the finger contacted the tissue.

8.2.1 Measured Model Based Haptic Rendering

One approach to perform this transformation is to use detailed models of the sensor, finger, and tissue to solve solid mechanics problems describing the contact of the sensor and finger with the internal organ. The first interaction to analyze is the contact between the sensor and remote tissue. By solving an inversion problem, realistic models of the material and structural properties of the internal organ can be determined from signals collected by the sensor. The second interaction is a hypothetical contact between the surgeon's finger and tissue model. This predicts the sensations the surgeon would feel and allows the production of appropriate feedback to the finger. Figure 8.1 shows the conceptual idea of this process. The motions and forces of the surgeon's hand are used to

drive the sensor inside the patient. As the sensor probes the organ, contact information is used to develop a simple model of the tissue that captures key aspects of the organ's properties. The more the sensor probes the organ, the better the tissue model becomes. The surgeon is able to palpate the internal organ by probing the tissue model using a haptic interface.

Implementing this signal processing technique requires the integration of many complex algorithms and hardware devices. Figure 8.2 shows the main components involved in the system and the flow of information between these parts. There are two main loops functioning in parallel, each using the motions and forces of the surgeon's hand as inputs. One loop is used to develop a 3D model of the remote organ from the sensation collected as the sensor probes the tissue. The second loop uses a haptic rendering algorithm to determine realistic tactile and kinesthetic sensations to display to the surgeon. It is useful to investigate both of these loops in detail to understand future research necessary to implement these ideas. This also shows how many of the findings of this thesis provide initial steps toward this goal.

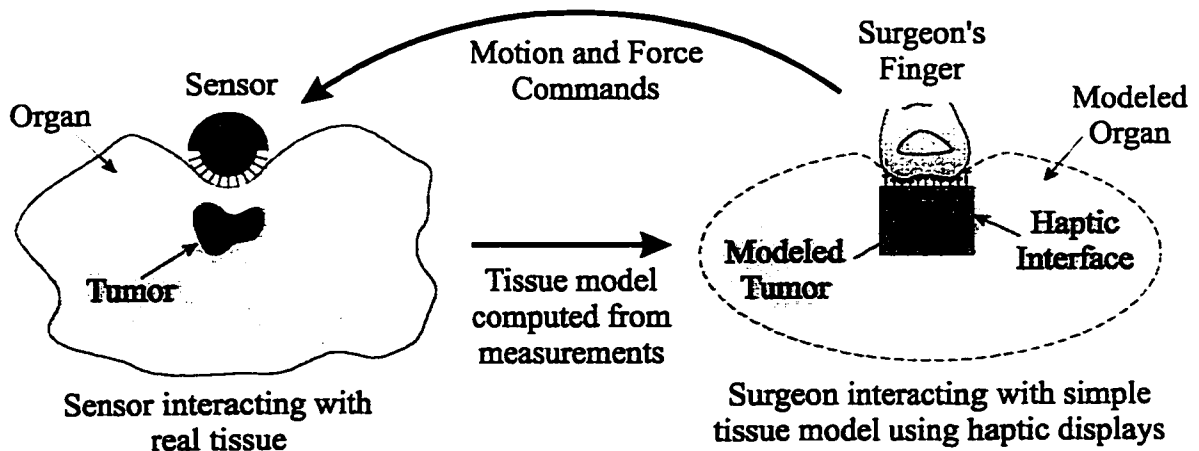


Figure 8.1. *Concept of Model-Based Haptic Rendering.*

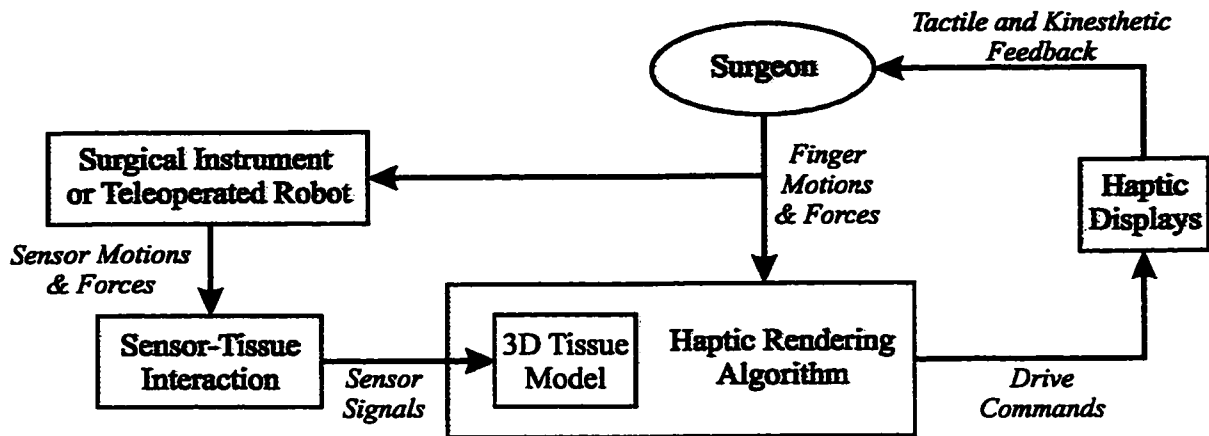


Figure 8.2. *Key Components and Flow of Information.*

8.2.2 3D Tissue Model Generation from Tactile Signals

The surgeon controls the motions of the contact sensors inside the patient's body through teleoperated robots or advanced instrument mechanisms. Internal tissues can then be probed to collect valuable contact information for the development of a 3D model of the tissue. It is important that these mechanisms allow smooth control of the motion of the sensor in relation to the tissue surface. This was shown to be crucial for the design of the prototype palpation instrument discussed in Chapter 7. If consistent contact between the sensor and tissue cannot be maintained, the signals measured will be difficult to interpret. The taxonomy presented in Chapter 6 also shows how hand configurations are chosen to maximize finger mobility for this reason. A significant amount of research is needed to develop teleoperated robots and instrument mechanisms that allow the surgeon to use natural hand and finger motions to smoothly control the sensor.

Determining properties of the internal organ from the contact sensor signals is a challenging task. It requires good control of the sensor motions, clean tactile signals, and

a thorough understanding of the relation between tissue properties and corresponding sensor measurements. Information about the tissue's local stiffness, shape, and embedded structures needs to be determined. This will require the solution of contact problems to determine how tactile sensations vary with these tissue properties. Then, real time processing techniques can be implemented to detect these predictable signals. The simple signal processing algorithm used in the prototype palpation instrument (described in Chapter 3) is an example of this process. The sensations induced by the homogeneous rubber were determined through experiment. By removing these signals from the pressure distribution, the sensations of the lump where the only stimulus the felt by operator through the tactile feedback system. It would be straightforward to compile this information into a 3D model of the tissue by measuring the position of the sensor relative to the tissue surface. Wellman and Howe [1998] implemented this idea for tactile mapping of breast tumors. A magnetic tracker was used to measure the relative position of a tactile sensor as it scanned across the breast tissue. The location of a lump was determined by integrating multiple passes of the sensor together. Solid mechanics models were used to determine properties of the lump based on measured tactile signals. This provided information about the lump's size, depth, and stiffness. Many more studies along these lines are needed to effectively interpret tissue properties from tactile signals.

Compiling the tissue properties into a 3D model involves constantly updating the model as more information is collected. This causes the model to continually increase in resolution as sensor probes the tissue. Some thought is required to determine how to do this. Important questions about the starting point for the model and what to do with conflicting information need to be resolved. Many of these issues can be answered by

trial and error methods, but results will highly depend on specific applications. To speculate a bit, it seems reasonable to start with a very simple model of the tissue and gradually refine it. For example, the initial state could be a half-space of homogeneous material. Then as contact positions are determined, the shape of the internal organ is slowly refined and perfected. Overall contact force and the shape of the pressure distribution can give information about the local stiffness of the material. Embedded objects could be detected by looking for pressure concentrations as the sensor glides over them. It may also be possible to incorporate other imaging modalities, such as MRI, CT scan, and visual information from the endoscope. This is a wide open research area that deserves attention.

A challenging sensing problem in this model-based approach is determining the motion of the sensor relative to the tissue surface. Many organs have very low stiffness and are easily deformed. This makes palpation possible, but hinders tracking of organ shape and position. If the relative position is not accurately determined, tactile features will appear to move or smear in the tissue model. This will greatly confuse the surgeon and hinder the palpation process. A simple solution is to rigidly fix the organ and only measure the position of the sensor relative to a fixed reference frame. An additional solution may come from the integration of image processing into the motion sensing process. Vision provides large quantities of useful information, but significant research is needed to determine real time algorithms for tracking low stiffness tissues.

8.2.3 Haptic Interface of Finger Contact with 3D Tissue Model

The second side of the signal processing technique involves using haptic rendering algorithms to determine what the surgeon's finger would feel by contacting the 3D tissue model, and thus the internal organ. The contact location between the finger and tissue is determined from measurements by the haptic interface. The rendering algorithms determine bulk forces, position, and distributed sensations on the finger by solving contact problems. This tactile and kinesthetic information is then displayed to the surgeon using haptic feedback devices. As the fingers probe different parts of the model, appropriate sensations are produced. At the same time, the motions of the surgeon's fingers are controlling the sensor and refining the model at that location. This causes tactile features of interest to have the highest resolution because they will be explored for longer intervals resulting in a more detailed model description.

There are many fundamental issues to address in this process. Many of these depend on understanding the interaction between the surgeon's finger and tissue model. As a first step, an understanding of the mechanics of the human fingerpad are needed. The structure and shape of the finger are difficult to describe and the material properties have been shown to exhibit nonlinear stress-strain behavior [Pawluk 1997]. Even with accurate models of the finger and tissue, the problems are far from over. Contact between two soft materials is difficult to predict due to the high strain levels and nonlinearity induced by the varying contact area. This makes numerical models challenging to implement, especially in real time. Analytic solutions offer quick results, but often require vast simplifications and assumptions. For example, the haptic control algorithm described in Chapter 3 modeled the contact between the finger and soft tissue

using a modified Hertz solution. The tissue was therefore described by a simple half-space of linear homogeneous material and the finger was parabolic in shape. More advanced features can be integrated into these simple models, as was done by including the nonlinearity of the finger pad. Much more work is needed to develop haptic rendering algorithms that accurately predict the sensations induced by contact with soft materials.

It is also important to understand the kinds of palpation motions the surgeon uses to explore an organ and what sensations are most beneficial to complete the task. This determines important design aspects of the haptic interface and helps simplify the goals of the contact rendering algorithms. Much of this thesis was devoted to understanding these issues and measuring quantities of this nature. The detection experiment is an excellent example of teasing out what humans are sensing during a palpation task and measuring the limitations of the sense of touch. The human factors study of finger speeds used during lump localization showed what search techniques surgeons use and quantified an important parameter of these motions. Because palpation is so complex and is used for such a variety of tasks, this work is just a small step toward understanding these issues. Significantly more effort is needed to understand other critical aspects of the natural palpation process.

The development of tactile and kinesthetic feedback devices is also a major hurdle. As was mentioned, this is the primary limiting factor. Signal processing algorithms are of no use if they cannot be implemented. Many of the design decision will need to be based on limitations in hardware performance. This should not diminish the importance of looking ahead and working to solve the challenging problems associated with

modeling and haptic rendering. New actuators will be introduced and the development of these devices will continue.

8.3 The Fundamental Importance of Touch

The sense of touch is an amazing sensory-motor process. A large part of the interaction with our world is through our fingers. We use it to explore, to build, to love, and even communicate. The development of remote palpation systems has very specific goals and objectives, but these ideas delve into this rich world of touch. Understanding how and why the sense of touch works is of value in and of itself.

Bibliography

1. Alacron A and Bergeur R, 1996. "A comparison of operating room crowding between open and laparoscopic operations," *Surgical Endoscopy*, **10**:916-919.
2. Baum J, Neena C, Netland P, Dreyer E, 1995. "Assessment of Intraocular Pressure by Palpation," *American Journal of Ophthalmology*, **119**(5):650-651.
3. Begej S, 1988. "Planar and finger-shape optical sensors for robotic applications," *IEEE J. of Robotics and Automation*, **4**(5):472-484.
4. Berguer R, 1996. "Ergonomics in the Operating Room," *The American Journal of Surgery*, **171**:385-386
5. Berguer R, Remler M, Beckley D, 1996. "Laparoscopic instruments cause increase forearm fatigue: A subjective and objective comparison of open and laparoscopic techniques," *Minimally Invasive Therapy & Allied Technology*, **5**:1-5.
6. Bliss JC, Katcher MH, Rogers CH, and Shepard RP, 1970. "Optical-to-Tactile Image Conversion for the Blind," *IEEE Transactions on Man-Machine Systems*, **MMS-11**(1):58-65.
7. Brocket RW, 1998. Harvard University, Division of Engineering and Applied Sciences, Personal Communication.
8. Chodak et al., 1986. "Comparison of Digital Examination and Transrectal Ultrasonography for the Diagnosis of Prostatic Cancer," *Journal of Urology*, **135**:951-954.
9. Cohn MB, Lam M, Fearing RS, 1992. "Tactile Feedback for Teleoperation," Das H, Ed., *Proc. Of Telemanipulator Technology, Proc. SPIE 1833*, pp. 240-254.
10. Cutkosky MR and Howe RD, 1990. "Human Grasp Choice and Robotic Grasp Analysis," n S. T. Venkataraman and T. Iberall, eds., *Dextrous Robot Hands*, New York, Springer-Verlag.

11. Dario P and Bergamasco M, 1988. "An Advanced Robot System for Automated Diagnostics Tasks through Palpation," *IEEE Transactions on Biomedical Engineering*, 35(2):118-126.
12. Emans MB, 1996. "A palpation instrument for use in minimally invasive surgery," Senior Design Project Report, Engineering Sciences 100hf, Harvard University.
13. Fearing RS, 1990. "Tactile sensing mechanisms," *International Journal of Robotics Research*, 9(3):3-23.
14. Fischer H, Neisus B, and Trapp R, 1995. "Tactile Feedback for Endoscopic Surgery," *Interactive Technology and the New Paradigm for Healthcare*. K Morgan, R.M. Stava, H.B. Siburg et al., Eds., IOS Press and Ohmsha.
15. Fischer H, 1997. "Sensor-Aktorsysteme für den Einsatz in der laparoskopischen Chirurgie, Forschungszentrum Karlsruhe, Wissenschaftliche Berichte FZKA5898, Karlsruhe.
16. Fung YC, 1993. "Biomechanics: Mechanical Properties of Living Tissues," Springer-Verlag, New York.
17. Goodwin, A.W. and Wheat, H.E., 1991. "Human tactile discrimination of curvature when contact area with the skin remains constant," *Experimental Brain Research*, 88: 447-450.
18. Grant D and Hayward V, 1997. "Controller for a High Strain Shape Memory Alloy Actuator: Quenching of Limit Cycles," *Proceedings of the 1997 IEEE International Conference on Robotics and Automation*, Albuquerque, New Mexico, pp. 254-259.
19. Hasser Christopher Hasser and Janet M. Weisenberger, 1993. "Preliminary Evaluation of a Shape-Memory Alloy Tactile Feedback Display," in H. Kazerooni, J. E. Colgate, and B. D. Adelstein, eds., *Advances in Robotics, Mechatronics, and Haptic Interfaces*, DSC-vol. 49, American Society of Mechanical Engineers Winter Annual Meeting, New Orleans, Nov. 29-30.
20. Hillis WD, 1982. "Active touch sensing," *Int. J. of Robotics Research*, 1(2):33-44.

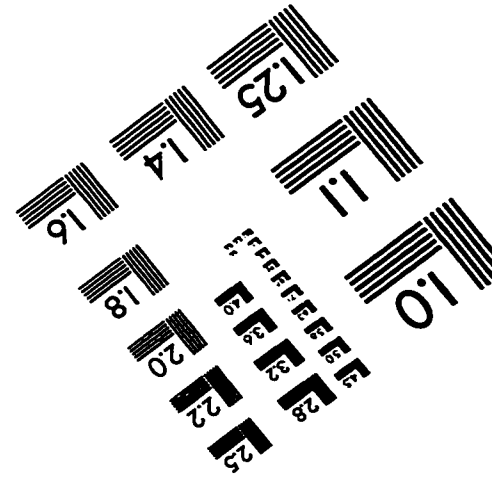
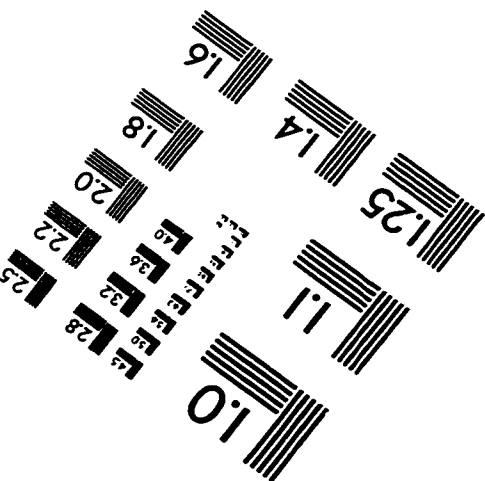
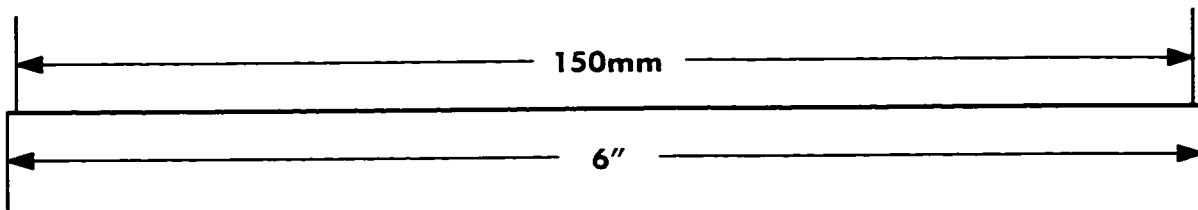
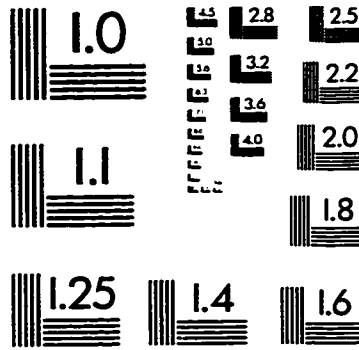
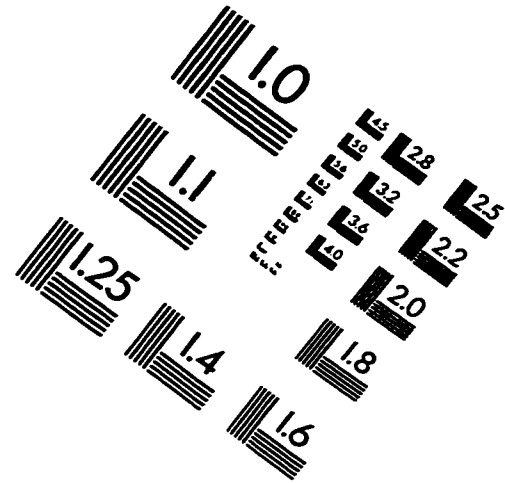
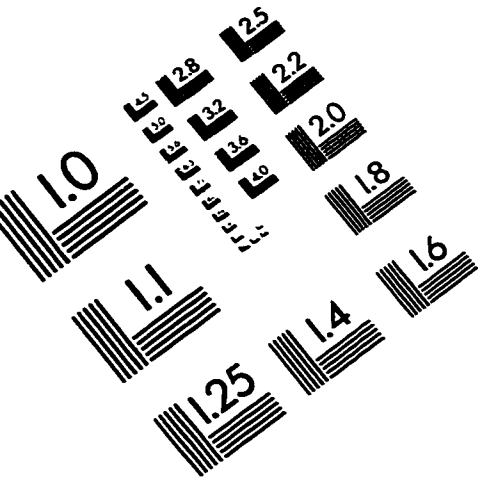
21. Howe RD, 1994. "Tactile sensing and control of robotic manipulation," *Journal of Advanced Robotics*, **8**(3):245-261.
22. Ikuta K, 1990. "Micro/miniature shape memory alloy actuator," *Proceedings of the IEEE International Conference on Robotics and Automation*, Cincinnati, pp. 2156-2161.
23. Ikuta K, Takamoto M, and Hirose S, 1990. "Mathematical Model and Experimental Verification of Shape Memory alloy for Designing Micro Actuator," *Proceedings of the IEEE Micro Electro Mechanical Systems*, pp.103-8, IEEE.
24. Johnson KO and Phillips JR, 1981. "Tactile Spatial Resolution. I. Two-Point discrimination, Gap Detection, Grating Resolution, and Letter Recognition," *Journal of Neurophysiology*. **46**(6):1177-1191.
25. Johansson RS and Vallbo AB, 1983. "Tactile sensory coding in the glabrous skin of the human hand," *Trends in NeuroSciences*, **6**(1): 27-32.
26. Kontarinis DA and Howe RD, 1993. "Tactile Display of Contact Shape in Dexterous manipulation," in *Advances in Robotics, Mechatronics, and Haptic Interfaces*, DSC-vol. 49, H. Kazerooni, J. E. Colgate, and B. D. Adelstein, eds., American Society of Mechanical Engineers Winter Annual Meeting, New Orleans, Nov. 29-30, pp. 81-88.
27. Kontarinis DA, Son JS, Peine WJ, and Howe RD, 1995. "A Tactile Shape Sensing and Display System for Teleoperated Manipulation," *Proc. of the 1995 Intl. Conference on Robotics and Automation*, Nagoya, Japan.
28. Kontarinis DA and Howe RD, 1995. "Tactile display of vibratory information in teleoperation and virtual environments," *Presence*, **4**(4):387-402.
29. Lai Fook SJ, Wilson, TA, Hyatt, RE, and Rodarte, JR, 1976. "Elastic Constants of Inflated Lobes of Dog Lungs," *J. Applied Physiology*, **40**:508-513.
30. Lederman SJ and Klatzky R, 1987. "Hand movements: A window into haptic object recognition," *Cognitive Psychology*, **19**(3), 342-368.

31. Loomis JM and Lederman SJ, 1986. "Tactile Perception," *Handbook of Human Perception and Performance*, Boff KB, Kaufmann L, Thomas J, Eds., Wiley, New York.
32. Mack MJ, Shennib H, Landreneau RJ, and Hazelrigg SR, 1993. "Techniques for Localizing of Pulmonary Nodules for Thoracoscopic Resection," *J. Thoracic Cardiovascular Surgery*. **106**(3): 550-553.
33. Melzer A, Schurr MO, Kurnert W, et al., 1993. "Intelligent surgical instrument system ISIS: Concept and preliminary experimental application or prototypes," *Endoscopic Surg Allied Technol* **1**:165-170.
34. Melzer A, Buess G, Cuschieri A, 1994. "Instruments and Allied Technology for Endoscopic Surgery," *Operative Manual of Endoscopic Surgery 2*, Cuschieri A, Buess G, Perissat J, Eds., Springer-Verlag, New York, pp. 1-69.
35. Naylor CD, 1994. "Physical Examination of the Liver," *JAMA*, **217**(23):1859-1865.
36. O'Reilly S and Keogh JAB, 1992. "Palpating enlarged kidneys," *Irish Medical Journal*, **85**(3):89.
37. Pawluk DTV, Son JS, Wellman PS, Peine WJ, 1998. "A Distributed Pressure Sensor for Biomechanical Measurements," *Journal of Biomechanical Engineering*, **102**(2):302-305.
38. Pawluk DTV and Howe RD, 1996a. "Dynamic Lumped Element Response of the Human Fingerpad." *ASME Journal of Biomechanical Engineering*, in press (April 1999).
39. Pawluk, DTV and Howe RD, 1996b. "Dynamic Contact of the Human Fingerpad Against a Flat Surface", submitted to *ASME Journal of Biomechanical Engineering*.
40. Pawluk DTV, Peine WJ, Wellman PS, and Howe RD, 1997. "Simulating Soft Tissue with a Tactile Shape Display," *ASME International Mechanical Engineering Congress and Exposition*, Dallas, Nov. 15-21, 1997, in B. Simon, ed., *Advances in Bioengineering*, *ASME BED*-Vol. 36.

41. Plunket MB, Peterson MS, Landreneau RJ, Ferson PF, Posner MC, 1992. "Peripheral pulmonary nodules: preoperative percutaneous needle localization with CT guidance," *Radiology*, 185:274-6.
42. Peine WJ and Howe RD, 1998. "Do humans sense finger shape or distributed pressure when detecting a lump in soft tissue?" in R.J. Furness, ed., *Proc. of the ASME Dynamic Systems and Control Division, ASME International Mechanical Engineering Congress and Exposition, Anaheim, Nov. 19-20, 1998, DSC-Vol. 64*, pp. 273-278.
43. Peine WJ, Foucher KC, and Howe RD, 1997. "Finger speed in single digit palpation," *Human Factors*, in press.
44. Peine WJ, Son JS, and Howe RD, 1994. "A Palpation System for Artery Localization in Laparoscopic Surgery," Proceeding of the First International Symposium on Medical Robotics and Computer Assisted Surgery, Pittsburgh, PA, August.
45. Pennypacker HS and Iwata MM, 1990. "MammaCare: A case history in behavioral medicine," in D.E. Blackman and H. Lejeune, eds., *Behaviour Analysis in Theory and Practice: Contributions and Controversies*, East Sussex, UK: Lawrence Erlbaum Associates Ltd., pp. 259-288.
46. Phillips JR and Johnson KO, 1981. "Tactile spatial resolution. III. A continuum mechanics model of the skin predicting mechanoreceptor responses to bars, edges, and gratings," *Journal of Neurophysiology*, 46: 1204-1225.
47. Slator S, 1993. "Palpation of the Thyroid Gland," *Southern Medical Journal*, 86(9):1001-1003.
48. Srinivasan MA and LaMotte RH, 1987. "Tactile discrimination of shape: Responses of slowly and rapidly adapting mechanoreceptive afferents to a step indented into the monkey fingerpad," *Journal of Neuroscience*, 7(6): 1682-1697.
49. Srinivasan MA and LaMotte RH, 1995. "Tactile discrimination of softness," *Journal of Neurophysiology*, 73(1): 88-101.

50. Taylor PM, Moser A, and Creed A, 1997. "The Design and Control of a Tactile Display Based on Shape Memory Alloys," *Proceedings of the 1997 IEEE International Conference on Robotics and Automation*, Albuquerque, NM, pp. 1317-1323.
51. Tendick F, Jennings R, Tharp G, and Lawrence S, 1993. "Sensing and Manipulation Problems in Endoscopic Surgery: Experiment, Analysis, and Observation," *Presence*, 2(1):66-81.
52. Vege-Bermudez F and Johnson KO, 1998. "Monkey cutaneous SAI and RA responses to multiple probes protruding from a uniform background: effects of number and baseline depth," *Technical Report*, Krieger Mind/Brain Inst. and Dept. of Neuroscience, Johns Hopkins University.
53. Wellman PS and Howe RD, 1995. "Towards Realistic Vibrotactile Display In Virtual Environments," *Symposium on Haptic Interfaces for Virtual Environment and Teleoperator Systems, Proc. of the ASME Dynamic. Systems and Control Division of the ASME*, DSC 57(2)713-718.
54. Wellman PS, Peine WJ, and Howe R D, 1997. " Mechanical Design and Control of a High-Bandwidth Shape Memory Alloy Tactile Display," in A. Casals and A.T. de Almeida, eds., *Experimental Robotics V. The Fifth International Symposium*, Barcelona, Spain, June 15-18, Springer-Verlag Berlin, pp. 56-66.
55. Wellman PS and Howe RD, 1998. "Tactile mapping for breast lesion localization," *Harvard BioRobotics Laboratory Technical Report*.

IMAGE EVALUATION TEST TARGET (QA-3)



APPLIED IMAGE, Inc
1653 East Main Street
Rochester, NY 14609 USA
Phone: 716/482-0300
Fax: 716/288-5989

© 1993, Applied Image, Inc., All Rights Reserved